

**DETERMINING PRESSURE COEFFICIENTS DUE TO
WIND LOADING ON GRAIN BINS**



By

HASAN VOLKAN KEBELI

**A DISSERTATION PRESENTED TO THE GRADUATE SCHOOL
OF THE UNIVERSITY OF FLORIDA IN PARTIAL FULFILLMENT
OF THE REQUIREMENTS FOR THE DEGREE OF
DOCTOR OF PHILOSOPHY**

UNIVERSITY OF FLORIDA

2002

Copyright 2002

by

Hasan Volkan Kebeli

To my lovely daughter, Melinda Kebeli, for filling me with joy and inspiration.

HOUGHTON
MIFFLIN
HARCOURT
190 N. ZEEB RD.
BOSTON, MA 02116

ACKNOWLEDGMENTS

The research for this dissertation was made possible by the support and encouragement I have received from many people. First of all, I would especially like to express my deepest gratitude and appreciation to my advisor and mentor Dr. Ray A. Bucklin for giving me the opportunity to work with him during my graduate studies at the University of Florida. I thank him for his advice, support, guidance, and encouragement over the years. It has been a privilege and an honor to work under his guidance. His dedication and enthusiasm have always been encouraging and motivating.

I want to extend my gratitude to Dr. Kurtis R. Gurley for his support, advice, and help in experiment setup and data analysis. His extensive contributions to this research were extremely valuable. I would also like to thank the other members of my supervisory committee, Dr. Arthur A. Teixeira, Dr. Michael T. Talbot, and Dr. Duane S. Ellifritt, for their guidance and support throughout this study. My committee's efforts on my behalf have left me indebted to them. In addition, I would like to acknowledge Dr. Timothy Reinhold for his collaboration, effort, help, and guidance for wind tunnel experiments at the Wind Load Test Facility in Civil Engineering Department, Clemson University.

I gratefully acknowledge the financial support of this study by the Turkish Ministry of Education for my graduate education in the U.S., The Grain Systems Inc. (GSI), Westeel Limited, Scafco Corp., and Brock Mfg.-CTB Inc. for their generous contributions towards this research.

I wish to express my appreciation to the faculty, staff and graduate students of the Department of Agricultural and Biological Engineering and the Department of Civil and Coastal Engineering. I especially thank Bob Tonkinson for his assistance in experiment setup and instrumentation. I also want to thank Larry W. Miller and Steve Feagle for their help and efforts.

My sincere thanks and appreciation go to my departed dearly loved father Cevat, my mother Vildan, and my brother Hakan for their unconditional love and affection throughout my life. I am grateful to them for giving me the best education possible and for the constant support and everlasting friendship they have provided.

Finally, my greatest appreciation and most special thanks go to my remarkably wonderful wife, Ayşegül, for her eternal love, companionship, support, patience, understanding, and encouragement through the culmination of this dissertation. I am also indebted to her for giving birth to our precious and charming daughter Melinda, to whom this dissertation is dedicated.

TABLE OF CONTENTS

	<u>page</u>
ACKNOWLEDGMENTS	iv
LIST OF TABLES	viii
LIST OF FIGURES.....	ix
ABSTRACT.....	xiv
 CHAPTERS	
1 INTRODUCTION.....	1
2 LITERATURE REVIEW.....	4
Wind Loads	4
Wind Loads on Shell Structures.....	16
Wind Loads on Grain Bins.....	21
Wind Load Requirements for Grain Bins in Building Codes and Standards.....	32
3 MATERIALS AND METHODS.....	38
Wind Tunnel Experiments	38
Wind Tunnel	41
Model Bins.....	42
Pressure Sensors and Data Acquisition System	44
Full-Scale Wind Experiments	55
Full-Scale Grain Bin	56
Pressure Taps and Sensors	56
Meteorological Towers	61
Data Acquisition System.....	62
4 RESULTS AND DISCUSSION	67
Wind Tunnel Tests.....	67
Velocity Profile and Turbulence Intensities of the Wind Tunnel Flow	68

Single Bin Configuration	75
Wall pressure coefficients.....	75
Roof pressure coefficients.....	77
Aspect ratio (H/D) effects	89
Grouping Effects.....	92
Wall pressure coefficients.....	92
Roof pressure coefficients.....	104
Full-Scale Tests.....	128
Wall Pressure Coefficients.....	131
Roof Pressure Coefficients.....	134
5 SUMMARY AND CONCLUSIONS	140
APPENDICES	
A CONTOURPLOTS OF ROOF PRESSURE COEFFICIENTS.....	148
B PEAK AND RMS PRESSURE COEFFICIENTS.....	154
LIST OF REFERENCES	187
BIOGRAPHICAL SKETCH.....	200

LIST OF TABLES

<u>Table</u>	<u>page</u>
2-1. Pressure coefficients for round structures given by ANSI A.58.....	34
2-2. Pressure coefficients for chimneys, tanks and similar structures.	34
3-1. Pressure tap placement on conical roofs.....	52
4-1. Measurements of velocity and turbulence intensities at the wind tunnel test section.....	71
4-2. Mean wall pressure coefficients for the full-scale bin.	132
4-3. Mean roof pressure coefficients at the top level of the full-scale bin.....	136
4-4. Mean roof pressure coefficients at the middle level of the full-scale bin.....	137
4-5. Mean roof pressure coefficients at the bottom level of the full-scale bin.....	138
B-1. Pressure coefficient data obtained from 25° smooth roof.	155
B-2. Pressure coefficient data obtained from 25° rough roof.....	159
B-3. Pressure coefficient data obtained from 30° smooth roof.	163
B-4. Pressure coefficient data obtained from 30° rough roof.....	167
B-5. Pressure coefficient data obtained from 35° smooth roof.	171
B-6. Pressure coefficient data obtained from 35° rough roof.....	175
B-7. Pressure coefficient data obtained from 40° smooth roof.	179
B-8. Pressure coefficient data obtained from 40° smooth roof.	183

LIST OF FIGURES

<u>Figure</u>	<u>page</u>
3-1. Boundary layer wind tunnel at WLTF, Clemson University, S.C.	45
3-2. Wind generating fans for the wind tunnel at WLTF.....	45
3-3. Test section of the wind tunnel at WLTF.	46
3-4. Pressure tap configuration on conical roof and cylindrical wall.....	47
3-5. Smooth and rough surface walls in the wind tunnel.....	48
3-6. Smooth and rough surface conical bins in the wind tunnel.	49
3-7. Wall modules for different aspect ratios.....	50
3-8. Model bin with aspect ratio of 2.5.	50
3-9. First bin grouping configuration with six model bins.	51
3-10. Second bin grouping configuration with three model bins.	51
3-11. Third bin grouping configuration with six model bins.....	52
3-12. First bin grouping configuration with six model bins.	53
3-13. Second bin grouping configuration with three model bins inline.....	53
3-14. Third bin grouping configuration with six model bins.	54
3-15. A map of the location where the full-scale tests were conducted.....	58
3-16. Full-scale grain bin.	58
3-18. The pressure tap on the sheet metal.	59
3-19. Clear tygon hose connectors from pressure sensors	60

3-20. Pressure sensor network for pressure measurements of 33 taps.....	60
3-21. Meteorological towers during the field experiment.....	65
3-22. Data acquisition hardware used for the pressure sensor data.	65
3-23. Schematics of wind tunnel and full-scale experiments.....	66
4-1. Mean velocity profile of the wind tunnel.....	73
4-2. Turbulence intensities at the wind tunnel.	74
4-3. Wall pressure coefficients of a single bin with smooth and rough wall surfaces. ...	76
4-4. Mean pressure coefficients for the 25° rough roof with an aspect ratio of 1.0.	79
4-5. Mean pressure coefficients for the 25° smooth roof with an aspect ratio of 1.0.....	80
4-6. Mean pressure coefficients for the 30° rough roof with an aspect ratio of 1.0.	81
4-7. Mean pressure coefficients for the 30° smooth roof with an aspect ratio of 1.0.....	82
4-8. Mean pressure coefficients for the 35° rough roof with an aspect ratio of 1.0.	83
4-9. Mean pressure coefficients for the 35° smooth roof with an aspect ratio of 1.0.....	84
4-10. Mean pressure coefficients for the 40° rough roof with an aspect ratio of 1.0.	85
4-11. Mean pressure coefficients for the 40° smooth roof with an aspect ratio of 1.0....	86
4-12. Comparison of the mean pressure coefficients (C_p mean) at the bottom level of the rough roof.....	87
4-13. Comparison of the mean pressure coefficients (C_p mean) at the top level of the rough roof.....	88
4-14. Mean pressure coefficients for the 25° rough roof with an aspect ratio of 1.5.	90
4-15. Mean pressure coefficients for the 25° rough roof with an aspect ratio of 2.5.	91
4-16. Wall mean pressure coefficients (C_p mean) for the first grouping with a spacing of 1/4 of the model diameter (G1-L1).....	95
4-17. Wall mean pressure coefficients (C_p mean) for the first grouping with a spacing of 1/2 of the model diameter (G1-L2).....	96
4-18. Wall mean pressure coefficients (C_p mean) for the first grouping with a spacing of 1/1 of the model diameter (G1-L3).....	97

4-20. Wall mean pressure coefficients (C_p mean) for the second grouping with a spacing of 1/10 of the model diameter (G2-L1).....	99
4-21. Wall mean pressure coefficients (C_p mean) for the second grouping with a spacing of 1/5 of the model diameter (G2-L2).....	100
4-22. Wall mean pressure coefficients (C_p mean) for the second grouping with a spacing of 1/2 of the model diameter (G2-L3).....	101
4-23. Comparison of wall mean pressure coefficients (C_p mean) at 0 degree wind direction for the second grouping (G2).....	102
4-24. Wall mean pressure coefficients (C_p mean) for the third grouping (G3).....	103
4-25. Roof mean pressure coefficients (C_p mean) for the first grouping at 0° wind direction (G1-L1, 0 degree).....	107
4-26. Roof mean pressure coefficients (C_p mean) for the first grouping at 45° wind direction (G1-L1, 45 degree).....	108
4-27. Roof mean pressure coefficients (C_p mean) for the first grouping at 90° wind direction (G1-L1, 90 degree).....	109
4-28. Roof mean pressure coefficients (C_p mean) for the first grouping at 0° wind direction (G1-L2, 0 degree).....	110
4-29. Roof mean pressure coefficients (C_p mean) for the first grouping at 45° wind direction (G1-L2, 45 degree).....	111
4-30. Roof mean pressure coefficients (C_p mean) for the first grouping at 90° wind direction (G1-L2, 90 degree).....	112
4-31. Roof mean pressure coefficients (C_p mean) for the first grouping at 0° wind direction (G1-L3, 0 degree).....	113
4-32. Roof mean pressure coefficients (C_p mean) for the first grouping at 45° wind direction (G1-L3, 45 degree).....	114
4-33. Roof mean pressure coefficients (C_p mean) for the first grouping at 90° wind direction (G1-L3, 90 degree).....	115
4-34. Roof mean pressure coefficients (C_p mean) for the second grouping at 0° wind direction (G2-L1, 0 degree).....	116
4-35. Roof mean pressure coefficients (C_p mean) for the second grouping at 45° wind direction (G2-L1, 45 degree).....	117

4-36. Roof mean pressure coefficients (C_p mean) for the second grouping at 90° wind direction (G2-L1, 90 degree).....	118
4-37. Roof mean pressure coefficients (C_p mean) for the second grouping at 0° wind direction (G2-L2, 0 degree).....	119
4-38. Roof mean pressure coefficients (C_p mean) for the second grouping at 45° wind direction (G2-L2, 45 degree).....	120
4-39. Roof mean pressure coefficients (C_p mean) for the second grouping at 90° wind direction (G2-L2, 90 degree).....	121
4-40. Roof mean pressure coefficients (C_p mean) for the second grouping at 0° wind direction (G2-L3, 0 degree).....	122
4-41. Roof mean pressure coefficients (C_p mean) for the second grouping at 45° wind direction (G2-L3, 45 degree).....	123
4-42. Roof mean pressure coefficients (C_p mean) for the second grouping at 90° wind direction (G2-L3, 90 degree).....	124
4-43. Roof mean pressure coefficients (C_p mean) for the third grouping at 0° wind direction (G3, 0 degree).	125
4-44. Roof mean pressure coefficients (C_p mean) for the third grouping at 45° wind direction (G3, 45 degree).	126
4-45. Roof mean pressure coefficients (C_p mean) for the third grouping at 90° wind direction (G3, 90 degree).	127
4-46. A sample of 15-minute wind speed data obtained under natural wind conditions at the field.	129
4-47. A sample of 15-minute wind direction data obtained under natural wind conditions at the field.	130
4-48. Mean wall pressure coefficients (C_p mean) for the full-scale bin.	133
4-49. Mean roof pressure coefficients (C_p mean) for the full-scale bin.	139
A-1. Contour plot of wind pressure coefficients (C_{pmean}) for 25° smooth roof.	149
A-2. Contour plot of wind pressure coefficients (C_{pmean}) for 25° rough roof.	149
A-3. Contour plot of wind pressure coefficients (C_{pmean}) for 30° smooth roof.	150
A-4. Contour plot of wind pressure coefficients (C_{pmean}) for 30° rough roof.	150

A-5. Contour plot of wind pressure coefficients (C_{pmean}) for 35° smooth roof.	151
A-6. Contour plot of wind pressure coefficients (C_{pmean}) for 35° rough roof.	151
A-7. Contour plot of wind pressure coefficients (C_{pmean}) for 40° smooth roof.	152
A-8. Contour plot of wind pressure coefficients (C_{pmean}) for 40° rough roof.	152
A-9. Contour plot of wind pressure coefficients (C_{pmean}) for full-scale roof.	153

Abstract of Dissertation Presented to the Graduate School
of the University of Florida in Partial Fulfillment of the
Requirements for the Degree of Doctor of Philosophy

DETERMINING PRESSURE COEFFICIENTS DUE TO
WIND LOADING ON GRAIN BINS

By

Hasan Volkan Kebeli

August 2002

Chairman: Ray A. Bucklin

Major Department: Agricultural and Biological Engineering

Wind loading is one of the factors that must be considered in structural analysis and design of grain bin structures. Structural design codes and handbooks in the U.S. only provide limited information about the local distribution of wind pressure on grain bins and conical roofs. This lack of reliable design data has contributed to wind-induced problems with these structures.

An experimental study was conducted to determine the effects of wind-induced pressures on the walls and the roofs of grain bin structures. The main objective of this research was to establish wind pressure distributions and thus pressure coefficients due to wind loading for grain bins with conical roofs. To achieve this goal, we conducted a series of wind tunnel experiments in a boundary layer wind tunnel using model grain bins with various sloped roofs and aspect ratios. The 1:60 scale model bins with variable height to diameter ratios of 1.0, 1.5, and 2.5; and four different roof configurations with

Abstract of Dissertation Presented to the Graduate School
of the University of Florida in Partial Fulfillment of the
Requirements for the Degree of Doctor of Philosophy

DETERMINING PRESSURE COEFFICIENTS DUE TO
WIND LOADING ON GRAIN BINS

By

Hasan Volkan Kebeli

August 2002

Chairman: Ray A. Bucklin

Major Department: Agricultural and Biological Engineering

Wind loading is one of the factors that must be considered in structural analysis and design of grain bin structures. Structural design codes and handbooks in the U.S. only provide limited information about the local distribution of wind pressure on grain bins and conical roofs. This lack of reliable design data has contributed to wind-induced problems with these structures.

An experimental study was conducted to determine the effects of wind-induced pressures on the walls and the roofs of grain bin structures. The main objective of this research was to establish wind pressure distributions and thus pressure coefficients due to wind loading for grain bins with conical roofs. To achieve this goal, we conducted a series of wind tunnel experiments in a boundary layer wind tunnel using model grain bins with various sloped roofs and aspect ratios. The 1:60 scale model bins with variable height to diameter ratios of 1.0, 1.5, and 2.5; and four different roof configurations with

angles of 25°, 30°, 35°, and 40° were used for pressure coefficient measurements of isolated bins in the wind tunnel. In addition, the effects of bin groupings were also investigated by running experiments with three different bin-grouping configurations. Grouping configurations were tested with a 30° roof, and a cylindrical wall with an aspect ratio of 1.0 at wind directions of 0°, 45°, and 90°. The mean pressure coefficients were calculated for each roof angle and cylindrical wall. In addition, a 4 m high and 4 m diameter full-scale bin was constructed in the field and wind pressure measurements were conducted with necessary instrumentation under natural wind flow conditions. Pressure distributions and pressure coefficients were determined based on wind speed and direction.

At the end of experiments, pressure coefficient data (C_p) were available for the walls and conical roofs of both model and full-scale bins. Contour plots of the data were drawn for each conical roof to be used as guidance tools in the design and analysis of grain bins.

Abstract of Dissertation Presented to the Graduate School
of the University of Florida in Partial Fulfillment of the
Requirements for the Degree of Doctor of Philosophy

DETERMINING PRESSURE COEFFICIENTS DUE TO
WIND LOADING ON GRAIN BINS

By

Hasan Volkan Kebeli

August 2002

Chairman: Ray A. Bucklin

Major Department: Agricultural and Biological Engineering

Wind loading is one of the factors that must be considered in structural analysis and design of grain bin structures. Structural design codes and handbooks in the U.S. only provide limited information about the local distribution of wind pressure on grain bins and conical roofs. This lack of reliable design data has contributed to wind-induced problems with these structures.

An experimental study was conducted to determine the effects of wind-induced pressures on the walls and the roofs of grain bin structures. The main objective of this research was to establish wind pressure distributions and thus pressure coefficients due to wind loading for grain bins with conical roofs. To achieve this goal, we conducted a series of wind tunnel experiments in a boundary layer wind tunnel using model grain bins with various sloped roofs and aspect ratios. The 1:60 scale model bins with variable height to diameter ratios of 1.0, 1.5, and 2.5; and four different roof configurations with

angles of 25°, 30°, 35°, and 40° were used for pressure coefficient measurements of isolated bins in the wind tunnel. In addition, the effects of bin groupings were also investigated by running experiments with three different bin-grouping configurations. Grouping configurations were tested with a 30° roof, and a cylindrical wall with an aspect ratio of 1.0 at wind directions of 0°, 45°, and 90°. The mean pressure coefficients were calculated for each roof angle and cylindrical wall. In addition, a 4 m high and 4 m diameter full-scale bin was constructed in the field and wind pressure measurements were conducted with necessary instrumentation under natural wind flow conditions. Pressure distributions and pressure coefficients were determined based on wind speed and direction.

At the end of experiments, pressure coefficient data (C_p) were available for the walls and conical roofs of both model and full-scale bins. Contour plots of the data were drawn for each conical roof to be used as guidance tools in the design and analysis of grain bins.

CHAPTER 1 INTRODUCTION

Agricultural grains are handled as bulk materials and are typically stored in thin-walled, stiffened cylindrical steel bins with conical roof systems. The roofs and walls of grain bins are usually fabricated from cold-formed corrugated or smooth steel panels. These panels are bolted together. The cylindrical shell is usually stiffened by vertical and circumferential stiffeners (wind rings). The conical roof is usually stiffened by purlins and rafters, especially in large diameter bins.

Bulk storage structures have a much higher failure rate than most other structures. The construction of an adequate, efficient storage system requires a large investment and should not be undertaken without thorough planning and a sound understanding of load conditions. Modern industry's demands for larger size bins, coupled with the need of higher rates of loading and discharge, flow improving devices, and changing storage conditions have complicated the task of structural engineers. A significant number of such bin structures suffer serious damage each year because of a variety of structural problems.

Wind loading is one of the major factors to be considered in structural analysis and design of grain bin structures. Severe wind events, such as hurricanes, create large economic losses each year along the eastern and southern coastlines of the United States. A considerable portion of the economic loss is generated by damage resulting from the failures of agricultural structures. Wind-related losses of all structures and buildings in

the U.S.A. were estimated to exceed \$3 billion annually (Mehta 1984, Reed 1987). The loss over 10 years was an estimated \$58 billion between 1985 and 1995, not including noncatastrophic windstorms and uninsured wind damage (Devlin 1997). This shows the importance of wind loads in the structural design process.

During the process of structural design of a grain bin, the first task is to determine the magnitude and the distribution of pressures caused by stored material within the structure. Grain-induced pressures are only important when the structure is loaded whereas the wind pressures become important when the structure is empty. A huge amount of work and research has been done focusing on stored material pressures and their distribution due to numerous effects. However, published work on the wind-loading design of grain bins with conical roofs is limited. Most of wind-related work has dealt with the wind loads on the shell structures. Most of the current building codes and design standards include detailed information about wind-loading provisions of rectangular shaped structures with common-type roofs. However, information is very limited for round, circular, and cylindrical shaped structures and for conical roofs (grain bins). This lack of information on the effects of wind-induced pressures on grain bins has contributed to many structural failures in the past.

The importance of understanding the effects of wind-related phenomena on grain bins has emerged recently as it has for other low-rise buildings. Most of the research on the wind load effects of these structures has focused on wind tunnel simulations. Although wind tunnel studies continue to be the workhorse for determining and defining wind loads on structures, there is a critical need for full-scale field data on wind characteristics and wind loads. The single most important use of full-scale data is

validating and comparing the results obtained from wind tunnel studies. A second role is that of an independent check of code provisions and standard requirements. The importance of comparing full-scale data and wind tunnel data should not be understated (Davenport et al. 1984). Full-scale field data are required to clarify questions applicable to full-scale situations and to validate pressure coefficients for geometrically similar models tested by different researchers. Nevertheless, additional wind tunnel model studies are needed to strengthen the building codes and standards and to append more information design engineers.

The overall goal of this research was to determine the effects of wind loads on cylindrical shaped grain bins with conical roof structures, and to develop guidelines for design. The specific objectives were as follows:

- To establish a wind tunnel test procedure and structural models for determining the effects of wind loads on grain bins.
- To plan and design a full-scaled experiment to validate the results obtained from wind tunnel model simulations.
- To find the wind pressure coefficients for isolated grain bin walls and roofs with different height to diameter ratios and roof slopes.
- To determine how pressures vary for a group of grain bins (grouping effects) compared to single bin.

CHAPTER 2 LITERATURE REVIEW

Wind Loads

When wind approaches and envelops a structure, the direction of flow is changed, and several aerodynamic phenomena occur near building surfaces. The effect of wind on a building depends on the features of the building geometry. The overall pattern of flow produces an inward-acting pressure across the windward wall, and outward-acting pressure on the leeward wall and the roof. The smooth flow of air cannot negotiate sharp angles; hence, the flow separates from some surfaces, with relatively low pressures occurring immediately downstream. Locally severe, outward pressures act on the surfaces within separation zones and are the principal forces initiating failures in many buildings (Liu 1991). The principal components of wind loads that act on buildings are as follows:

- Uplift forces. Uplift forces tend to lift the roof membrane, thus resulting in either tearing of the connection between wall and roof or between wall and foundation.
- Drag forces. Drag loads tend to overturn the structure about a point on the leeward side. It produces a shear force and an overturning moment at the foundation level.

In addition to the flow-separation phenomenon, pressure differences occur across roofs and walls when openings appear in the structure, either by design or through failure. Windward wall openings cause an increase in pressure within the building. This increase in pressure combined with the outward pressures already acting externally on the roof, the leeward wall, and the sidewalls; intensify the net, outward-acting pressures on these

surfaces. Conversely, an opening in a sidewall or leeward wall causes a decrease in pressure within the building because air is drawn out of the building. Such increases in pressure, combined with the external pressure across the windward wall, increase the net pressure on this surface. However, the decrease in internal pressure reduces the net force on the roof, sidewalls, and leeward walls.

Many researchers have worked on modeling of wind behavior and studied the parameters that affect wind pressures (Changery 1979, Cook 1993, Corotis and Jaria 1979, Davenport and Surry 1974, Davenport et al. 1977, Davenport et al. 1978, Ellingwood 1983, Gurley and Kareem 1997, Gurley et al. 1997, Iannuzzi and Spinelli 1987, Islam et al. 1990, Kareem et al. 1998, Lew and Hart 1979, Moriarty 1985, Reed 1987, Simiu et al. 1985, Solari 1988, 1989 and 1985, Stathopoulos 1984, Stathopoulos and Kozutsky 1985, Stathopoulos and Luchian 1989, Stathopoulos and Saathoff 1994, Wen 1983). The wind forces acting on a structure are dynamic and random in nature. In conventional design practices, wind loads are usually treated as quasi-static. Although this simplification has the potential to significantly advance the practice of structural engineering as far as design for wind is concerned, wind-structure-interaction phenomena exist that cannot be analyzed using quasi-static methods. For example, an array of structures produces multiple disruptions of airflow that may interfere with each other. Interference phenomena can reduce or enhance air pressure and airflow effects on structures. Initial attempts have generalized these effects as functions of building geometry, array geometry, and wind direction (Peterka and Cermak 1975). Specific geometries for specific urban area configurations are routinely analyzed in wind tunnels.

The analysis of large shell structures, such as cooling towers, under wind-loading has been widely studied by researchers (ASCE 1961, Dyrbye and Hansen 1996, Gould and Abu-Sitta 1980, Kundurpi et al. 1975, Maher 1966; Niemann 1980, Purdy et al. 1967, Prabhu et al. 1975, Rao and Ramanjaneyulu 1993, Sachs 1977, Simiu and Scanlan 1996, Singer et al. 1966, Sollenberger et al. 1980, Sollenberger and Scanlan 1974, Wang and Billington 1974). Recently, for structural engineers, the wind-loading effects on tall buildings has become the main research area of wind load effects on structures (Adrezin et al. 1996, ASCE 1987b and 1988, Balendra et al. 1989, Bogs and Peterka 1989, Bose and Datta 1994, Chan 1998, Chen 1994, Chen and Ahmadi 1992, Ellingwood 1984, Fur 1996, Jesien et al. 1993, Kareem 1985a and 1985b, Krauthammer et al. 1987, Noakowski and Gerstle 1990, Samali et al. 1985, Tallin and Ellingwood 1984 and 1985, Torkamani and Promono 1985). In the agricultural engineering field, several researchers have conducted experiments to determine wind effects on agricultural structures such as greenhouses, open-shelter roofs, livestock barns and roofs of post-frame structures (Aldrich and Weaving 1979, Aldrich and Wells 1979, Hoxey 1984, Hoxey and Richardson 1984, Mahoney et al. 1978, Mahoney 1984, Mahoney and Fryrear 1985, Mcfadden et al. 1991, Richardson 1993, Robertson and Moran 1984, Robertson et al. 1985, Srinivasan 1993). However, published work on the wind-loading design of grain bins with conical roofs is limited.

The equation that characterizes fluid flow embodies a complete statement of the energy principle, or the essential balance between kinetic energy and potential energy over every part of a streamline in steady fluid flow. This equation is known as the Bernoulli theorem (Rouse, 1938).

$$\frac{\rho V^2}{2} + p + \gamma h = \text{constant} \quad (2-1)$$

where ρ : mass density (kg/m^3),
 γ : specific weight (kN/m^3),
 V : velocity (m/sec),
 p : pressure intensity (kPa), and
 h : elevation (m).

The two most important parameters that influence airflow are viscosity and inertia. The interaction of these forces characterizes the type of flow as either laminar or turbulent. This interaction is expressed as a dimensionless parameter, known as the "Reynolds number." It is shown as

$$\text{Re} = \frac{V * L}{\nu} \quad (2-2)$$

where V : approaching wind speed (m/s),
 L : representative dimension (m), and
 ν : kinematic viscosity (m^2s^{-1}).

It is evident from the above equation that when Re is large, inertial effects predominate, when Re is small, the viscous effects are stronger.

Under certain conditions of flow, particularly flow over "bluff" bodies (bodies with a broad and flattened nose) a separation of flow from the sharp edges occurs (Davenport 1960). The point at which separation occurs is a point on that streamline that divides the oncoming flow from the reverse flow in the region of discontinuity. The region of discontinuity downstream from the flow-separation point is called the wake. The wake is characterized by energy dissipation that takes place due to the action of viscosity. It is a region with very little pressure gradient and pressure compared to those existing at the separation points. In view of the energy loss due to viscosity, it is not

possible to use the Bernoulli equation to relate pressure and velocity. The pressure at any point on a bluff body is usually expressed as a dimensionless pressure coefficient (C_p).

$$C_p = \frac{P_a - P_s}{\frac{1}{2} * \rho * V^2} \quad (2-3)$$

where P_a : actual pressure at a point(Pa),
 P_s : free stream pressure of wind flow (Pa),
 V : velocity of air at referenced height(m/sec), and
 ρ : mass density of flow (kg/m^3).

The local pressure at a point on an immovable surface in the path of a wind stream normal to the surface is given by

$$P = \frac{1}{2} * C_p * \rho * V^2 \quad (2-4)$$

where p : wind pressure (Pa)
 C_p : pressure coefficient,
 ρ : mass density of air, and
 V : velocity of air at referenced height(m/sec).

ASCE 7-98 (ASCE 1998, Mehta and Marshall 1997) gives the velocity pressure at elevation (z) as

$$q_z = 0.6134 * V^2 \quad (2-5)$$

Alternatively, the equation can be written as

$$q_z = 0.6134 * K_z * K_{zt} * V^2 * I \quad (2-6)$$

where q_z : velocity pressure evaluated at height z above ground (N/m^2),
 K_z : velocity pressure coefficient evaluated at height z ,
 K_{zt} : topographic factor,
 V : basic wind speed (m/s) corresponds at a 3-sec gust speed at 10 m height, and

I: importance factor.

The design pressure is given by

$$q_D = C_p * q_z \quad (2-7)$$

The literature contains numerous presentations of similar procedures for assessing the response of structures in strong gusty winds (Ambrose and Vergun 1994, Davenport, 1961, Hands and Clarkson 1968, Smart et al. 1967). Generalized treatment of the interaction of gusty winds with elastically responding structures leads to two response functions:

- A function in which the classic Equation (2-1) term relates drag force per unit area to the square of wind velocity (described as the "drag" term).
- A function in which the response of the structure is associated with the acceleration of the wind (described as the "acceleration" term).

The coefficient of drag C_d in the drag term can be associated with a mean wind speed value. The acceleration term is more important for winds whose speed and direction change rapidly relative to fundamental frequencies of structural vibration. Wind-field conditions in severe thunderstorms and in hurricanes may violate the assumptions of stationary wind flow that are fundamental to the formulation. In stationary flow there is no measurable fluid-structure interaction, thus the problem can be solved by traditional means of static analysis. This concern has validity in application to analysis of complete structures with small frequencies of vibration. However, most often the systems of interest for analysis are structural components (e.g., walls, wall panels, roof panels) with large frequencies of vibration. In these situations, the assumptions of stationary wind flow are valid, even in severely turbulent conditions. Principles of mechanics can be used

to define the pressure p (in psf or N/m^2) that will cause a given building or building component to fail. Then the wind speed that produces this pressure can be calculated with expressions that contain only the "drag" term as defined in many publications. The most commonly used reference by engineers was published by the American Society of Civil Engineers (ASCE 1961, 1998, and 2000), as in Equation (2-6).

Wind loads on most structures vary with the wind direction and the resistance of structures to horizontal wind force. The importance of accurate estimates of wind speed is self-evident because wind pressures are a function of the square of the wind speed. Therefore, the modification of wind speeds for use in design has a nonlinear influence on design loads (Lew and Hart 1979). The effect of wind direction is obviously an important factor for consideration in wind-loading response of structures. When the wind direction has to be considered, the use of annual maximum wind speed in the reliability analysis becomes questionable. The annual maximum wind may come from a direction that may cause less severe effect than a wind of a lower intensity. However, it may come from a direction that the structure is most vulnerable. In practice, a commonly used procedure is to assume that the wind comes from a direction that would cause the most critical effects in the structure. This can be called the worst direction assumption. Wen (1983) conducted a study to investigate the applicability of theoretical prediction of long-term effects based on short-term data. He calculated the wind speed, direction statistics, and power spectra. The probabilities of annual maximum response of structures with various orientations were evaluated both from theory and directly from data. The analytical method based on short-term data was found to correctly predict the mean values of the annual maximum response. In addition, it correctly identified the most unfavorable orientation of the

structure and gave reliable estimates of the sensitivity of structural response to change in orientation. The width of the direction trace produced by a standard anemograph raises considerable uncertainty as to the appropriate direction for given large gusts, and a consequent uncertainty about the expected extreme gusts calculated for particular sectors. Further uncertainty is added when the calculated expected extreme gusts are applied to a wide area around the observing site (Moriarty 1985). Reed (1987) categorized the field parameters involved in wind engineering that influence the reliability of conditions as meteorological, structural, or aerodynamic in nature. Parameters in each field were identified, along with distributions and associated levels of uncertainty provided by research in the field. Griffis (1993) suggested that the two most influential parameters in the context of structural reliability under wind-loading were the structural damping ratio and the description of the fluctuating component of the wind.

A structure will not respond fully to the impact of a gust that is only a small fraction of the structure's size. A gust, to be fully effective, must have sufficient spatial extent to envelop both the structure itself and the flow patterns on the windward and leeward sides. These two flow patterns are responsible for the maximum loads on the structure. A correlation function could be defined which accounts for the fact that wind gusts are unlikely to act simultaneously over the full extent of the structure (Vellozzi et al. 1968). The gust correlation function could vary from unity for completely correlated flow to zero for uncorrelated flow. Wind loads on a structure can be derived from a mean wind speed plus the effects of a fluctuating wind speed. The response of the structure depends on the mean wind speed, the correlation between gust size and structure size, and the correlation between gust frequencies and structural frequencies of vibrations.

Definitions or determinations of wind speed have major implications in the determination of wind-loadings. The same wind record would provide different wind speeds depending on the averaging time interval used. National standards around the world use different definitions of wind speed. For example, the National Building Code of Canada (NRCC 1990 and 1990a) uses mean hourly wind speed, the American National Standard ASCE 7-98 (2000) use 3-second gust speed, and the British (BSI 1972) and Australian (SAA 1989) Standards use 2-second gust speeds.

Several major codes and standards permit or encourage the use of a wind tunnel, especially when structures are of unusual shape or character. In instances where the geometry of the structure is such that the code-specified wind load provisions are not applicable, the conduction of a wind tunnel analysis should be considered (Chiu and Perry 1997). There are two basic types of wind tunnels; aeronautical and boundary layer. Wind tunnels for aeronautical purposes developed rapidly during the first half of the twentieth century, especially during the two World Wars. The main development period for wind tunnels to study wind effects on ground-based structures has been within the last 35 to 40 years and resulted in the emergence of the boundary layer wind tunnel in its various forms. Up to the end of the 1950s, all model tests for wind-loading of ground-based structures were carried out in smooth flow aeronautical wind tunnels. About this time, Jensen and Franck (1965) in Denmark illustrated the importance of carrying out tests in a turbulent boundary layer representative of the atmospheric boundary layer. Davenport (1960 and 1961) has pioneered in the application of boundary layer wind tunnels to the design of wind sensitive structures, the description of urban wind climates and other problems involving the action of wind. He founded a boundary wind tunnel laboratory

and conducted many experiments with the boundary layer wind tunnel at The University of Western Ontario (Davenport and Isyumov 1968, Davenport and Surry 1974). The results of his wind tunnel studies were referenced in many publications including ASCE-7. Natural growth methods of boundary-layer development require test sections of length greater than ten times the height of the tunnel. Mean velocity and turbulence profiles similar to those existing in the atmosphere can be simulated. Coriolis forces generated by the earth's rotation cannot be modeled, and the Ekman spiral effect caused by ground resistance to the Coriolis force cannot be reproduced. However, these are the natural events that produce extreme wind effects, and in wind tunnel simulations, are not necessary to replicate. In Australia, the trend has been to use fetch lengths of six to eight times the tunnel height. Turbulence producers such as tapered spires are often used at the start of the test section to produce extra turbulence and to stimulate boundary layer growth in a relatively short test section. For modeling flow around low-rise structures at scales of 1/150 or 1/100, it has been found that plain fences at the start of the test section are able to provide the large turbulence scales, as well as turbulence intensities required. In Britain, attempts have been made to use even shorter fetch lengths, four to five times the test section height, with auxiliary devices such as vortex generators, fences and screens. Although these methods have produced apparently satisfactory flows at the test section, they are likely to be non-equilibrium boundary-layer flows. This type of flow may produce incorrect results in some types of tests in which the downstream length of the model is large. In the U.S., universities such as Colorado State University, Clemson University, Texas Tech University, and Notre Dame University have wind tunnels in

which simulated atmospheric boundary layer tests can be conducted and the wind data can be analyzed.

A number of full-scale field investigations measured wind pressures on low-rise buildings. All but one of the buildings involved were specifically built or set aside for use in wind tunnel studies. The one exception was a training and education center where the focus was on wind resistance. The monitoring system was seen as part of the project. During the 1970's, the National Bureau of Standards (now called as the National Institute of Standards and Technology) conducted several field studies to measure wind loads in low-rise buildings. These studies included building an instrumented house in Montana (Marshall 1973), two houses in the Philippines (Marshall et al. 1976), and a mobile home at the Gaithersburg Campus of the National Bureau of Standards (Marshall 1977). In the early 1980's, a full-scale two-story house was constructed at Aylesbury, England to determine wind-induced pressures (Vickery 1984). Texas Tech University began collecting full-scale wind speed and wind pressure data at their Wind Engineering Research Field Laboratory (WERFL) located in Lubbock, Texas more than a decade ago. The WERFL includes a 50-m tall micrometeorological tower with instruments placed at six height levels and a flat-floor building with 100 pressure taps mounted on the roof and the walls of the building. The building can be rotated 360° for changing azimuth angles. (Levitan and Mehta 1991a and 1991b, Tielman et al. 1993). To improve construction practices in Southern Shores, North Carolina, the town initiated a project. This project included the construction of the Kern Center, which is intended to serve as an educational center for high-wind construction techniques. The center was instrumented by John Hopkins University to measure wind-induced pressures and wind characteristics

(Porterfield and Jones 1997). This system included 13 sensors permanently installed on the second floor of the building. The Silsoe Research Institute (SRI) in Bedford, UK is well known for years of research concerning wind loads on full-scale buildings. Field studies being conducted at the SRI are designed to provide data on wind pressure distributions over the building surfaces and wind patterns around the structures. The cube-shape structure can be rotated 360° , and can be lifted on an edge to a slope of 5° . Differential pressure transducers are housed inside the test building and measure data from taps drilled through the wall and roof surfaces (Hoxey and Richardson 1984; Michot 1999).

Extensive examinations of wind-induced building failures from around the world support the following general observations. The overall wind effects tend to push windward walls in, pull sidewalls out, and lift roofs. Local wind effects tend to break windows at building corners, lift roofs at eaves and roof corners, and peel roofs at ridge lines downwind from separation points. Wind forces may affect the stability of empty bins—both single bins and bin groups; particularly those made from steel. In many cases, wind-loading of the empty bin is an important consideration. Common failure modes are buckling of the windward wall under positive wind pressure, overturning failure, anchorage failure, and loss of roof. The more common and less disastrous damage is local buckling on the windward wall, which has been found on many grain storage structures. Large numbers of grain storage bins have been designed and constructed with either little or unreliable data on the design for wind effects. Structural design codes and handbooks in the U.S. do not have adequate information on the local distribution of wind pressure on

grain bins and conical roofs. This lack of reliable design data has contributed to a number of wind-induced failures of these structures.

Wind Loads on Shell Structures

For circular cylinders, the boundary layer is laminar; and flow separation occurs upstream of the point of lowest pressure at low values of Reynolds number ($40 < Re < 10^5$) (Macdonald 1975). This phenomenon causes a large wake with correspondingly large drag coefficients. Wake vortices are shed alternatively from either side of the cylinder, causing a fluctuation in the point of separation. This produces a fluctuating lateral force that can cause a cylinder to vibrate across the flow stream.

Gopalacharyulu and Johns (1979) investigated the problem of a cantilever cylindrical shell subjected to an assumed wind pressure distribution by using Donnell's shell theory. Billington (1982) compared the results of a linear finite element analysis with those obtained with the membrane theory for cylindrical, conical, and hyperbolic shells under wind-loading. He reported that the behavior of very thin wall structures was predicted by membrane theory reasonably well, while the behavior of thick concrete structures approached that of a cantilever beam. However, most of these shells in use have dimensions such that they fall under long cylindrical shell category (height/diameter ≥ 3) while grain bins are usually built with aspect ratios ranging from 0.5 to 1.5. Such long cylindrical shells can be analyzed using Schorer's theory (Chandrashekhara 1989). Chandrashekhara found stress resultants and displacement results based on Schorer's theory very similar to those found by Gopalacharyulu and Johns (1979).

In contrast to beams, the response of thin-walled axisymmetric structures to wind-loading is not only a function of the resultant base shear and overturning moment, but

also sensitive to the distribution of the forces around the circumference. For the flow pattern past a cylinder, three independent strips may be considered:

- A vertical strip at a given circumferential angle
- A circumferential strip in the frontal region
- A circumferential strip in the wake region (Gould and Abu-Sitta 1980)

There is no correlation between the frontal and wake regions, and quadrature spectra are negligible. Also cross-correlations and cross-spectra are independent of location, except along the front circumferential strips. The pressure distribution and the subsequent response of cylindrical structures are very sensitive to the boundary of the frontal and wake regions as characterized by the angle of flow separation which is strongly dependent on the Reynolds number. In addition, the roughness of the surface is important in this regard.

Holroyd (1983, 1985a, and 1985b) conducted experiments to take measurements of pressure distributions on the surfaces of open-top oil storage tanks in a 1/250 scale atmospheric boundary wind tunnel. He presented the mean, rms, and spectral components of the pressure distribution over the surface of the cylindrical shape tank. He concluded that the changes in structure itself and in the structure of the incident air flow affect both air flow and pressure distribution near the tank. In addition, he included derived calculations and results on flow-induced vibrations in circular cylindrical structures. It was suggested that the vibration induced by the turbulence in the air stream played the significant role in initiating the collapse of open-topped oils storage tanks in high speed wind events.

Jerath and Sadid (1985) investigated the stability of cylindrical shells made of corrugated steel under the action of wind loads. The shells were analyzed by considering the material orthotropic and by using the principle of minimum potential energy in conjunction with Ritz's approach given in Almroth (1962). The buckling loads and the buckling configurations were obtained for short cylinders made of corrugated steel sheets subjected to wind pressure. The study was made on cylindrical shells of various dimensions, which were simply supported at the base and open or closed at the top. Buckling load curves for these shells were given for different length-to-radius and radius-to-thickness ratios. They concluded that the external lateral pressure causing buckling was greater for closed cylinders than open ones for short cylinders having length-to-radius ratios less than one.

Uematsu and Uchiyama (1985) conducted a series of wind tunnel tests to determine the wind pressure distribution on the shell surface and to determine the buckling behavior of cylindrical shells. Wind tunnel tests were performed in a wind tunnel (6.5 m long and 1.4 m wide) with a smooth flow. Flexible cylindrical shell models were constructed from polyester film, and were tested inside the wind tunnel. Their results indicated that buckling occurred in shorter shells, which they did not expect to happen. For the longer ones, the pre-buckling deflection and amplitude became quite large.

Pecknold (1989) described load-transfer mechanisms in wind-loaded cylindrical shells, and interpreted them using a simple analytical model. His model generalized the well-known beam-on-elastic foundation analogy to higher load harmonics ($n > 1$), useful for axisymmetric pressure loading cases. His model provided an easily visualized model of

Vlasov's semi membrane theory, accurately replicated the most important bending effects in closed thin-walled cylinders, and explained very long lengths of edge loading in an intuitively appealing way. He suggested that the slowly decaying bending solution of his model could be considered as an improved membrane theory, which automatically transitioned to ring bending when the height-to-diameter ratio or the load-harmonic ratio was large. This transition from membrane action to ring-bending behavior was primarily responsible for the moderating influence of shell bending on the membrane stresses in wind-loaded cylinders. A single shell parameter $L/a \sqrt{h/a}$ (where L is height of cylinder, and a is radius of cylinder, and h : wall thickness), which can be regarded as the length of the shell relative to the effective decay length of edge disturbances, fully described the behavior of wind-loaded cylinders according to his theory. For the wind load distribution based on ASCE 7-88 (ASCE 1988), a fixed-free cylinder responded for $L/a \sqrt{h/a}$ less than about 0.1, and the membrane theory overestimated the axial membrane stress at the base by a factor of 3 when $L/a \sqrt{h/a}$ was equal to 1.0.

With increase in the height of cylindrical steel structures, resistance to dynamic forces such as earthquakes and wind loads becomes critical. Such structures, if flexible and lightly damped, may exhibit large deflections or unstable oscillations due to wind-loading. When two flexible cylinders are put in tandem in line with the wind flow direction, the rear cylinder may vibrate with either larger or smaller deflection than a single cylinder. When two cylinders are placed in tandem with the flow direction, the rear one is subjected to two kinds of forces:

- Its own vortex stream
- The buffering force from the wake of the upstream cylinder

The phase angle between two forces and the amplitude of the rear cylinder's motion are dependent on the relative position of two cylinders. Bishop and Hassan (1964) found from their test results that the lift force was increased with the amplitude of cylinder motion. They also concluded that the fluctuating lift force acting on the cylinder is a self-excited oscillatory mechanism in the flow field. One of the most successful mathematical models was introduced by Hartlen and Currie (1970). They assumed that the oscillating lift force on the cylinder could be represented by an equation in the form of the van der Pol equation. When this equation was coupled to the equation of motion of a cylinder and the parameters appearing in the model were approximately chosen, the observed behavior was qualitatively reproduced. Skop and Griffin (1975) formulated a model to predict the vortex-excited resonant response of bluff elastic cylinders. Their results were in good agreement with the experimental data. Zdravkovich (1985) observed the flow-induced oscillations of two elastic circular cylinders and concluded that the resulting oscillations induced by vortex shedding were considerably modified by, and strongly dependent on the arrangement of two cylinders. According to Zdravkovich, the maximum amplitude of vibration of the rear cylinder was around the spacing ratio of 4.7 when two cylinders were in line with the wind direction. Shiau and Yang (1987) developed a model based on this equation for predicting the vortex-excited resonant response of two cylinders in line with the wind direction. Their mathematical model relied on experimental results for the determination of introduced constants. They used the modified Van der Pol equation to account for the effect of fluctuating lift force on the cylinder, and this equation was coupled with that for oscillatory motion of the cylinder. They concluded that their mathematical model successfully predicted the motion of an

elastically mounted cylinder in the wake of another cylinder. Shiau (1989) developed a semi empirical mathematical model to predict the vortex-excited resonant response of two flexible cylindrical structures in line with wind direction. He concluded that the model could be used to predict the motion of a cantilevered cylinder in the wake of another cylinder.

Wind Loads on Grain Bins

Most of the studies conducted on cylindrical shell structures dealt with unstiffened cantilevered shells with open tops or with flat roofs. However, typical grain bins are much more complicated structures. The roof and walls of steel grain bins are bolted together. The cylindrical shell is usually stiffened by vertical and circumferential stiffeners. Cylindrical storage structures gain storage capacity by the use of roof slopes that range from 25° to 30° because grain piles in a cone with a slope of 25° to 30° . Therefore, it is a widely used practice to design grain storage bins with a conical roof. The conical roof is usually stiffened by purlins and rafters, especially in large diameter grain bins. In addition, the spatial variation of the wind pressure results in a distribution of forces in the structure, which is very different from that produced by uniform loading. Such a complicated structural system under non-uniform wind-loading behaves neither as a cantilever beam, nor according to membrane theory. Rather, an interactive mechanism is developed between the shell and the stiffeners to resist wind loads (Blackacker 1983). The conical roof of the bin is also an interesting structural system whose behavior under wind-loading has not been adequately described in the literature. The roof system is subjected to suction due to the wind, and is loaded at eave level by circumferentially nonuniform edge forces due to the wind-loading on the bin walls.

Wickstrom (1980) suggested that the wind pressures act perpendicular to the surface, so wind forces would act similarly on cones to the way they act on curved roofs. He also suggested that the ASAE Standard 288.3 (ASAE 1980) was the most accurate source for calculating wind loads on grain bin roofs in spite of the fact that it gave the most conservative results for grain bins.

Gaylord and Gaylord (1984) suggested wind pressure coefficients for cylindrical shape grain bins as 1.2 for diameter to square root of velocity pressure ratio smaller than 2.5 ($d/\sqrt{q} < 2.5$), and 0.8 for $d/\sqrt{q} > 2.5$. They also suggested pressure ratios for moderately smooth round bins with height to diameter ratios 1 and 7 as 0.5 and 0.7. To determine the wind loads on circular cylindrical bins during construction and in service, a number of wind-tunnel tests were performed by Esslinger et al. (given in Gaylord and Gaylord 1984) on cylinders. One of the cylindrical bins was 570 mm in diameter and 420 mm in height, and the other one was 570 mm in diameter and 840 mm in height. Pressures were determined for three conditions: open top, roof with inlet open, and roof with the inlet closed. The maximum resultant pressure on the windward surface of an open bin was about double the pressure on a bin with a roof. The difference was due to the internal suction in an open bin, which was numerically additive to the pressure on the outer surface. Furthermore, the pressure on an open bin was compressive on the windward as well as on the leeward surface, while the pressures on a bin with a roof were compressive on the windward surface and suction on the leeward surface. This suggested that an open bin was likely to be more susceptible to buckling than the one with a closed roof. The pressures on an empty bin with an open inlet on the roof were approximately intermediate between the pressures on an open bin and one with the roof inlet closed.

Esslinger et al. also made wind-tunnel tests on the two cylinders, 570 mm in diameter and 840 mm height, in a line with wind direction. They were placed 86 mm apart from each other. Maximum pressures on the windward side were about 30% larger in windward direction and 50% larger in leeward direction than the corresponding pressures for the single bin, and the differential wind pressure coefficient for two bins was about -2.5 compared to about -2 for a single bin.

Kurth (1985) analyzed the wind-loading on the three-dimensional structural system of the Eurosilos framework. Eurosilos are high-capacity silos, ranging from $10,000 \text{ m}^3$ to $100,000 \text{ m}^3$ storage capacity and capable of operating at filling and emptying rates of 500 to $2,500 \text{ m}^3/\text{h}$. Eurosilos consist of an inner and of an outer part. The inner part comprises a light internal wall, which is usually made of corrugated steel sheets and horizontal ring girders. The columns and the steel frame belong to the outer part of silo. The wind load analyses for the structural systems of Eurosilos are normally based on approximations. Kurth calculated wind pressures and loads on the structure based on DIN 1055 (DIN 1987). In the horizontal section of the silo, wind loads were assumed to be radial and tangential forces, and in the vertical section, the load application points were spaced at distances of $1/8$ of height. The structural analysis calculations were performed on a computer by using a finite element modeling software package, and results were given for varying dimensions of columns and different types of frames for Eurosilos.

When the bin is empty, external pressures due to wind-loading induce small hoop compressions in the cylindrical wall. These stresses are very small, but if the wall is only slightly curved (R/t is large), the wall will be sensitive to buckling failure. The variation of pressure around the bin circumference is an important factor in design for wind-

loading. The front half of bin wall generally carries almost all of the horizontal force caused by wind. The maximum vertical compressive force in the wall develops at about 70° from the windward direction (Greiner 1988). This is an important factor in design of connection bolts and wind stiffener rings. The wind pressure around an isolated grain bin structure depends on many parameters that highly affect the pressure ratio and suction force components around the circumference. Those parameters are:

- Reynolds number and wind flow
- The surface properties of the wall
- Aspect ratio of the bin structure (H/D)
- The position of the cylindrical structure to the ground level
- Terrain where the structure will be constructed
- The shape and the configuration of the roof
- The size of the openings in the roof

Briassoulis and Pecknold (1986a) conducted a finite element analysis to find the anchorage requirements of empty bins under wind-loading for three type bins defined as tall, intermediate, and shallow with height to diameter ratios of 2.40, 0.92, 0.49; respectively. The wind-loading pattern with no internal pressure was applied on the cylindrical wall, along with an approximate pattern of wind-loading proposed for a conical roof system. Their analysis indicated that the axial tensile forces were dominant in the tall bin case, while the shear force controlled anchorage requirements in the shallow bin. A cantilever beam approach resulted in unsafe predicted anchorage requirements, while a membrane theory solution for wind loaded cylinder yielded rather conservative

results. They concluded that the anchorage requirements for all three types of bins could be predicted with a good accuracy by using membrane theory reduced by a factor depending on the height to diameter ratio of the cylinder. The relative importance of the roof load increased dramatically with the decrease of the height to diameter ratio.

Briassoulis and Pecknold (1986b) used a Finite Element Modeling (FEM) analysis of three stiffened steel bins under non-uniform wind-loading. They used three different steel bin geometries, representing tall, intermediate, and shallow bins. In their paper, buckling and material failure effects were not considered. The major behavioral characteristics that they found from their FEM analysis were as follows:

- The downwind deflection at eave levels was negligible for all three-bin structures.
- The system of vertical stiffeners was the basic mechanism for resisting to overturning moments in the tall bin. However, in the shallow structure, the contribution of the cylindrical shell wall was as important as the vertical stiffeners.
- The wind rings in the tall bin developed axial forces and circumferential moments in an attempt to withstand large flexural requirements over a stiff region. This caused the development of severe hoop stresses distributed near the wind rings. These large hoop stresses likely resulted from composite like action between bin wall and wind ring.
- In large diameter bins, the large upward forces on the roof resulted in development of very high compressive hoop stresses in the upper portion of the cylindrical wall.
- The larger portion of vertical moment distribution developed at the top and the base of the vertical stiffeners in the tall bin. The distribution of moments was significantly smaller in intermediate and shallow bin.
- The circumferential bending moments developed in the cylindrical shell were not large, but their contribution to the hoop stress concentrations in the corrugated shell in the region of the wind rings was significant in the tall bin structures.
- In the tall, small diameter bin, the non-uniform wind pressure on the bin wall played a major role in the structure's behavior. In shallow, large diameter bins, the upward wind load on the roof was of primary importance.

Briassoulis and Pecknold (1988) carried out detailed linear elastic finite element analyses of three typical stiffened steel bins to aid in development of simple conceptual models to describe behavior of empty bins under wind-loading. The wind-loading on the bin wall was simulated according to ANSI A58.1 (1982). Details of the wind-loading simulation were given in Briassoulis (1985). Three typical steel bin structures were selected with different height to diameter ratios as a tall (72/30), intermediate (66/72) and a shallow bin (51/105). They concluded that the wind load behavior of stiffened steel bins in the linear elastic range was sensitive to bin geometry. The stiffened and unstiffened roof systems behave quite differently under wind-loading pressure on the roof and edge disturbances arising from interaction with the upper part of cylinder. Their results can be summarized as follows:

- The moments developed in the unstiffened roof shell of the tall bin were much higher near the center collar than in the other parts of shell structure.
- The center collar of unstiffened roof systems was under high tensile axial forces and high positive bending moments due to wind-loading. In the stiffened roof systems, the axial forces varied circumferentially from compression to tension. The bending moments in the stiffened systems depended on the details of connection and were not significant.
- The purlins were under high tensile forces depending on the diameter of the structure and the stiffeners of roof.
- The rings (plates) at the eaves could be under very high compressive axial forces due to composite action with the adjacent parts of the shell, especially in large diameter bin structures.
- They found very large moments and axial forces in the lower part of the rafters, near the junction with the wall.

Sabransky and Melbourne (1987) carried out tests on grain bins with roof slopes of 15° , 27° , and 45° and aspect ratios of 0.66, 0.78, and 1.16 by using a turbulent

boundary layer wind tunnel. They assumed an approaching terrain of open country and a geometric scale of 1/125. They used Reynolds numbers from 1.5×10^5 to 3×10^5 , and a group of three bins for grouping effects. They measured mean, standard deviation, and peak pressures at a reference point at eave height. Their work was limited by a wide angular spacing of 22.5° between measurement points, which limited the ability to determine the peaks in the mean pressure distribution. They reported mean roof pressure coefficients ranging from -0.3 to -1.7. Detailed results of the pressure coefficients of conical roofs were given in their published paper. It was found that a significant increase in rms pressure values occurred at the point of closest spacing between bins. A large mean suction of about -2.5 was observed on the side of the center bin at a wind direction of 22.5° to the normal of the line of the bins.

Macdonald et al. (1988) conducted a series of tests to determine circumferential wall pressure and roof pressure distributions caused by wind loads on circular grain bins. Wind tunnel tests were conducted in a 2.13×1.52 m closed-loop concrete wind tunnel that was capable of producing wind speeds up to 35 m/s in the 2.25 m long section. They used an augmented method combined with triangular spires and roughness elements to simulate the boundary layer flow for model conditions. They controlled their model's mean wind velocity profiles, turbulence intensity profiles, Reynolds stress profiles, and turbulence length scale and spectrum at a reasonable level. Model bin structures were constructed from a number of cylindrical modules of 200 mm external diameter and various heights. The modules were manufactured from 5mm thick clear acrylic tube and the ends of modules interconnected to form a continuous outer surface. Two of the segments (each 25mm in length) were fitted with pressure taps circumferentially spaced

at 7.2°. Sufficient untapped modules were constructed to enable the use of different bin heights of 100, 200, and 400 mm. A flat roof without pressure taps and two conical roofs with 25° slope with 50 pressure taps were manufactured. They conducted series of tests with nine different configurations of model bins that included three aspect ratios ($H/D = 0.5, 1, \text{ and } 2$), and three roof configurations (open top, flat roof, and a conical roof with 25° slope) in the wind tunnel. Internal pressures were measured for open top models, and the effects of Reynolds number of the flow and the height of pressure were also determined. They presented the pressure measurement results as mean, standard deviation, maximum and minimum defined with respect to mean wind velocity at wall height. Their conclusions could be summarized as:

- In turbulent boundary layer flow where the turbulence intensity was high, the wall pressure distributions were independent of Reynolds number.
- Maximum mean pressures occurred at 60-90% of the height of the bin. The mean pressures decreased significantly below 50% of the height.
- Increasing the aspect ratio increased the magnitude of mean suction at wall from 1.0 at an aspect ratio of 0.5:1 to mean suction of 1.8 at a ratio of 2:1.
- The mean roof pressure distributions showed high suctions occurring near the leading edge, and near the conical apex of roof.
- Although their mean wall and roof pressures were in a reasonable agreement with other full scale and model studies, the standard deviation pressures were lower.

Macdonald et al. (1990a) conducted experiments to determine the effects of a grouping of grain bins arranged in an in-line group of five. The models used for group bin studies were manufactured from 100 mm diameter acrylic tubing. Two of 13mm length segments were fitted with pressure taps. A group of five model bins was placed on a 3mm thick steel strip. For grouping effects, nine different types of grouping configurations with

spacing to diameter ratios ranging from 1/8 to 3 were tested. Wind tunnel, simulation parameters, and test methods were similar to those described in Macdonald et al. (1988). Their results indicated that the contributions of mean and rms pressures on a bin within an in-line group depended upon the spacing between the individual bins, the wind direction, and the position within the group. At small spacing, the positive circumferential pressure showed a significantly larger factor than an isolated bin. For the central model bin in a group, a wind direction of 20° to the normal to the line of bins produced a high negative pressure zone on the windward direction. At wind directions parallel to the line of bins, the windward end bin faced similar positive pressures but lower magnitude negative mean pressures compared to the isolated bin configuration. They observed higher rms pressures near the point of shortest distance to the adjacent bins at wind directions near normal to the line of bins. The rms pressures were relatively uniform around the circumference of structure at wind directions both parallel and oblique to the line of bins.

Macdonald et al. (1990b) developed spatial distributions of the fluctuating and peak pressures by using eigenvector analysis and coincident peak sampling methods. Pressures from pairs of panels on the bin walls were sampled and joint or two-point statistics of the fluctuating pressures derived. Detailed experimental techniques and material used can be found in Macdonald et al. (1988). With the eigenvector analysis, the upwind turbulence accounted for more than 70% of the pressure fluctuations on isolated grain bin structures. They found that the grouping of the bins in a row of five produced a reduction in the proportion of fluctuating pressure due to upwind turbulence as the spacing increased. Coincident peak analysis resulted in pseudo-instantaneous peak

pressure distributions which were believed more realistic than the traditional quasi-steady peak pressure distributions. Quasi-steady pressure distributions were unconservative for buckling loads because they gave too small angular sectors of positive pressure. However, they gave conservative drag coefficients which were attributed to very high suctions on the leeward side.

Harmon et al. (1992) conducted a tour covering four counties in the states of North Carolina and South Carolina after the Hurricane Hugo hit the region to evaluate the failures that occurred in agricultural structures. They observed 15 grain bins and 50 other agricultural structures during that time period. They found four overturned hopper-bottom bins caused by improper anchorage. These bins were mounted to a concrete pad using 7.6 cm lag screws with lead anchors. It was reported that one group of 3.6 m diameter grain bins was destroyed with the metal deposited about 800 m from the site. These bins were merely set down over the outside of the concrete slab with little visible means of anchorage. At another site, a 9.1 m diameter bin, which was on the windward side of a group of bins, blew from its foundation. Anchorage consisted of four 8.9cm lag screws with lead anchors. This bin impacted another bin, loosening it from its foundation. All of these hopper-bottom bins and grain bins were empty during the hurricane. They found a grain bin that was 11m in diameter with a capacity of 780 m^3 containing 280 m^3 corn at the time of hurricane Hugo. The anchors on this bin were extracted and the bin was bent at the grain level. The roof of the bin detached, with many fasteners pulling through the metal. They also reported two concrete stave bin failures; however, the reason of the failure was attributed to a material strength problem. They concluded that only one out of

15 bins that they observed had not failed during hurricane Hugo. It should be noted that Hurricane Hugo had peak wind gusts of 48.7 m/s at that region.

Grossman (1993) addressed the problem of not having a standard in the U.S. that gives detailed information on wind load distribution on the conical roof of grain bins. He also suggested that the Australian code could not be directly applied in the U.S. because of the complexity and difficulty of the Australian code for design engineers in practical applications.

Kebeli and Bucklin (1999) reviewed the causes to wind-loading related failures of grain bin structures. They also discussed the results of failures and failure modes due to excessive wind pressures on grain bins. Kebeli et al. (2001a and 2001b) presented pressure coefficients for conical roofs of grain bins obtained from a boundary layer wind tunnel study. These data included conical roofs with slopes of 25°, 30°, 35°, and 40° with rough and smooth surfaces. The wind pressure coefficient data for conical roofs will also be presented in this dissertation as a part of results section.

Andrade et al. (2001) presented a paper including a detailed review of current literature for the structural behavior of grain bins under wind-induced loads. They reviewed and discussed the problems regarding to mechanics of the structures, shell elastic behavior, numerical analysis of grain bins under the assumption of quasi-static wind-loading, wind tunnel tests with bin models, and general wind engineering parameters. They indicated that they would conduct further experiments to study the buckling behavior of empty bins under wind-loading.

Wind Load Requirements for Grain Bins in Building Codes and Standards

In the United States, the federal government does not adopt codes building codes for cities and states. Therefore, cities, counties, and some states have their own codes. It has been estimated that there are nearly 5000 different building codes in the U.S. However, most of these codes are the variations of International Building Code (IBC), Uniform Building Code, Standard Building Code, and Basic Building Code; four major codes. In addition to building codes, there are also standards for general design loads on buildings and structures. Most of the current building codes and design standards include detailed information about the wind-loading provisions on rectangular shape structures with common type roofs. However, loading guidance is very limited for round, circular, and cylindrical shape structures and for conical roofs (grain bins). A brief summary of the wind-loading provisions on the round shaped structures in major building codes and design standards follows.

The ANSI A.58 Standard (ANSI 1982) covered all types of loads including wind loads. The procedure for wind load calculation was very similar to that of today's version (ASCE 7-98 1998). However, ANSI A.58 Standard gave very limited information about the pressure coefficients on round shape structures. It gave only four pressure coefficients based on surface type and aspect ratio as shown in Table 2-1.

The ASCE 7-98 (ASCE 1998) and previous versions (starting with ASCE 7-88) are based on ANSI A.58 with slight changes over the years. The most significant change starting with ASCE 7-95 is the use of 3-second gust speed instead of fastest-mile wind speed. ASCE 7-93, 95 and 98 Standards do not have any information for cylindrical structures with conical roofs. However, they cover round structures briefly and give force

coefficients for tanks, chimneys, and similar structures based on cross-section shape (square, hexagonal or octagonal, round) and h/d ratios in a table (Table 6-7 in ASCE 7-98). However, it should be noted that these values are obtained from the wind tunnel studies in Australia conducted by Macdonald et al. (1988). A summary table (Table 2-2) that shows the pressure coefficients (C_p) for only round structures is given below.

The ASAE EP288.5 (ASAE Standards 1998) gave pressure coefficients on bins or tanks having height to diameter ratios smaller than five based on wind direction angle. However, it gave only one case and it was very limited. There was no information about the pressure coefficients of grain bins with conical roofs in the standard. It should also be noted that these values were referenced from ASCE 7-88 (ASCE 1988).

The ACI 318.83 (1986) refers to ANSI A.58.1 for wind load provisions while the newest version of the standard (ACI 318.99 1999) suggests using general building codes for load calculations. No specific information is available for wind-loading on circular structures.

The Uniform Building Code (1982, 1991 and 2000) gives multiplying factors for chimneys and tanks that are factors by which the pressure coefficient for a rectangular building must be multiplied to obtain the pressure coefficient for a round shape structure. In the Uniform Building Code, wind pressures are obtained using the following general equation:

$$p = C_e * C_q * q_s * I \quad (2-8)$$

where C_e : height, exposure, and gust factor coefficient,
 C_q : pressure coefficient for structure or a portion of it,
 q_s : dynamic wind pressure equal to $0.6134V^2$, and
 I : importance factor (not the same I as in ASCE 7).

Table 2-1. Pressure coefficients for round structures given by ANSI A.58 (1982).

Type of surface	H/D=1	H/D=7
Smooth	0.5	0.6
Rough ($D'/D \geq 0,02$)	0.7	0.8

Where H: height of the structure (m),

D: diameter of the circular cross section (m), and

D': depth of protruding elements such as ribs and spoilers (m).

Table 2-2. Pressure coefficients for chimneys, tanks and similar structures ASCE7-98 (1998).

Cross section	Type of surface	H/D=1	H/D=7	H/D=25
Round ($D \cdot q_z^{(1/2)} > 2.5$)	Smooth	0.5	0.6	0.7
	Rough ($D'/D \geq 0,02$)	0.7	0.8	0.9
	Very rough ($D'/D \geq 0,08$)	0.8	1.0	1.2
Round ($D \cdot q_z^{(1/2)} \leq 2.5$)	All	0.7	0.8	1.2

Where D: diameter of circular cross section (m),

q_z : velocity pressure (N/m^2), and

H: height of structure (m).

The wind load provisions of BOCA-87 were a drastic revision of BOCA-84. It is based on ANSI A58 (1982). The BOCA-93 National Building Code (1993) refers mostly to ASCE-7 for wind-loading calculations. A table for the force coefficients of chimneys, tanks and similar structures is available with the same coefficient values given in ASCE-7 (ASCE 2000). In the National Building Code, wind pressures for main wind force resisting systems are obtained using the following general equation.

$$P = P_v I [K_z G_h C_p - K_h (GC_{pi})] \quad (2-9)$$

where P_v : basic velocity pressure,

I : wind load importance factor (not the same I as in ASCE 7),

K_z : velocity pressure exposure coefficient, at height of interest (z),

G_h : gust response factor evaluated at height (h),

C_p : external pressure coefficient,

K_h : velocity pressure coefficient, evaluated at the mean roof height (h),

GC_{pi} : product of gust response factor and internal pressure coefficient, and

h : mean roof height.

The Standard Building Code (1997) gives wind-loading provisions similar to ASCE-7 while using fastest-mile wind speed. There are pressure coefficients for walls and roofs for rectangular structures but no information is available for round structures.

Development of the structural provisions in the International Building Code (IBC 2000) began in 1996. An International Code Council (ICC) Drafting Structural Subcommittee of code official members from BOCA, ICBO and SBCCI, along with extensive input and assistance from construction materials industry representatives. The technical provisions in the 2000 IBC have been subjected to the most extensive review of any structural code requirements in the United States. Since the publication of the IBC

Working Draft, more than 1,000 proposed structural code changes from hundreds of interested parties have been considered and more than 400 changes have been approved and incorporated into the structural provisions of the 2000 International Building Code. The wind load map and the technical requirements in the IBC reflect the latest wind load criteria in the 1998 ASCE 7 standard. The text of the IBC includes new simplified wind requirements. Generally, the simplified wind provisions can be used for buildings having a mean roof height not exceeding the least horizontal dimension of the building or 60 feet, whichever is less, along with certain other restrictions. The code includes tables of calculated wind pressures that apply to the simplified wind design method. A conversion table of equivalent basic wind speeds for 3-second gust wind and fastest mile wind speed is provided. This will allow the use of referenced documents based on fastest mile wind speeds to be used with the code wind requirements based on the 3-second gust wind speed.

The Florida Building Code (2000) classifies the wind loads for all buildings and structures depending on whether their location is in a high-velocity hurricane zone. The minimum design wind load for all structures in the high-velocity hurricane zone is given as 30 psf (1.44 kN/m^2) while it is recommended as 10 psf (0.48 kN/m^2) for all other structures. However, no specific information is available in the building code for wind-loading provisions on circular or round shape structures.

There are also some major international standards that cover wind-loading information on round structures. Australia has been in the forefront of developing and modernizing wind load provisions of building codes and standards because most of Australia's coastline is threatened by devastating cyclones. The Australian Standard

(1996) is based on 3-second gust speeds, and gives the most detailed information about wind-loading on round and circular shape structures. The Australian Standard gives external pressure coefficients for circular bins, silos and tanks for different wind directions. It also recommends the negative pressure coefficient of -0.8 be used for unroofed containers, containers under construction, or containers having large self-opening vents. In addition, pressure coefficients for conical shape roofs are given for two cases: (1) For roof slope $\leq 10^\circ$, -1.0 in windward direction and -0.5 in leeward direction. (2) For roof slope $\geq 15^\circ$, -1.0 in windward direction and -0.5 in leeward direction. It should be noted that the Australian standards are based on mostly the experimental results conducted by Macdonald et al. (1988, 1990a, and 1990b).

The DIN 18914 (DIN 1985) suggests that for conical roofs, the pressure coefficients of gable roofs be used while a pressure coefficient of 0.7 is given for cylindrical shell walls. Eurocode 1 (European Prestandard 1995) gives wind load factors as 0.6, 0.5, and 0.4 to use in calculating design wind loads in cylindrical shape structures.

The wind-loading information and provisions on round shape structures and buildings in building codes, design standards, and published research papers are very limited while those on conventional type buildings (rectangular shape) have been widely studied and available in most codes and standards. Therefore, it is obvious that there is a need for further studies of the wind-loading effects on round shaped (circular cylinder) structures, such as grain bins.

CHAPTER 3 MATERIALS AND METHODS

The overall goal of this research was to explore the effects of wind loads on grain bins. Therefore, the main task was to determine wind pressure coefficients on grain bin structures. Determining the wind pressure coefficients was accomplished by both a series of wind tunnel tests with numerous model bins and a field study with a full-scale grain bin structure. Hence, the experimental phase of this research has been conducted in two main parts as wind tunnel and full-scale tests.

Wind Tunnel Experiments

Major codes and standards permit or encourage the use of a wind tunnel, especially when structures are of "unusual shape or character". In instances where the geometry of the structure is such that the code-specified wind load provisions are not applicable, wind tunnel testing should be considered. Wind tunnel technology has reached a stage where wind tunnel model studies are reasonably standardized. The American Society of Civil Engineers has published a manual on engineering practice on Wind Tunnel Model Studies of Buildings and Structures (ASCE 1987) that assists practicing professionals as well as wind tunnel technologists to conduct wind-tunnel tests.

The wind-loading of structures is essentially a highly fluctuating and dynamic phenomenon. The approach used in Codes and Standards of specifying equivalent static loads can only be regarded as an approximation to reality. The characteristics of the fluctuating point pressures acting on exposed internal and external surfaces of full-scale

structures can be reproduced in the boundary layer wind tunnel, but information on these point pressures is not what structural designers really require. There is an increasing tendency for wind tunnel laboratories to attempt to give structural engineers information on the fluctuating load effect parameters that are really required; such as, foundation loads, overturning moments, bending moments, deflections, etc. Wind tunnel testing techniques have developed extensively over the last eighty years or so, to the point where it is now possible to reproduce the important features of airflow around bluff bodies such as ground based structures. It is important in present-day wind tunnel tests that the turbulent flow features of the atmospheric boundary layer be reproduced. In recent years there have been increasing attempts to provide information directly relevant to the structural engineers rather than the standard point pressure data. Some of the advances in wind tunnel technology and their application were summarized at the workshop held at the National Institute of Science and Technology (previously the National Bureau of Standards) in Gaithersburg, Maryland (Reinhold 1983).

According to similitude theory normally introduced in fluid mechanics, all model tests must be conducted under geometric, kinematic, and dynamic similarities (Liu 1991, Sachs 1977, Simiu and Scanlan 1986 and 1996). Geometric similarities require that the shape of the model, its surrounding structures, and topographical properties must be same as the prototype. Kinematic similarity means that the velocity field and flow streamline pattern must be similar. Finally, dynamic similarity requires the pressure distribution and the forces caused by wind must be similar. It should be noted that these three similarities are not independent of each other. Therefore, the same dimensionless parameters that give kinematic similarity also ensure dynamic similarities. For flow around a stationary

object, the pressure at any point (p) is a function of the velocity of flow (V), the density of the fluid (ρ), the dynamic viscosity (μ), the bulk modulus of elasticity (E_b), and a characteristic length of the structure (L), which can be given as:

$$p = \Phi(V, \rho, \mu, E_b, L) \quad (3-1)$$

Dimensional analysis of Equation (3-1) yields to:

$$C_p = \Phi(Re, Ma) \quad (3-2)$$

Equation (3-2) implies that the pressure coefficient at any location on a stationary structure depends on Mach number (Ma) and Reynolds number (Re). However, the effect of Mach number is negligible when for $Ma < (1/3)$. Assuming that the Reynolds number scaled back to prototype and the density of the air in a model test identical to that of the full-scale wind, Equation (3-2) becomes:

$$\frac{P_m}{P_p} = \left(\frac{V_m}{V_p} \right)^2 \quad (3-3)$$

where P_m : pressure at the model (Pa),
 P_p : pressure at the prototype (full-scale structure) (Pa),
 V_m : surrounding air velocity at the model (m/sec), and
 V_p : surrounding velocity at the prototype (m/sec).

Since force (F) is equal to pressure times area and area is proportional to the square of characteristic length (L), Equation (3-3) results in:

$$\frac{F_m}{F_p} = \frac{P_m * L_m^2}{P_p * L_p^2} = \left(\frac{L_m}{L_p} \right)^2 * \left(\frac{V_m}{V_p} \right)^2 \quad (3-4)$$

Where F_m and F_p are the forces on the model and prototype (full-scale) structures, and L_m/L_p is the scale ratio. Equations (3-2) through (3-4) are the scaling laws for predicting full-scale behavior from model test results. They can be used for both static and dynamic loads as long as the structure is stationary (not vibrating). These scaling laws were applied to the models for the wind tunnel testing part of this study.

Wind Tunnel

For this research, all wind tunnel experiments were carried out in the boundary layer wind tunnel at the Wind Load Test Facility (WLTF) located in the Civil Engineering Department at Clemson University (Figure 3-1). The wind tunnel at WLTF consists of four parts; fans, settling chamber, contraction section, and test section. The wind tunnel has an open return design and it is powered by a pair of fans with a diameter of 1.8m that are capable of producing steady speeds of 4 to 18 m/s (Figure 3-2). The nominal size of the test section is 3 m in width and 2 m in height. The height of the tunnel is adjustable so that the pressure gradient along the length of tunnel can be controlled. The wind tunnel has a nominal length of 30 m, and the length from the end of the contraction to the middle of the turntable is 16 m. The test section was covered with roughness elements of various sizes and spacing densities to create appropriate turbulent boundary layers at the test location inside the wind tunnel. The specific combination of spires, trip boards, and floor roughness elements were selected for the tests to generate necessary aerodynamic parameters for an open country terrain flow simulation. The settling chamber consists of a honeycomb grill and screens to create uniform flow conditions. The honeycomb has a length to diameter ratio of eight to one, which straightens any rotation of the air stream caused by the fans. The screens that are located

upwind and downwind of the honeycomb cause backpressure to prevent flow separation and serve to break up small turbulent eddies. The contraction section of the tunnel reduces the cross sectional area of the flow to the size of the test section. To ensure that the model being tested is only subjected to the boundary layer generated by the spires and roughness elements and not that of the walls and ceiling and to prevent abnormal pressure gradients, the ratio of the maximum cross section of the model to the cross section of tunnel is kept below 10%. A picture of the wind tunnel section is given in Figure 3-3. Further details regarding the wind tunnel sections at WLTF and the open country terrain flow simulation can be found in Monroe (1996).

Model Bins

Three model bins with variable height-to-diameter ratios of 1.0, 1.5, and 2.5, and four different conical roof configurations with angles of 25°, 30°, 35°, and 40° were constructed at 1:60 scale for pressure coefficient measurements of isolated bins in the wind tunnel. Grouping experiments were conducted with model bins that had aspect ratio (h/d) of 1.0 and 30° conical roof. The bin models were fabricated from clear acrylic cylindrical modules of 15.24 cm external diameter and heights of 15.24 cm and 7.62 cm. Four conical roof models were fabricated from Plexiglas (acrylic plastic) with 25°, 30°, 35°, and 40° slopes. A total of 177 pressure taps were placed on each conical roof at 8 different levels (From A to H) along the roof height. At three lower levels, pressure taps were located at every 10° around the circumference (36 pressure taps at each level), every 20° at 3 middle levels (18 taps at each level), every 40° at the next level (9 taps), and every 60° at the peak level (6 taps). For the cylindrical wall, 36 pressure taps at every 10° around the circumference were placed at the middle height of the cylindrical modules.

Figure 3-4 shows the placement of the pressure taps on a model roof and wall. Detailed pressure tap locations are given in Table 3-1. All single unit tests were conducted with both smooth and rough surfaces of conical roofs and walls to observe Reynolds number effects (Figure 3-5 and 3-6) because the absolute value of Reynolds number partly depends on the surface roughness (Liu 1991, Simiu and Scanlan 1996). To determine the aspect ratio effects, two additional wall modules were constructed. One module with half height of the normal model module, and one wall with the full height of the normal model wall. Figures 3-7 shows the wall modules, and Figure and 3-8 shows the model bin with height to diameter ratio of 2.5. The wall pressure coefficient measurements were conducted only with the 30° conical roof. In addition, a number of dummy models with an aspect ratio of 1.0 and a conical roof angle of 30° were constructed to use in grouping configurations.

Three different configurations were chosen for grouping effect tests. The first grouping consisted of six bins, 2 rows of 3 in-line bins (Figure 3-9). Pressure data was collected only from the center model bin in the back row (shaded bin in the figure). The other five bins were dummy models. To determine the effects of the spacing between bin rows (L), three spacing configurations ($L_1=d/4$, $L_2=d/2$, and $L_3=d$ where $d=15.24$ cm) were tested. For the second grouping experiments, three in-line model bins with three different spacing distances ($L_1=d/10$, $L_2=d/5$, and $L_3=d/2$ where $d=15.24$ cm) between the model bins were tested (Figure 3-10). The model bin at the center was used for data acquisition and the other two were dummy models. Finally, as seen in Figure 3-11, six model bins were placed in a circle-like arrangement for the third grouping configuration.

Figures 3-12 through 3-14 show pictures of the grouping configurations. All grouping configurations were tested under three wind directions of 0°, 45°, and 90°.

Pressure Sensors and Data Acquisition System

Pressure data were obtained from the wind tunnel for each tap location by Scanivalve Model 48JMG-48 port pressure switches and eight Setra Model 239 differential pressure transducers. These eight 48 port switches make it possible to test 384 different tap locations without changing the model setup. The reference pressure for the transducers was the static pressure obtained from a reference pitot tube located near the top of the wind tunnel (approximately 165 cm high) where the flow is less turbulent. The method by which pressure measurements are taken at the WLTF begins with the establishment of an electrical zero by applying the static reference pressure to both sides of the differential transducer. Once the electrical zero is set, the Scanivalve steps to the total reference pressure port. The mean voltages from this port minus the electrical zero provide an electrical voltage proportional to the mean dynamic pressure for reference pitot tube. Next, the Scanivalve switches from port to port to measure local pressure at each pressure tap. The data acquisition program then divided the local pressure tap measurements on each model by the reference mean velocity pressure to obtain pressure coefficients at each tap location. Another pitot tube located at the mean roof height of the models was used to adjust the pressure coefficients to a mean roof height reference as used by ASCE 7-98 (ASCE 1998). The following equation was used in the conversion:

$$C_{p(adjusted)} = C_{p(tap)} * \frac{(total_{ref} - static_{ref})}{(total_{tap} - static_{tap})} \quad (3-5)$$



Figure 3-1. Boundary layer wind tunnel at WLTF, Clemson University, S.C.

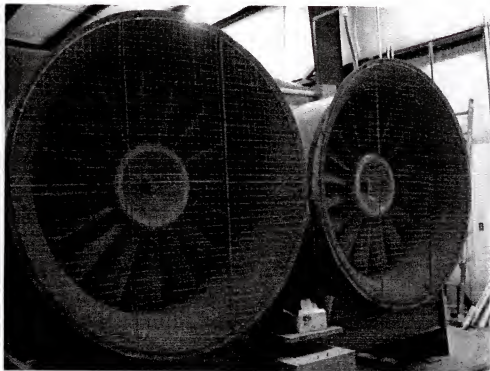


Figure 3-2. Wind generating fans for the wind tunnel at WLTF.



Figure 3-3. Test section of the wind tunnel at WLF.

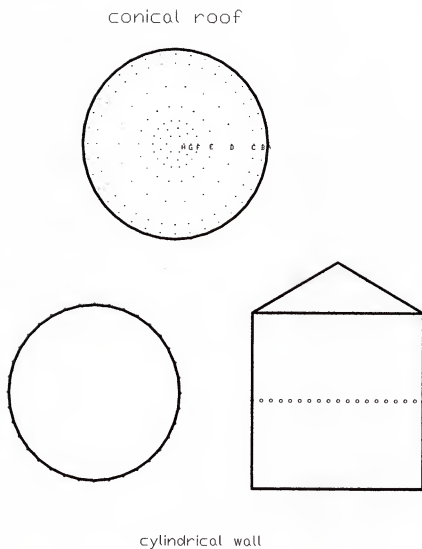


Figure 3-4. Pressure tap configuration on conical roof and cylindrical wall.

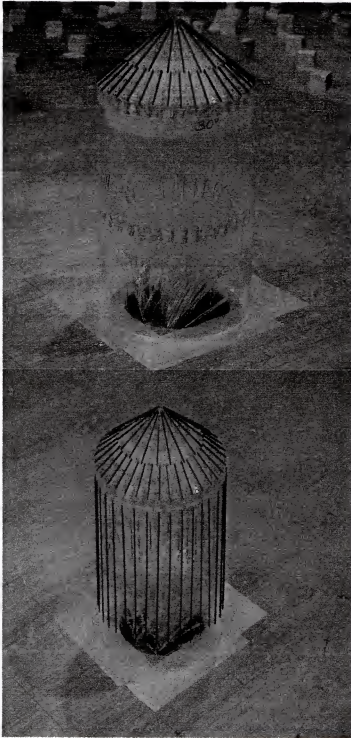


Figure 3-5. Smooth and rough surface walls in the wind tunnel.

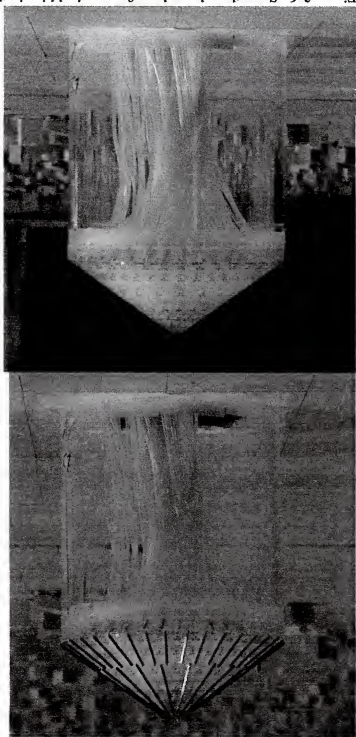


Figure 3-6. Smooth and rough surface conical bins in the wind tunnel.

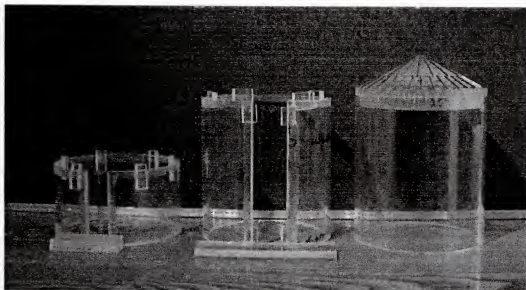


Figure 3-7. Wall modules for different aspect ratios.

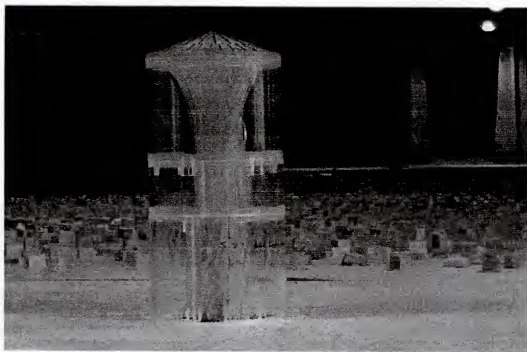


Figure 3-8. Model bin with aspect ratio of 2.5.

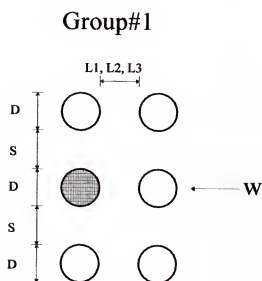


Figure 3-9. First bin grouping configuration with six model bins.

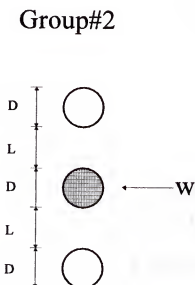


Figure 3-10. Second bin grouping configuration with three model bins.

Group#3

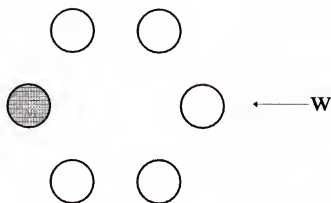


Figure 3-11. Third bin grouping configuration with six model bins.

Table 3-1. Pressure tap placement on conical roofs.

Pressure tap	Radial distance (cm) (From outer wall to center)				Height (cm) (From the floor level)			
	25°	30°	35°	40°	25°	30°	35°	40°
A	0.05	0.04	0.04	0.04	15.26	15.27	15.27	15.27
B	0.41	0.40	0.37	0.35	15.43	15.47	15.50	15.50
C	1.15	1.45	1.58	1.50	15.78	16.08	16.35	16.36
D	2.97	3.04	3.04	2.92	16.62	16.99	17.37	17.43
E	4.60	4.58	4.54	4.44	17.39	17.88	18.42	18.56
F	5.76	5.46	5.62	5.45	17.92	18.39	19.17	19.32
G	6.33	6.34	6.28	6.19	18.19	18.90	19.64	19.87
H	6.91	7.00	6.91	6.99	18.46	19.28	20.08	20.47

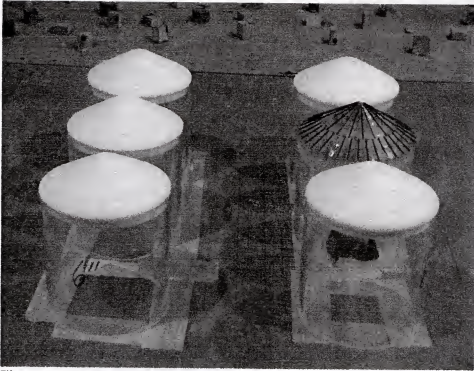


Figure 3-12. First bin grouping configuration with six model bins.

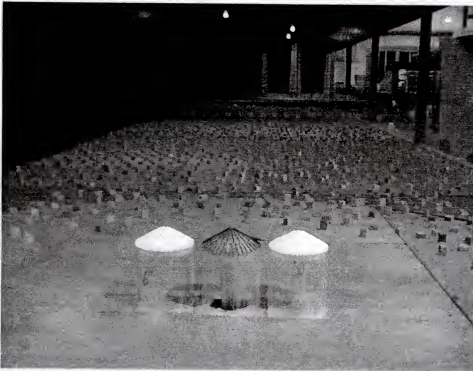


Figure 3-13. Second bin grouping configuration with three model bins inline.



Figure 3-14. Third bin grouping configuration with six model bins.

The adjusted pressure coefficients are then converted to 3-sec gust coefficients by dividing with a constant of 2.34 as suggested in the commentary section of ASCE 7-98 (ASCE 1998).

Testing was conducted with the wind tunnel set at 80% of maximum fan speed. This corresponds to an approximate wind velocity of 8 m/s (mean hourly) at mean roof height. A reasonable full-scale wind speed at mean roof height for a strong hurricane is approximately 35 m/s (125 km/h). This would correspond to a fastest mile speed of 48 m/s (172 km/h) and a 3-second gust wind speed of 58 m/s (209 km/h). Based upon the ratio of model to full-scale wind speeds and the full-scale time, a 90 second sample time period was selected for all the models. To capture an estimate of the variability of the results, each test was repeated 6 to 8 times. Mean, maximum, minimum, and root-mean-square (rms) pressure coefficients were recorded for each tap location.

Full-Scale Wind Experiments

Full-scale tests were conducted approximately 3.5 km south west of University Florida main campus in Gainesville, Florida. Figure 3-15 shows a map with the test field marked with a star. In spite of the fact that the test location was within the city limits, the surrounding area was very similar to the open country terrain because the selected area was originally for animal research and was very similar to actual farm surrounding. The main advantage of this location was being close the campus so that the control of experiment and transportation were easy.

The full-scale experiments were conducted between August 2001 and December 2001, a 3 month span, with numerous experimental sets. The average time of a single experiment was approximately 2 days. During continuous data acquisition of wind speed,

wind direction, and wind pressure with a sampling rate of 100 samples per second. A total number of 22 experiment sets was run for this full-scale wind pressure measurement research project.

Full-Scale Grain Bin

A 3.5 m in diameter and 3.5 m high ($H/D = 1$), 10.2 cm (4") corrugated steel grain bin structure with a 30° conical roof with a total height of 4.5 m, donated by The Grain Systems Inc. (GSI) for this research project, was used for wind pressure measurements (Figure 3-16). The effort was to be able to obtain the smallest bin possible due to its manageability, which also would still reasonably reflect the full-scale behavior. The smaller the bin, the easier to place the pressure taps and make necessary changes. There were originally two vent openings on top of the roof that could affect the pressure readings of the taps. Hence, they were removed from the roof and the openings were closed with 20 gauge steel sheet. The bin was constructed on a concrete floor, and it included a service door for easy access in and out of the bin.

Pressure Taps and Sensors

A total of 33 pressure taps were placed on the bin. Twenty-four of them were on the roof and nine were on the bin wall. On the roof, pressure taps were placed at three height levels. There were 6 pressure taps at every 60° around the roof at the top level, 9 pressure taps at every 40° at the middle level, and again 9 pressure taps at every 40° at the bottom level. Nine pressure taps at every 40° were placed at the mid-height of the bin wall. Figure 3-17 shows the placement of pressure taps on both the roof and the wall. The sheet metal was first drilled to have 0.5 cm in diameter openings, and then a 0.32 cm (1/8") diameter two-way metal hose fitting with treads were placed on the holes (Figure

3-18). They were fixed to the wall and roof bodies with the help of metal glue. The outer edge of the fitting was cut off, so it was flush with the metal sheet. These fittings were connected to the pressure sensors by 0.32 cm inside diameter and 0.48 cm (3/16") clear tygon tubes (Figure 3-19). Pressure measurements were performed by using 33 on-line absolute pressure transducers. Motorola MPX2010GP (side port attached) type pressure sensors were chosen for this research. They were not only economical but also were temperature compensated and self calibrated reliable sensors. The MPX2010/MPXT2010 series silicon piezoresistive pressure sensors provide a very accurate and linear voltage output, directly proportional to the applied pressure (Motorola 2000). These sensors house a single monolithic silicon die with the strain gauge and thin-film resistor network integrated on each chip. The sensor is laser trimmed for precise span, offset calibration, and temperature compensation. Their operation range is 0 to 10 kPa (0 to 1.45 psi) with the full-scale span output of 25 mV (Figure 3-20). The typical supply voltage is rated as 10 Vdc, with a sensitivity of 2.5 mV/kPa. Their pressure hysteresis is given as $\pm 0.1\%$ (supply voltage). The pressure sensors were found to be quite reliable. However, the calibration of all the pressure sensors used in this research was controlled and checked frequently by a Proscientific Inc. digiquartz portable pressure standard with an operating pressure range of 0-160 kPa (0-23 psi). The excitation voltage for all 33 pressure sensors was supplied by Kenwood regulated DC power supply (Kenwood PR18 1.2 A DC Power Supply 18 V/1.2 A) with a voltage range of 0 to 18 V. 10 V constant excitation supply was chosen for the pressure sensors. Kenwood PR18's voltage regulation characteristics were: Line regulation: 0.01%+2 mV (3.8 mV), load regulation: 0.01%+2 mV (3.8 mV), and ripple/noise: 0.5 mVrms.

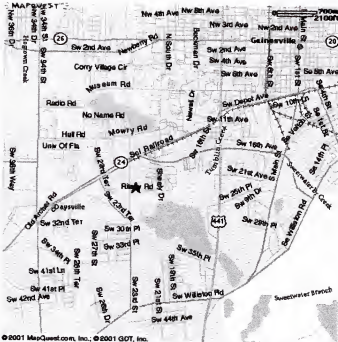


Figure 3-15. A map of the location where the full-scale tests were conducted.



Figure 3-16. Full-scale grain bin.

Pressure Tap Configuration

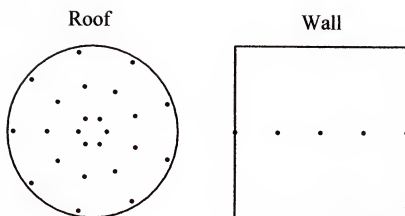


Figure 3-17. Placement of the pressure taps on the roof and wall of full-scale bin.



Figure 3-18. The pressure tap on the sheet metal.



Figure 3-19. Clear tygon hose connectors from pressure sensors

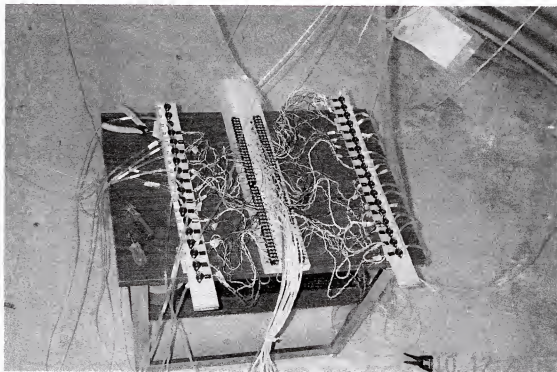


Figure 3-20. Pressure sensor network for pressure measurements of 33 taps.

Meteorological Towers

Wind speed, wind direction, and ambient pressure data were measured and recorded by two mobile meteorological towers originally constructed for the Hurricane Research Center, Clemson, South Carolina. Two mobile trailers have been outfitted with high quality instrumentation and recording systems for deployment in the event of a hurricane making land fall near one or more of the retrofitted/ pre-wired homes to obtain high quality wind data. The trailers are equipped with a 10 m folding tower, which holds three fixed axes RM Young gill propeller anemometers at the 5 m and 10 m levels (to obtain 3-components of velocity using an iterative solution technique that applies corrections for anemometer directional response), and a RM Young propeller vane anemometer at 10 m height. Additional instrumentation in the trailers includes RM Young sensors for barometric pressure, temperature, relative humidity and rainfall. The trailers are designed to resist overturning at gust speeds of 90 m/s (200 mph) under self-weight without the use of guywires or earth screws. With soil anchors (included) the trailers are designed to withstand gusts up to about 112 m/s (250 mph). The trailers include all instrumentation, a computer, backup power from batteries and a portable generator, earth screw anchors, an installation device for the earth screws, tools, surge brakes, and a spare tire. They were placed in a north-south direction with respect to of the bin with approximately 10 m away from the structure. The data acquisition was carried out by the computers located in the trailers. The system has a data recording frequency of 100 Hz with a capability of recording 15-channels of meteorological data at the same time. (Figure 3-21). Tower software that interacts with the raw data obtained from the towers' data acquisition system was used for analyzing the raw data. Tower software

(Nelson and Reinhold 1999) was capable of converting raw data to graphs of wind speed and wind direction. The tower software collected data as 15-minute segments during the data recordings. Therefore, it has functions for calculating 15-minute mean speed, highest 15 minute, 10 minute, 2 minute, 1 minute, and 3 second wind speed calculations. In addition, it can convert data to other various data formats, which enables the ability of opening and editing with many different programs.

For this research, the towers were programmed to collect 200 fifteen-minute data files for each experiment, which corresponded approximately to a two-day period of data acquisition. However, since one of the towers' computers had a problem during the experiments, only one tower was primarily used to collect wind data. The wind speed and direction data obtained from the mobile wind data collection tower were also checked against the daily meteorological data obtained from U.S. National Weather Service (2001).

Data Acquisition System

A signal conditioning card for pressure sensors, an excitation and conditioning accessory, a data acquisition board (I/O board), a personal computer, and software were used for data acquisition in this study. A personal computer with a 120 MHz Pentium processor was used to store and process the pressure sensor data Lab VIEW 5.0 (National Instruments 2000) instrumentation and analysis graphical programming language software was used for analyzing and storing data by writing a specific program for this study.

Since there were 33 pressure sensors, to accomplish a fast and multiple channel data acquisition, a complete analog signal conditioning and data acquisition setup by

National Instruments (SCXI system) was used for this study. This system included two 32-channel signal conditioning and multiplexing board (SXCI 1100) and for easy connection a SCXI-1303 front terminal block for each board, a chassis to house boards (SXCI 1000), and a 16-channel data acquisition board, and a computer. The SCXI-1100 module operates as a fast 32-channel differential multiplexer with an onboard programmable gain instrumentation amplifier (PGIA). The SCXI-1100 is a module for signal conditioning of thermocouples, volt sources, millivolt sources, 4 to 20 mA current sources, and 0 to 20 mA process-current sources. If external excitation is provided, it can also be used to measure thermistors, strain gauges, and RTDs. With the SCXI-1100 modules and SCXI-1303 terminal blocks, the SCXI chassis can serve as a fast-scanning signal conditioner accessory (National Instruments 2001). The SXCI system was connected to PCI-6035E (National Instruments 2001) multifunction I/O board for windows. The PCI-6035E is the lowest cost 16-bit data acquisition board using E-Series technologies to deliver reliable measurements in a wide range of applications. It has a sampling rate of 200 kS/s, with 16 channel 16-bit single-ended analog inputs. The PCI-6035E also has two 12-bit analog outputs where the PCI-6034E does not. Depending on the hard drive, the PCI-6035E can stream to disk at rates up to 200 kS/s. Figure 3-22 shows the SXCI system, power supply, and the computer. A program was setup with Lab View software to control data acquisition and data storage for the data obtained from pressure sensors.

All raw data obtained from pressure sensors and wind towers were analyzed afterwards with the help of numerous engineering software packages, such as Math Lab

R12 (Math Works Inc. 2001), Tower software (Nelson and Reinhold 1999), Microsoft Excel 2000 (Microsoft Co. 2000), and Sigma Plot 2001 (SPSS Inc. 2001).

Figure 3-23 shows the schematics of the wind tunnel and full scale experiments. In wind tunnel experiments, wind speed measurements were taken at the hot-wire anemometer and pitot tube level (approximately 165 cm high). Wind flow was generated by two axial fans that provided almost constant wind velocities during experiments. In field experiments, wind flow measured at 5 and 10 m with gill and vane anemometers. Wind flow was natural flow, and pressure taps were placed on a full-scale bin.

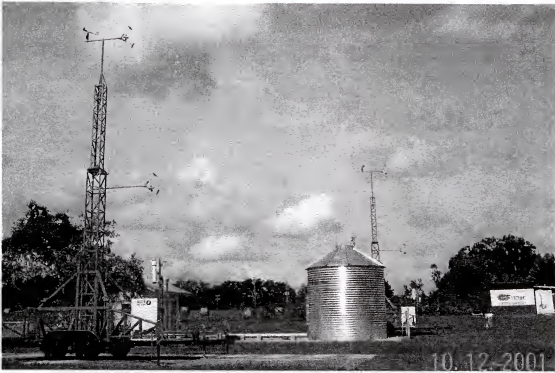


Figure 3-21. Meteorological towers during the field experiment.

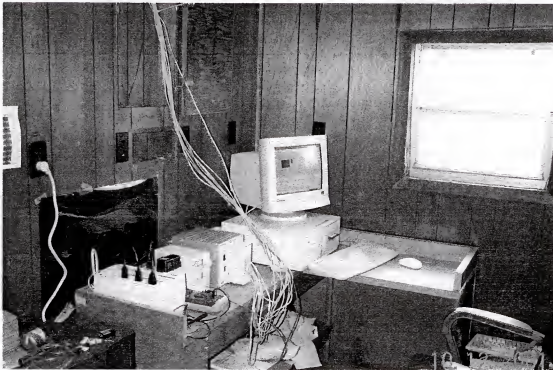


Figure 3-22. Data acquisition hardware used for the pressure sensor data.

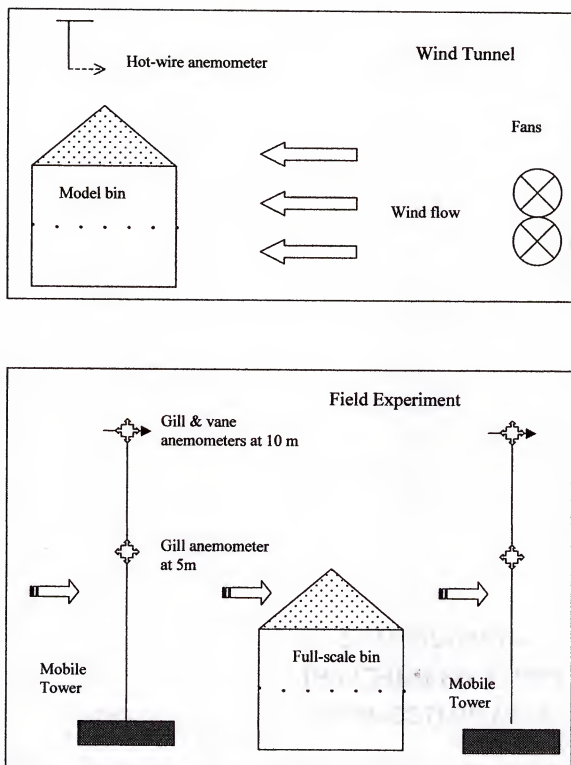


Figure 3-23. Schematics of wind tunnel and full-scale experiments.

CHAPTER 4

RESULTS AND DISCUSSION

The research to determine wind pressure coefficients was accomplished in two phases. The first task was to run wind tunnel experiments with model grain bins under open country terrain conditions. During wind tunnel experiments, many different single model bin configurations and different bin groups (grouping effects) have been tested under different wind angles of attacks (Azimuth angles). These were grouped under subsections of wind tunnel test results. The second phase of the study was to conduct a full-scale test in the field under natural wind flow. A full-scale grain bin was instrumented with pressure taps and sensors to measure wind pressures during natural wind events. Thus, the results section of this dissertation was divided into two main categories:

- Wind tunnel test results
- Full-scale test results

Wind Tunnel Tests

The testing of the scaled models in the boundary layer wind tunnel was a multiple step process. The first step in the process was the development of the flow, which was discussed in previous chapters. The second step in the model experiments was testing models in the established boundary layer flow. The third and the final step was the comparison of the resulting pressure coefficients with existing data from previous works, data from full-scale experiments, and comparisons with code values. The results obtained

from the wind tunnel tests were grouped into two main sections that were consisted of single (isolated) units and grouping results (effects of bin groupings). These two groups then were divided into two sections; wall pressure coefficients and roof pressure coefficients. In single unit tests, conical roofs with four different slopes and walls with three different aspect ratios were tested. A total of 21 different grouping configurations with changing spacing between bins, different grouping geometries, and different wind directions were tested under open country terrain simulated atmospheric boundary layer conditions. Each model test was repeated with smooth and rough surfaces as described in Chapter 3. The data are presented in this section in terms of mean pressure data (C_p mean), while the rms and the peak values of pressure coefficients will be presented in the corresponding appendices.

Velocity Profile and Turbulence Intensities of the Wind Tunnel Flow

When modeling or testing the wind effects on and around a structure in a wind tunnel, the first task is to simulate the boundary layer type suitable to the real conditions in which the structure will be located. Grain bins are almost always located in open country terrain conditions as defined in ASCE-7 (ASCE 1998). For a successful wind tunnel model study, the simulation of atmospheric boundary layer between full-scale conditions and model conditions should be similar with respect to parameters such as wind velocity profile, turbulence intensity, Reynolds number, and flow spectrum and length. The boundary layer wind tunnel at WLTF was already configured to give the necessary Reynolds stress profile and flow length. However, the measurements of velocity profiles and turbulence intensities at the height that the pressure taps were located were necessary before the tests.

Mean wind velocity profiles for the open country exposure were obtained for the reference pitot tube located 1.65 m above the floor and the second pitot tube was placed at the varying heights, such as the corresponding mean roof heights of conical roofs (Table 4-1). Table 4-1 includes the wind velocities at the reference height (pitot tube height, 1.65 m), mean velocities at the measured heights, turbulence intensities at reference height and measured heights, ratio of velocities (R), mean of the ratios, and standard deviations. Figure 4-1 shows the measured mean wind velocities at 16 different heights ranging from 6 cm to 40 cm from the floor base. Ten of these measurements were taken at the levels that the roof pressure taps were located. In addition, at each level, at least three repeated measurements were taken, and then they were averaged for each location. The log law and the power law estimated profile lines are also presented in Figure 4-1. Average Reynolds number during wind tunnel experiments was in the order of 8×10^5 . Turbulence intensities, in other words the root mean square values of the fluctuating horizontal component of the wind flow, were also measured at the same heights that the velocity profiles measured. Figure 4-2 shows the turbulence intensities measured at 16 different height locations in the test section. As seen in the figure, turbulence intensities were in the order of 0.2 (20%). Based on the velocity profile at the mean roof height for each conical roof, correction ratios for each pressure tap were obtained by applying Equation 3.5, because the pressure ratios calculated within the data acquisition system of wind tunnel were based on the reference pitot tube readings. After these conversions, the pressure coefficients were in terms of a mean hourly wind speed and referenced to the static and dynamic pressure at the mean roof height. However, the pressure data in design codes and standards are generally presented in terms of 3-second

wind speed values. Therefore, it should also be noted that the coefficient data presented here are converted to 3-second gust wind speeds by a factor of 2.34, based on the recommended conversion chart presented in ASCE-7 (ASCE 1998).

Table 4-1. Measurements of velocity and turbulence intensities at the wind tunnel test section.

Height (m)	Velocity 1	Velocity 2	Turb. Int. 1	Turb. Int. 2	R: V2/V1	Avg. R	St.D. (R)
0.061	13.276	7.248	0.106	0.227	0.546	0.546	0.000
0.076	13.479	7.747	0.106	0.225	0.575	0.575	0.000
0.122	13.541	8.218	0.106	0.218	0.607	0.607	0.000
0.152	13.255	8.033	0.097	0.215	0.606	0.606	0.010
	13.272	8.216	0.099	0.212	0.619		
	13.337	8.073	0.096	0.215	0.605		
	13.464	8.013	0.096	0.225	0.595		
0.159	13.128	8.043	0.101	0.220	0.613	0.620	0.007
	13.209	8.315	0.100	0.215	0.629		
	13.340	8.350	0.098	0.214	0.626		
	13.318	8.169	0.095	0.216	0.613		
0.165	13.241	8.218	0.098	0.218	0.621	0.621	0.001
	13.303	8.280	0.095	0.213	0.622		
	13.497	8.365	0.095	0.220	0.620		
	13.319	8.282	0.101	0.211	0.622		
0.168	13.516	8.643	0.108	0.210	0.639	0.645	0.009
	13.605	8.812	0.102	0.206	0.648		
	13.571	8.788	0.107	0.206	0.648		
0.171	13.310	8.388	0.100	0.217	0.630	0.626	0.006
	13.337	8.390	0.098	0.217	0.629		
	13.420	8.287	0.096	0.215	0.618		
	13.537	8.486	0.096	0.214	0.627		
0.178	13.322	8.452	0.095	0.202	0.634	0.628	0.005
	13.270	8.262	0.100	0.213	0.623		
	13.410	8.446	0.096	0.212	0.630		
	13.434	8.423	0.096	0.206	0.627		
0.184	13.189	8.387	0.099	0.204	0.636	0.640	0.005
	13.276	8.457	0.101	0.204	0.637		
	13.241	8.574	0.100	0.201	0.648		
	13.349	8.547	0.099	0.212	0.640		
0.191	13.135	8.360	0.095	0.208	0.636	0.647	0.009
	13.329	8.558	0.093	0.199	0.642		
	13.406	8.744	0.099	0.201	0.652		
	13.311	8.726	0.100	0.209	0.656		

Table 4-1. —continued.

Height (m)	Velocity 1	Velocity 2	Turb. Int. 1	Turb. Int. 2	R: V2/V1	Avg. R	St.D. (R)
0.197	13.203	8.562	0.097	0.203	0.648	0.650	0.005
	13.388	8.692	0.095	0.210	0.649		
	13.346	8.636	0.096	0.212	0.647		
	13.342	8.767	0.096	0.203	0.657		
0.201	13.500	9.028	0.108	0.202	0.669	0.667	0.001
	13.488	9.002	0.105	0.203	0.667		
	13.624	9.075	0.101	0.200	0.666		
0.203	13.171	8.579	0.095	0.206	0.651	0.654	0.005
	13.218	8.729	0.093	0.205	0.660		
	13.278	8.683	0.107	0.214	0.654		
	13.323	8.645	0.092	0.207	0.649		
0.254	13.401	9.357	0.106	0.196	0.698	0.698	0.000
0.406	13.425	9.922	0.110	0.176	0.739	0.739	0.000

Where Velocity 1: Wind velocity at the reference pitot tube height (1.65m) (m/s),
Velocity 2: Wind velocity at the measurement height (m/s),
Turb. Int. 1: Turbulent intensity at the reference pitot tube height (1.65m),
Turb. Int. 2: Turbulent intensity at the measurement height,
R: correction ratio,
Avg. R: average value of the correction ratio, and
St.D: Standard deviation of the correction ratio.

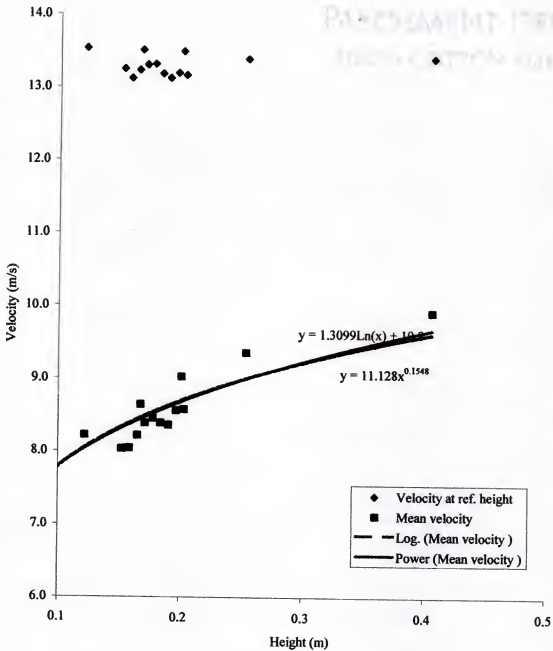


Figure 4-1. Mean velocity profile of the wind tunnel.

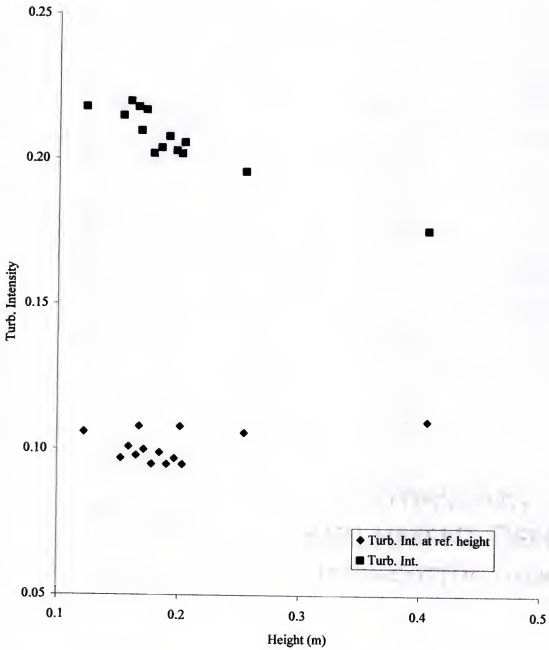


Figure 4-2. Turbulence intensities at the wind tunnel.

Single Bin Configuration

This part deals only the model test experiments conducted with single units (single model bins). Four different conical roofs (25° , 30° , 35° , and 40°) and three different aspect ratios (1.0, 1.5, and 2.5) were tested. The results will be presented in two groups; wall pressure coefficients and roof pressure coefficients.

Wall pressure coefficients

Since there is abundant information available on the wind pressure coefficients of cylindrical walls of bin structures, the experiments regarding wall pressure measurements were only limited to one type model bin, and the pressure taps were placed at only one level along the height of the wall. The wall pressure measurements for a single unit were conducted with the model bin that had an aspect ratio of (h/d) 1.0 with 30° conical roof. The tests were repeated with smooth and rough surface walls.

Figure 4-3 shows the mean pressure coefficient (C_p -mean) data obtained from both smooth surface and rough walls. The circumferential wind pressure distributions were symmetrical about the windward line in both cases. The pressure coefficients ranged from +0.4 to -0.8 for smooth wall, and from +0.4 to -0.4 for rough wall. The highest negative pressures were observed at 90° on the cylindrical wall, which can be attributed to the flow separation phenomena on cylindrical shaped objects (Simiu and Scanlan 1986, Liu 1991). The flow becomes more turbulent around the curved sides, which creates a backflow near the surface referred to as separation zones. Even though it is known that the flow separation angle depends on the surface roughness, results showed that both wall types displayed similar behavior. ANOVA (Analysis of Variance) results showed no significant difference between two data sets ($p > 0.05$). However, magnitudes of the peak

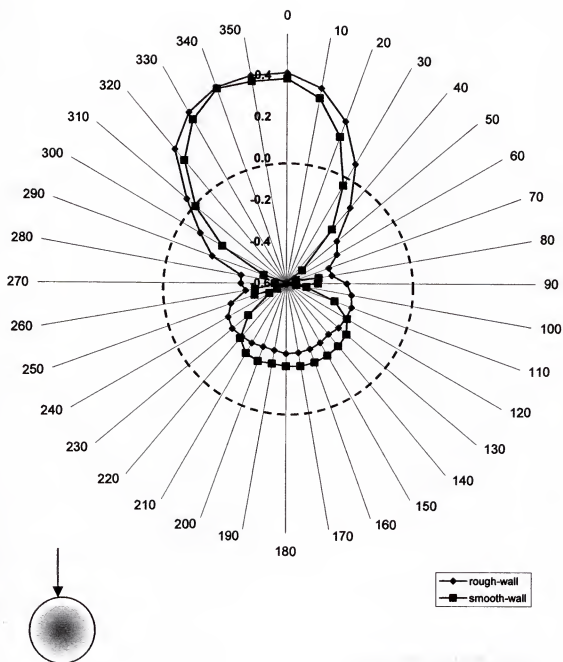


Figure 4-3. Wall pressure coefficients of a single bin with smooth and rough wall surfaces.

pressure coefficients were different in two cases. The highest positive pressures were on the windward face for both wall configurations.

Roof pressure coefficients

Point pressure measurements at each tap location were taken on 25°, 30°, 35°, and 40° angle conical roofs for a single unit. In addition, bins with aspect ratios of 1.0, 1.5, and 2.5 were tested with the 25° conical roof as a single unit.

The average values of mean pressure coefficients (C_p mean) obtained by eight repeated tests for a rough surface 25° conical roof are presented in Figure 4-4. The mean C_p values are different not only around the circumference but also along the roof height at different levels (From A to H). Detailed information regarding the tap locations can be found in Chapter 3 of this dissertation. The mean pressure ratio ranged from -0.05 to -0.32 on the 25° conical roof. The absolute values of C_p mean were highest at the lower levels of roof (A and B), and lowest at the middle levels of the roof (D and E). The same tests were conducted with the smooth surface 25° conical roof; and the results are presented in Figure 4-5. The mean pressure coefficients ranged from -0.10 to -0.70. As Figures 4-4 and 4-5 indicate, the pressure coefficients for the smooth surface roof were higher than those for the rough surface roof as expected due to aerodynamic theory regarding surface roughness. Statistical analysis of the data (ANOVA) indicated that there were significant differences between two roof surfaces ($p < 0.05$). In addition, the differences of pressure coefficients among the roof levels (A to H) were more distinct for the smooth surface roof than the rough one. The average mean pressure coefficients obtained for the 30°, 35°, and 40° roofs with rough and smooth surfaces are shown in Figures 4-6 through 4-11, respectively. The local pressure coefficient data showed similar

behavior for all the roof angles. However, as the angle of roof increased, the range between maximum and minimum values increased while the average differences of pressure distribution among the height levels decreased. Positive mean pressures were observed at the middle levels starting with the 30° roof while all pressure coefficient values were negative for all the tap locations at all levels for the 25° roof. The highest absolute values of pressure coefficients for all roof angles were observed at the wind directions of 90° and 270° around the circumference. The average mean local pressures for rough surface roofs were in the range of +0.03 to -0.33 for the 30° roof, +0.08 to -0.34 for the 35° roof, and +0.12 to -0.41 for the 40° roof while those for the smooth surface roofs were 0.00 to -0.50 for the 30° roof, +0.04 to -0.45 for the 35° roof, and +0.15 to -0.65 for the 40° roof. Statistical analysis (ANOVA) of mean pressure coefficients obtained for each roof angle tests did not detect any significant difference among replications ($p > 0.05$). However, ANOVA tests indicated that there were significant differences among the data obtained for different roof angles ($p < 0.05$). This suggests that changing in the conical roof angle significantly affects the mean pressure coefficient values. Figures 4-12 and 4-13 show the comparison of C_p mean values obtained from four rough-surface conical roofs (25°, 30°, 35°, and 40°) at the bottom and the top levels of the roof, respectively. As seen in the figures, the differences among roof angles were more noticeable at the bottom level of the roof while the differences were less pronounceable at the bottom level. The range between the maximum and minimum values of C_p mean at the bottom level changed as the roof slope increased. This might be contributed to the sudden shape and slope change at the bottom of the roof, which is a transition area from wall to roof.

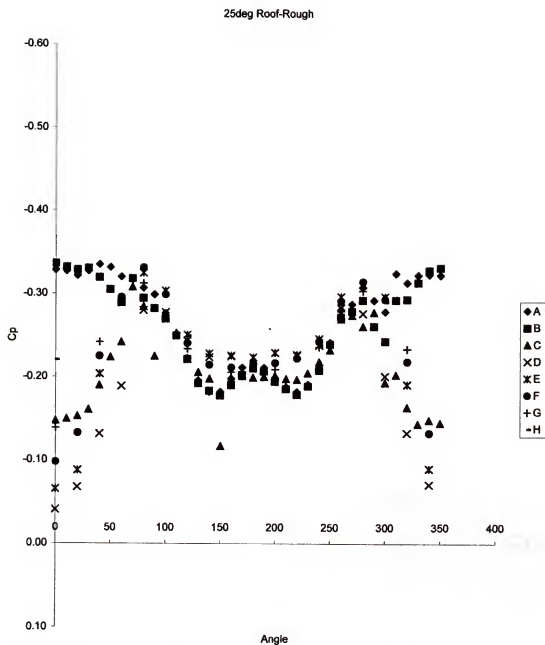


Figure 4-4. Mean pressure coefficients for the 25° rough roof with an aspect ratio of 1.0.

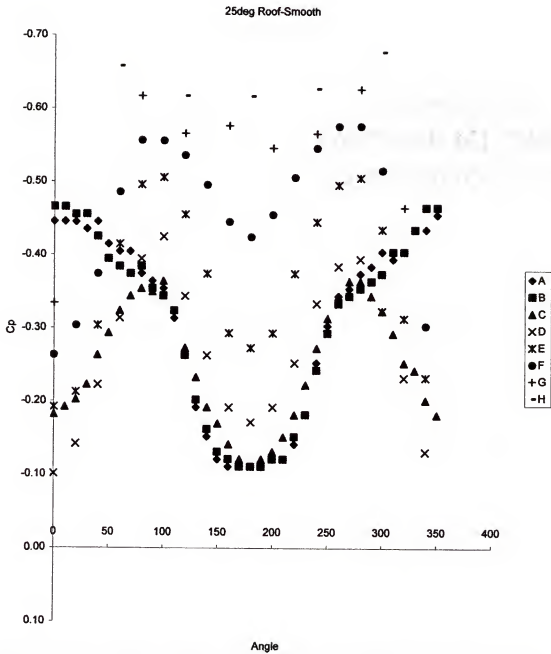


Figure 4-5. Mean pressure coefficients for the 25° smooth roof with an aspect ratio of 1.0.

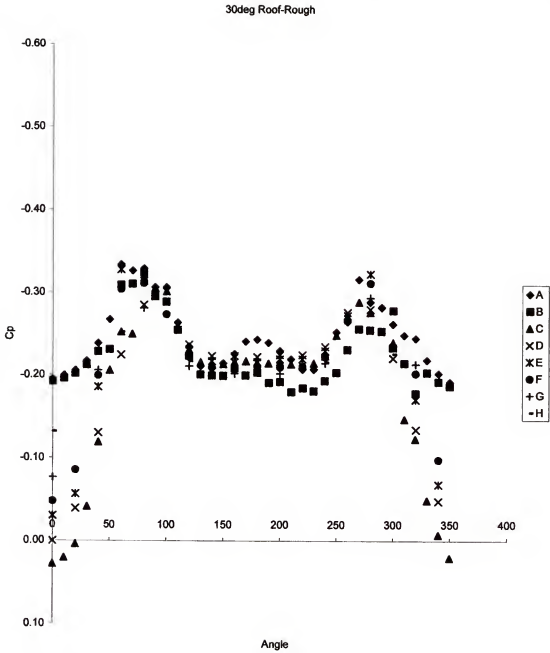


Figure 4-6. Mean pressure coefficients for the 30° rough roof with an aspect ratio of 1.0.

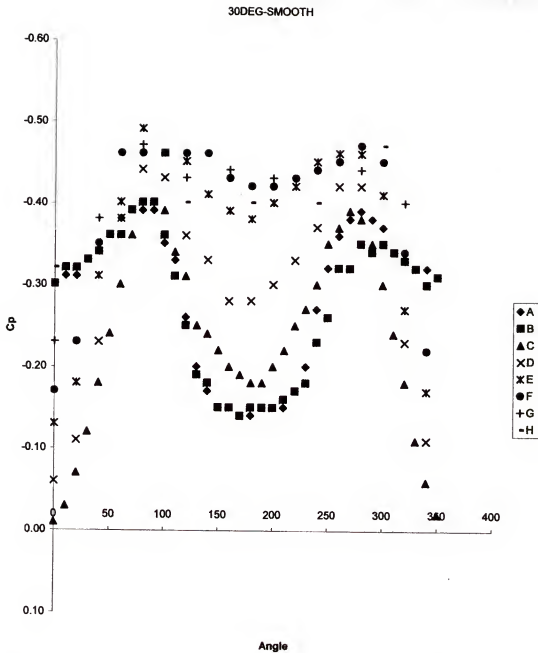


Figure 4-7. Mean pressure coefficients for the 30° smooth roof with an aspect ratio of 1.0.

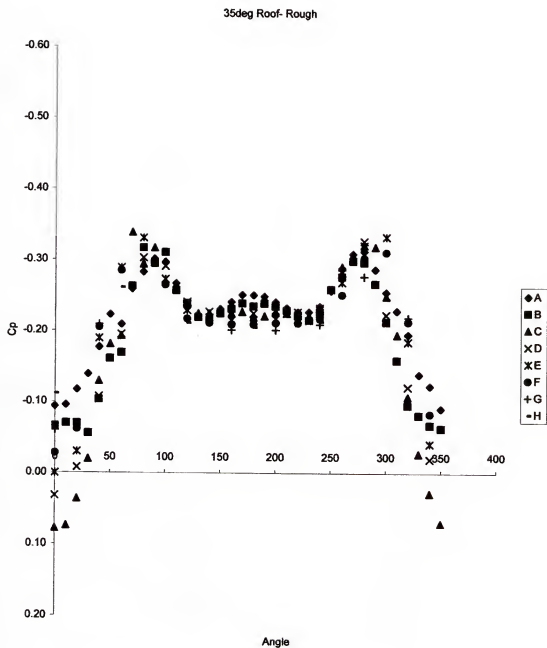


Figure 4-8. Mean pressure coefficients for the 35° rough roof with an aspect ratio of 1.0.

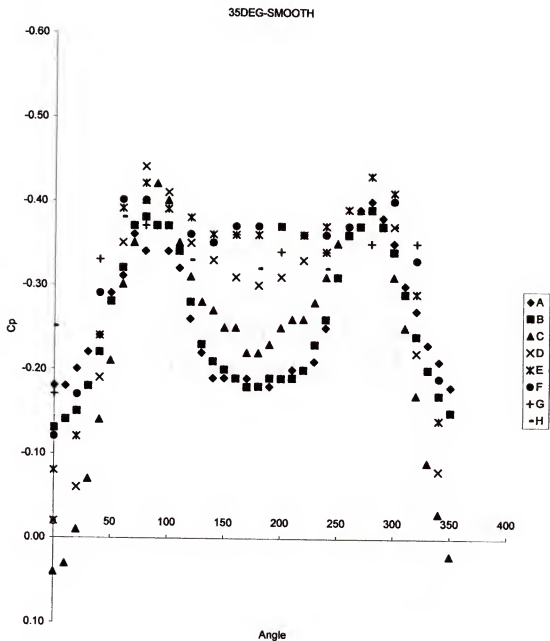


Figure 4-9. Mean pressure coefficients for the 35° smooth roof with an aspect ratio of 1.0.

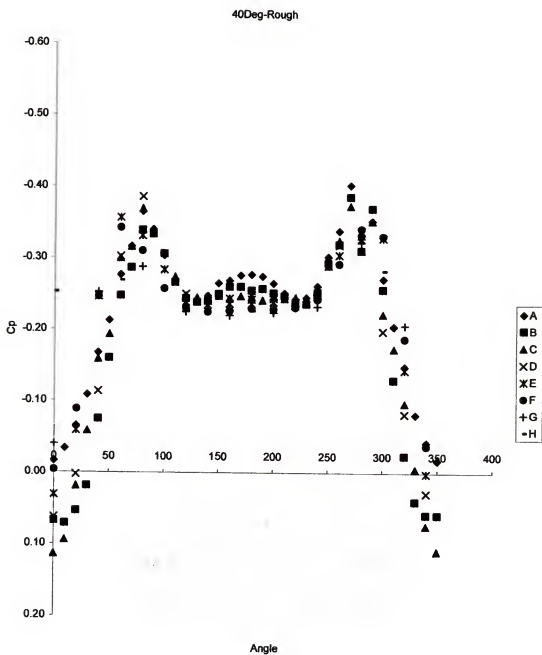


Figure 4-10. Mean pressure coefficients for the 40° rough roof with an aspect ratio of 1.0.

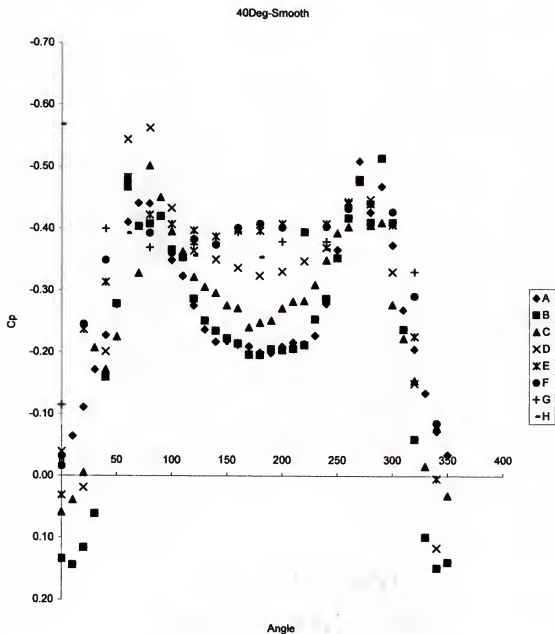


Figure 4-11. Mean pressure coefficients for the 40° smooth roof with an aspect ratio of 1.0

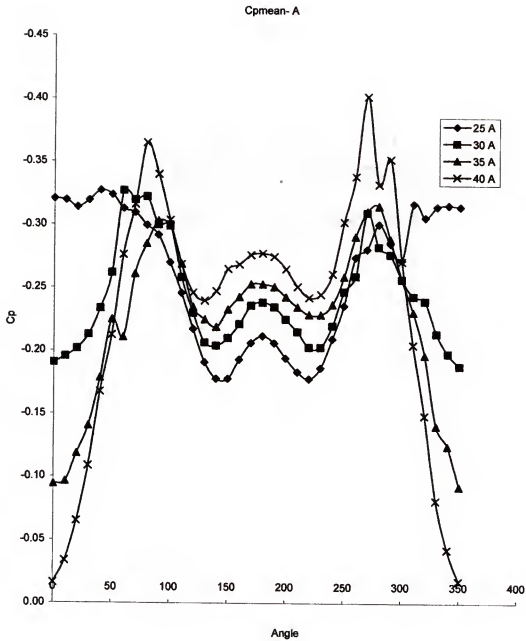


Figure 4-12. Comparison of the mean pressure coefficients (C_p mean) at the bottom level of the rough roof.

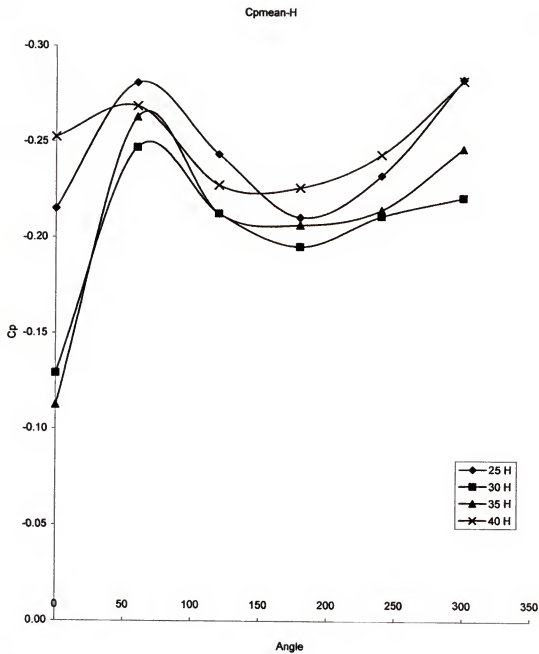


Figure 4-13. Comparison of the mean pressure coefficients (C_p mean) at the top level of the rough roof.

Aspect ratio (H/D) effects

To determine the effects of the height to diameter ratio of the bin structure, the wind tunnel tests for the 25° angle conical roof were repeated with changing aspect ratios (H/D) of the cylindrical wall. Figures 4-14 and 4-15 show the mean pressure coefficient values of conical roof for aspect ratios of 1.5 and 2.5, respectively. It should be noted here that the aspect ratio tests were performed with a rough surface roof only. The change in the aspect ratio (h/d) of the cylindrical bin from 1.0 to 1.5 and 2.5 resulted in a significant difference ($p < 0.05$) among the mean pressure coefficient values. As shown in the figures, the mean C_p values increased as the aspect ratio changed from 1.0 to 1.5 and 2.5. The mean C_p values ranged from -0.07 to -0.48 for the aspect ratio of 1.5 while it was between -0.11 and -0.71 for aspect ratio of 2.5. These results were expected because wind speeds were higher and the flow was less turbulent as the height of the roof increased above the ground level as in boundary layer flow conditions.

Contour maps of the mean pressure coefficient data were plotted for each single bin unit roof. They were presented along with the contour plot of full-scale roof in Appendix A. Figures A-1 through A-8 show the contour plots of $C_{p, \text{mean}}$ values for each roof. The peak and the rms values of pressure coefficient data obtained for the single unit model wind tunnel tests are presented in Appendix B in the corresponding order to this part. Tables B-1 through B-8 showed the maximum and minimum values and the root mean square values for the pressure coefficient data. This might be helpful when determining extreme conditions or for conditions when the variation of wind pressure coefficient is a concern for the designer.

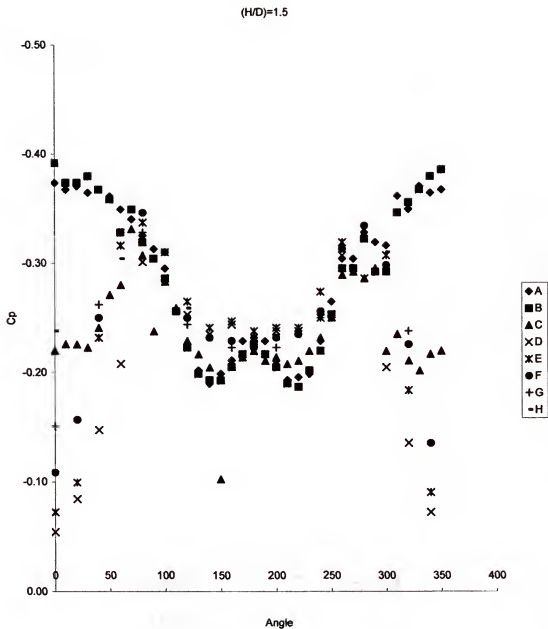


Figure 4-14. Mean pressure coefficients for the 25° rough roof with an aspect ratio of 1.5.

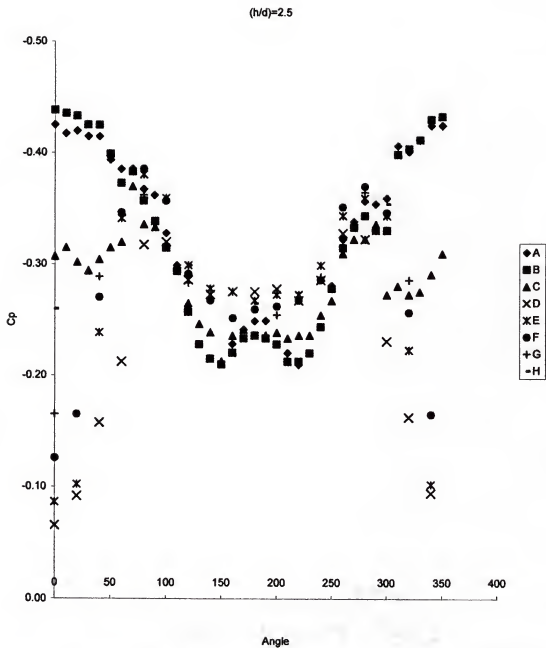


Figure 4-15. Mean pressure coefficients for the 25° rough roof with an aspect ratio of 2.5.

Grouping Effects

Significant changes in pressure coefficients are possible when structures are placed in close proximity to one another. Thus, following the experiments with a single-isolated bin model, additional tests were conducted to determine the effects of bin groupings on wind pressure coefficients. For this purpose, three different bin-grouping configurations were chosen, which are presented in detail in Chapter 3 (Materials and Methods) of this dissertation. In addition to the grouping geometries, spacing effects among bins within bin groupings, and wind direction effects were investigated. Pressure data for grouping configurations were measured for only the model bins with 30° conical roof and smooth wall surface. However, one test was performed with rough surface wall to compare the results as well as to determine the effects of surface roughness. As in the previous part, the results are presented within two main groups for grouping effects, which were wall pressure coefficients and roof pressure coefficients. The first grouping configuration (G1) was consisted of six bins placed in two rows of 3-in-line bins. The second bin grouping (G2) consisted of a single row of 3-in-line bins. Finally, the third bin grouping (G3) was a rose-like shape of 6 bins in-circle.

Wall pressure coefficients

The first set of experiments was conducted with the first grouping. The spacing between bin rows was changed to three different values ($L1=1/4D$, $L2=1/2D$, and $L3=D$) to determine the spacing effects as well as wind direction effects. Figure 4-16 shows the wall pressure coefficients obtained from G1-L1 configuration under three azimuth angles (0, 45, 90 degrees). The C_p mean values showed similarities except for the 80° slice of the cylinder that corresponds between 240° and 320° around circumference. While the results

from 0° and 90° wind attack degrees remained close, those from 45° showed higher positive pressure coefficients. This might be attributed to the orientation of two rows of bin groups, which caused the positive pressure to be generated on that part of the circumference. Nevertheless, statistical analysis of the results indicated that the differences among azimuth angles were not statistically significant ($p > 0.05$). Figure 4-17 and 4.18 show the C_p mean values measured for G1-L2 and G1-L3, respectively. Statistical analysis results did not indicate any significant differences among the azimuth angles for G1-L2 and G1-L3 configurations. In addition, it was obvious that the wall pressure coefficients were very similar for the three different spacing configurations. Figure 4-19 shows the C_p mean values obtained from three different spacing configurations for the 0° wind direction. ANOVA results indicated that the spacing was not a significant factor on the results of pressure coefficients.

The second set of grouping experiments were conducted with three bins in-line (G2) at three wind directions. In this case, the spacing between bins changed from $1/10^{\text{th}}$ of the model bin diameter (L1) to $1/5^{\text{th}}$ (L2), and from $1/5^{\text{th}}$ to $1/2^{\text{nd}}$ of the diameter (L3). Figures 4-20 through 4-22 show the C_p mean results obtained from G2-L1, G2-L2, and G2-L3, respectively. As seen in the figures, behavior and magnitude of the pressure coefficients were different from those obtained from G1. The wind direction was statistically significantly to affect the results obtained from G2-L3 while that was not the case for G2-L1 and G2-L2. In the G2-L3 configuration, the spacing was half of the model bin diameter, which was 5 times longer than L1, and 2.5 times than L2. Furthermore, the spacing distance was significantly effective for the second grouping configuration for all

three wind directions ($p < 0.05$). Figure 4-23 shows the C_p values obtained from 3 different spacing configurations for the 0° wind direction for the second configuration.

Figure 4-24 shows the mean wall pressure coefficient data (C_p mean) obtained from the circular shaped grouping (G3) with wind directions of 0° , 45° , and 90° . The pressure distribution corresponded to the changes of windward direction. Statistical analysis indicated significant differences among the data sets obtained from each windward direction. In addition, the magnitude of the pressure coefficients for 0° wind direction were less than those for a single unit as expected due to geometric orientation of the bins in the grouping. The highest magnitude of pressure coefficients was measured with 90° wind attack angle (Azimuth angle). This was assumed the result of geometric orientation of the bins within the grouping.

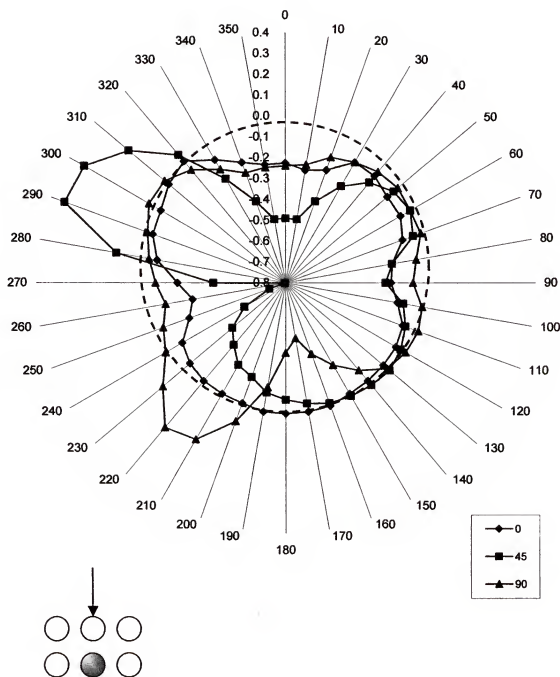


Figure 4-16. Wall mean pressure coefficients (C_p mean) for the first grouping with a spacing of 1/4 of the model diameter (G1-L1).

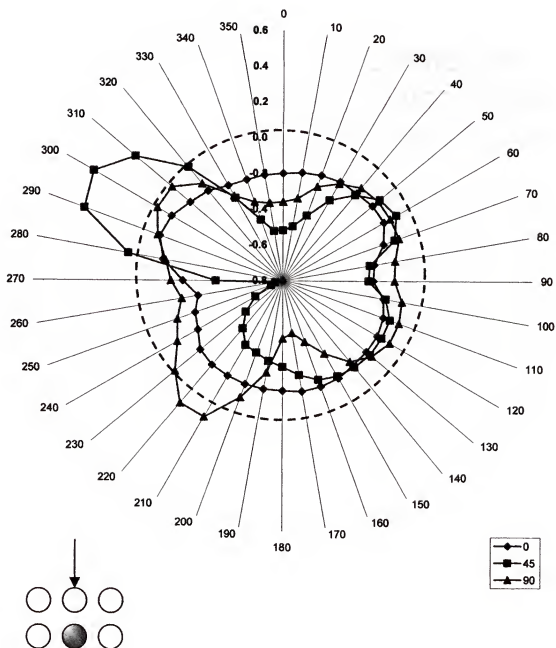


Figure 4-17. Wall mean pressure coefficients (C_p mean) for the first grouping with a spacing of $1/2$ of the model diameter (G1-L2).

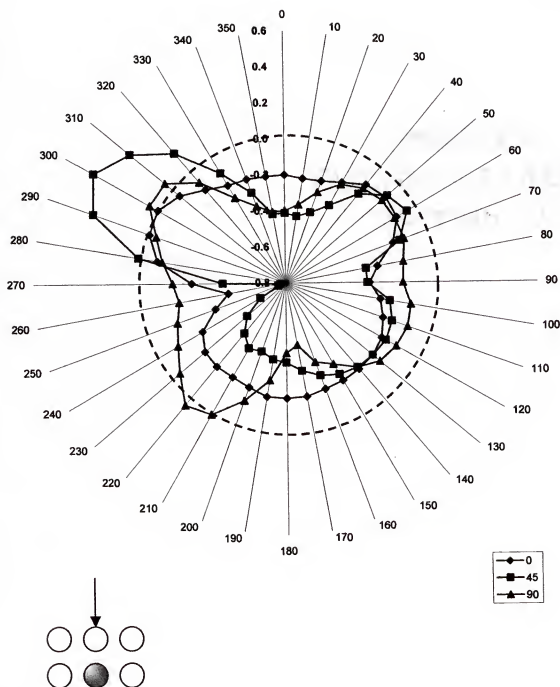


Figure 4-18. Wall mean pressure coefficients (C_p mean) for the first grouping with a spacing of 1/1 of the model diameter (G1-L3).

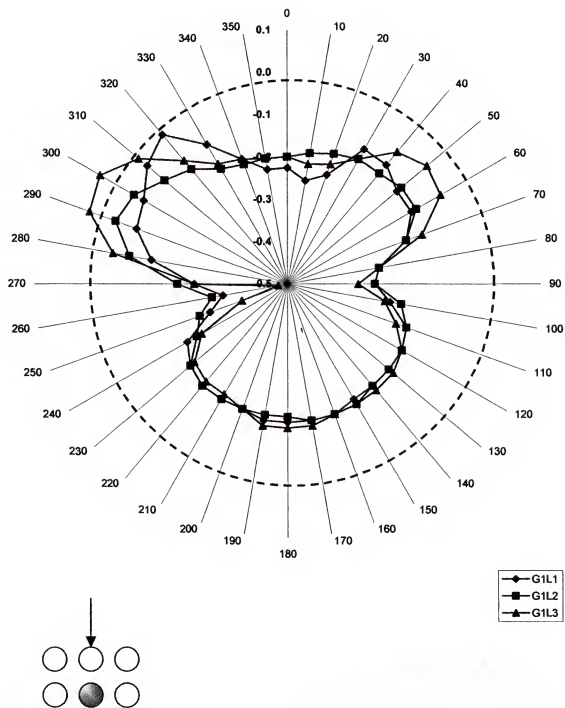


Figure 4-19. Comparison of wall mean pressure coefficients (C_p mean) at 0° wind direction for the first grouping (G1).

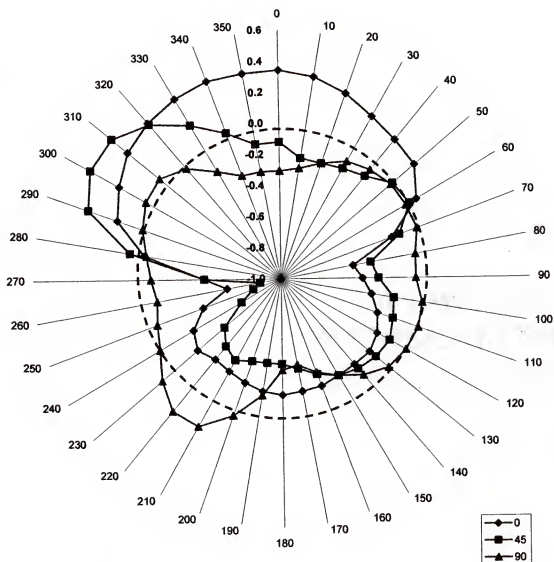


Figure 4-20. Wall mean pressure coefficients (C_p mean) for the second grouping with a spacing of $1/10$ of the model diameter (G2-L1).

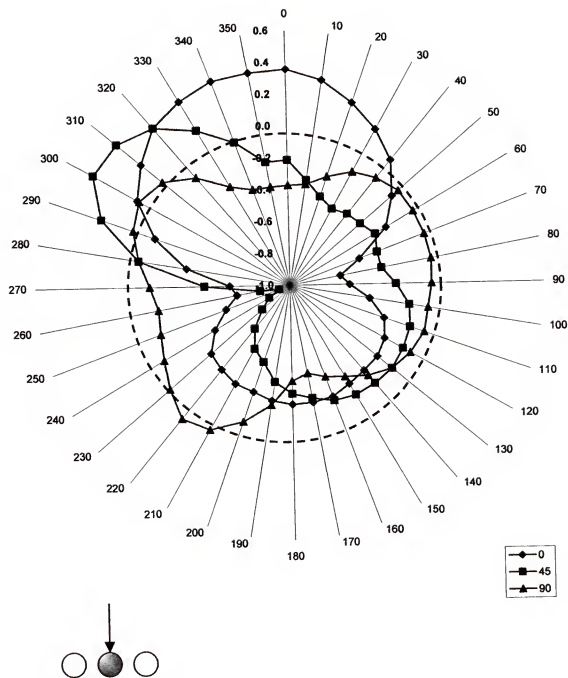


Figure 4-21. Wall mean pressure coefficients (C_p mean) for the second grouping with a spacing of $1/5$ of the model diameter (G2-L2).

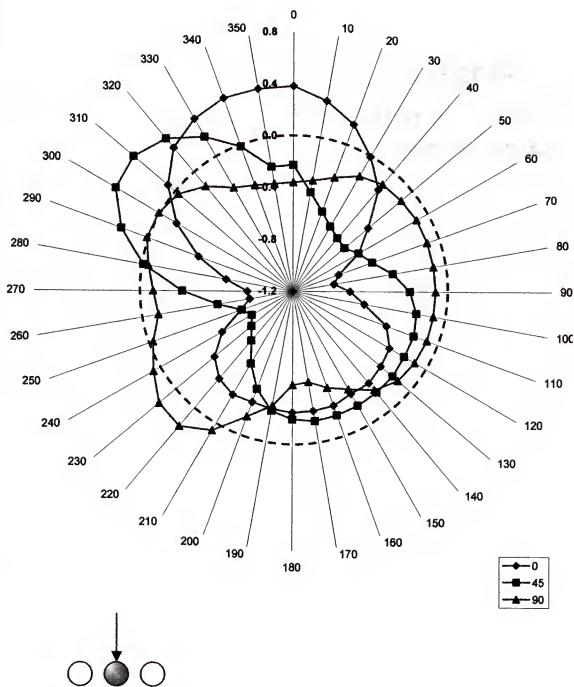


Figure 4-22. Wall mean pressure coefficients (C_p mean) for the second grouping with a spacing of $1/2$ of the model diameter (G2-L3).

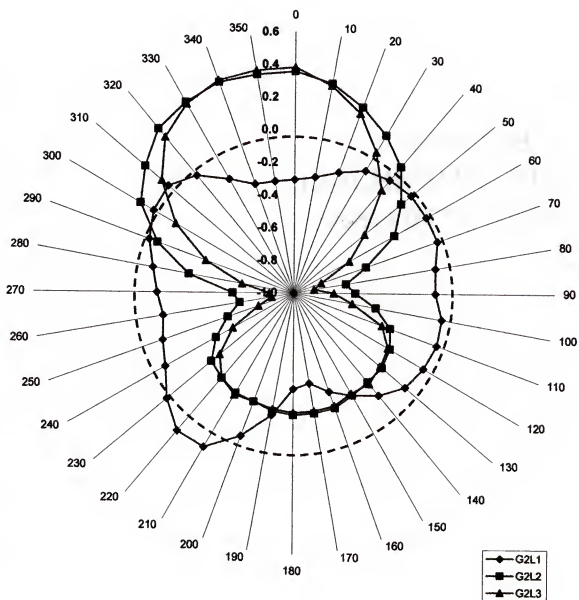


Figure 4-23. Comparison of wall mean pressure coefficients (C_p mean) at 0 degree wind direction for the second grouping (G2).

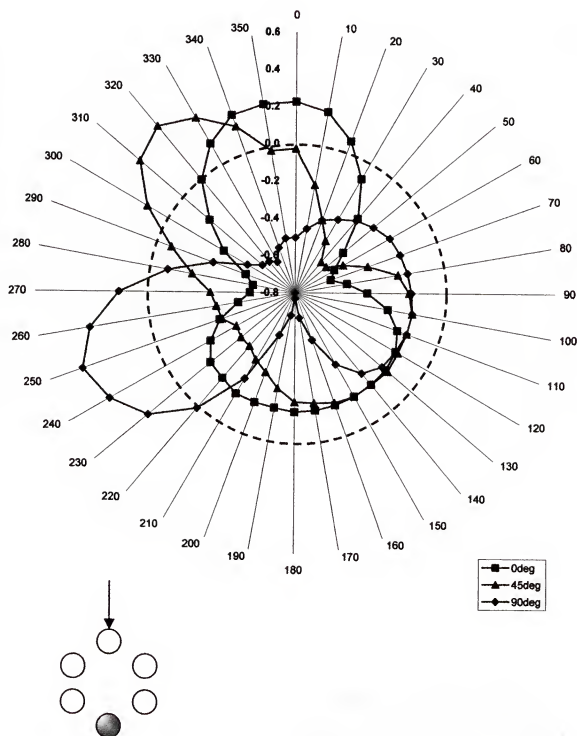


Figure 4-24. Wall mean pressure coefficients (C_p mean) for the third grouping (G3).

Roof pressure coefficients

To determine the grouping effects on roof pressure coefficients, measurements were taken with 30° conical roof for the three bin grouping configurations. For flow separation effects, measurements were taken at three wind directions at 45° and 90°, as well as for the normal direction (0°). Initial experiments indicated that the pressure distribution changes in azimuth angles of 30° and 60° were not significantly distinct. Therefore, only three wind direction angles were included in the experiments.

Figures 4-25 through 27 show the mean roof pressure coefficient data (C_p mean) obtained with the first grouping configuration (G1-L1) at three wind directions; 0, 45, and 90 degrees, respectively. Compared to each other, the differences among three wind direction data were easily noticeable. As seen from the figures, the C_p mean showed positive (+) values between 220° and 320° at 90° wind attack angle. The magnitude of highest negative (-) C_p mean values also dropped from -0.35 for 0 and 45 degrees to -0.25 for 90 degrees. However, when compared with the single unit with 30° rough conical roof, the results were similar with G1-L1 at 0 degree wind direction. The most noticeable difference between two groups of data was the distribution of wind pressures at the eight height levels of the conical roof. The difference among roof levels (A to H) for a single unit was much less than those for the grouping configuration. Further tests were conducted with two more spacing configurations; each at three wind directions. Figures 4-28 through 30 show the C_p mean data obtained from G1-L2 (spacing is 0.5 D) at 3 wind directions; 0°, 45°, and 90°; respectively. Figures 4-31 through 33 show the C_p mean data obtained from G1-L3 ($L=D$) at the same three wind directions. The pressure distribution and C_p values obtained from L2 and L3 showed similar behaviors to those obtained from

L1. In fact, the statistical analysis of roof pressure coefficients for the first grouping configuration (G1) indicated that the spacing was not a significant factor. However, changing wind direction within grouping configuration had a statistically significant effect on the C_p mean values.

As for the wall pressures, the roof wind pressure tests were conducted with the second bin grouping configuration, which consisted of 3 bins in-line. The bin at the center had pressure taps with two dummy bins on its sides. Figures 4-34 through 42 show the results obtained from G2-L1, G2-L2, and G2-L3 at wind directions of 0° , 45° , and 90° . The C_p mean data for all three spacing distances for the second grouping configuration showed similar pressure distributions for different levels of the roof. However, the statistical analysis results revealed that the effects of wind direction were significant enough to affect the pressure distribution on the roof. In addition, the magnitudes of the C_p means were higher for G2 than those obtained from G1. The highest negative pressure coefficients were in the range of -0.45 for G2 at 0° azimuth angle while they were in the range of -0.35 for G1. In spite of the fact that the pressure distributions looked similar between the single unit and G2 under the normal wind direction (0°), the magnitudes of C_p were different. Groupings of the bins might presumably cause increased suction around the roof, which resulted higher negative pressures for the bin inside grouping than the single bin.

Figures 4-43 through 45 show the mean roof pressure coefficient data (C_p mean) obtained from a circular shape grouping with six bins (G3) under three wind direction angles. Measurements were made on the back-central model bin with a 30° rough surface conical roof with five dummy model bins each having 30° conical roofs. The values of

pressure coefficients increased as the wind direction changed from 0° to 45° , and 45° to 90° . The difference among the pressure coefficients due to wind direction was statistically significant ($p < 0.05$). The pressure distributions at 0° azimuth angle were very similar to those obtained from the single unit with 30° rough surface roof in spite of the fact that the magnitudes of pressure coefficients were different. Furthermore, positive pressure regions (positive pressure coefficients) were observed for the cases of 45° and 90° azimuth angles.

Comparison of the results obtained from this study can be made with a number of previously published works. Even though there were modeling differences, similar pressure distribution results for the cylindrical wall were reported by Sabransky and Melbourne (1987) and Macdonald et al. (1988) for a single bin. However, magnitudes of the pressure coefficients around the cylindrical wall were different. Macdonald et al. (1988) reported mean roof pressure distribution and pressure coefficients for a 25° roof with an aspect ratio of 1.0. Their mean pressure coefficients were in the range of +1.2 to -1.6, and positive pressure ratios were observed in the wind direction. The differences in magnitude of the mean pressure coefficients might be attributed to the fact that they used smooth surface models and 50 pressure taps at every 36° around the circumference of the roof. It should also be noted that an aeronautical type wind tunnel with a relatively short test section was used in their experiments.

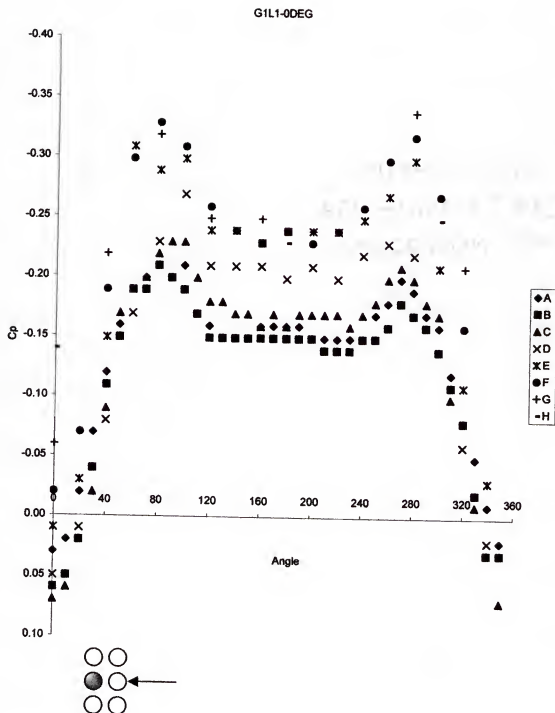


Figure 4-25. Roof mean pressure coefficients (C_p mean) for the first grouping at 0° wind direction (G1-L1, 0 degree).

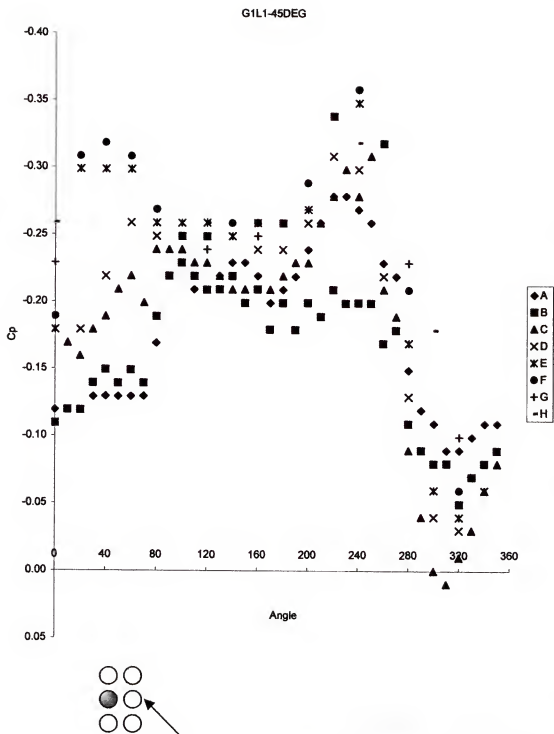


Figure 4-26. Roof mean pressure coefficients (C_p mean) for the first grouping at 45° wind direction (G1-L1, 45 degree)

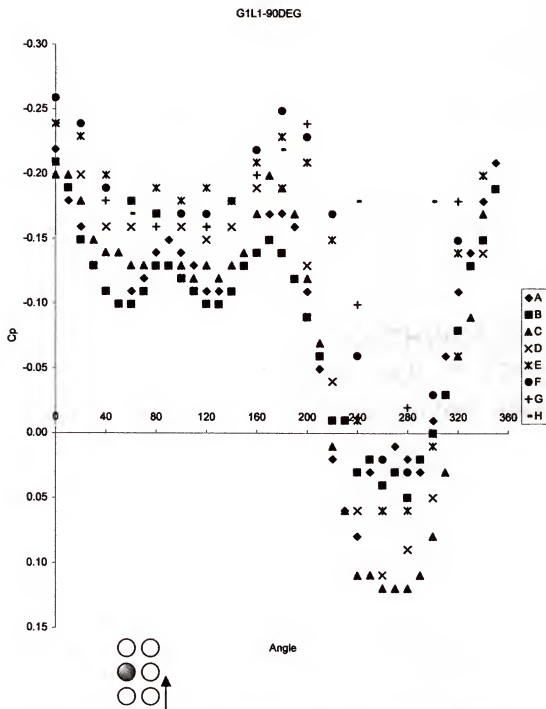


Figure 4-27. Roof mean pressure coefficients (C_p mean) for the first grouping at 90° wind direction (G1-L1, 90 degree).

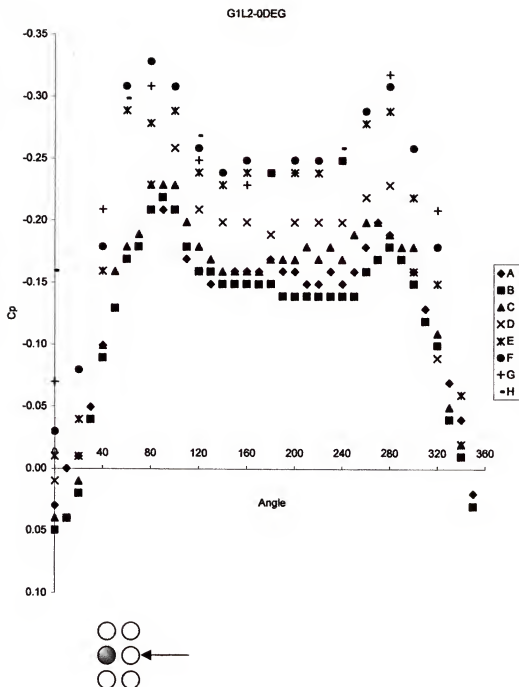


Figure 4-28. Roof mean pressure coefficients (C_p mean) for the first grouping at 0° wind direction (G1-L2, 0 degree).

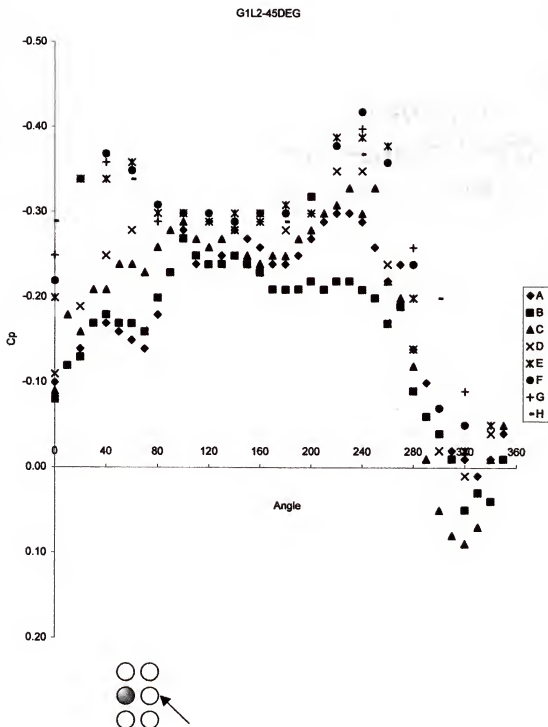


Figure 4-29. Roof mean pressure coefficients (C_p mean) for the first grouping at 45° wind direction (G1-L2, 45 degree).

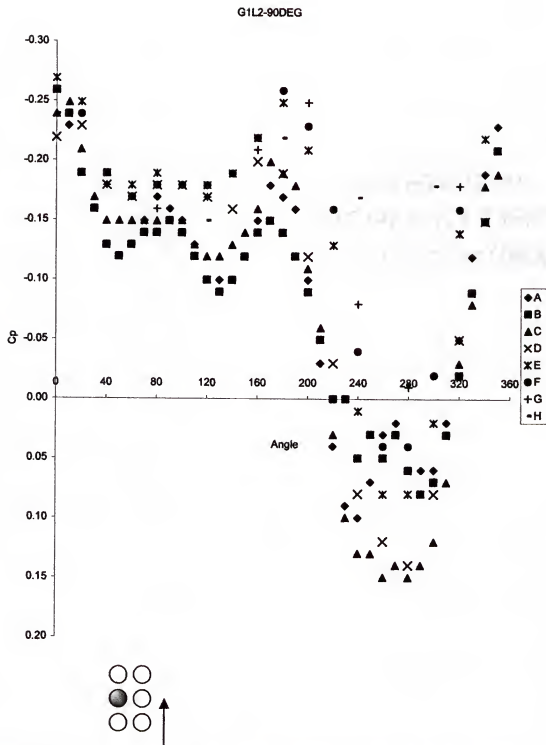


Figure 4-30. Roof mean pressure coefficients (C_p mean) for the first grouping at 90° wind direction (G1-L2, 90 degree).

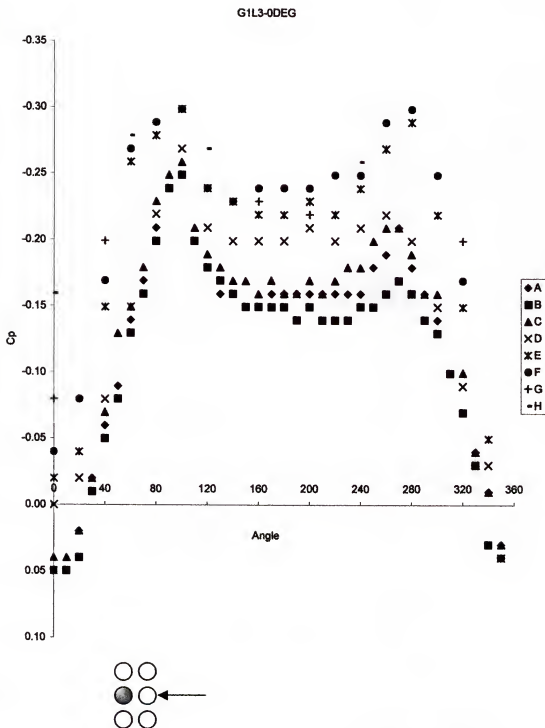


Figure 4-31. Roof mean pressure coefficients (C_p mean) for the first grouping at 0° wind direction (G1-L3, 0 degree).

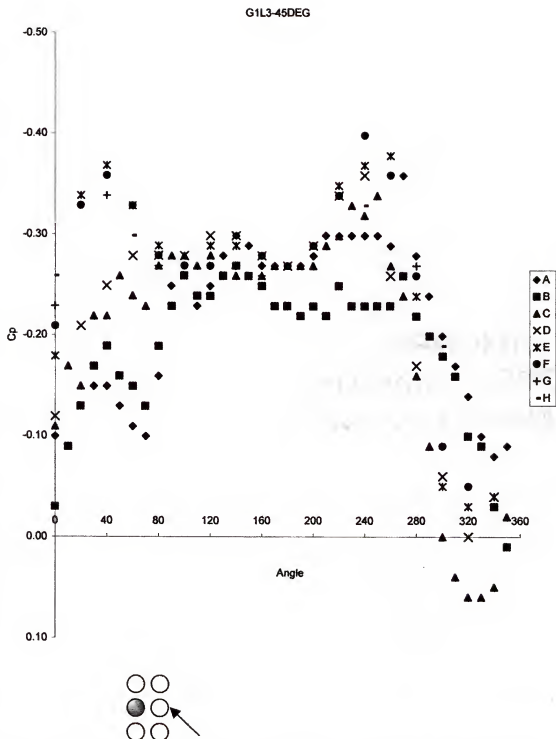


Figure 4-32. Roof mean pressure coefficients (C_p mean) for the first grouping at 45° wind direction (G1-L3, 45 degree).

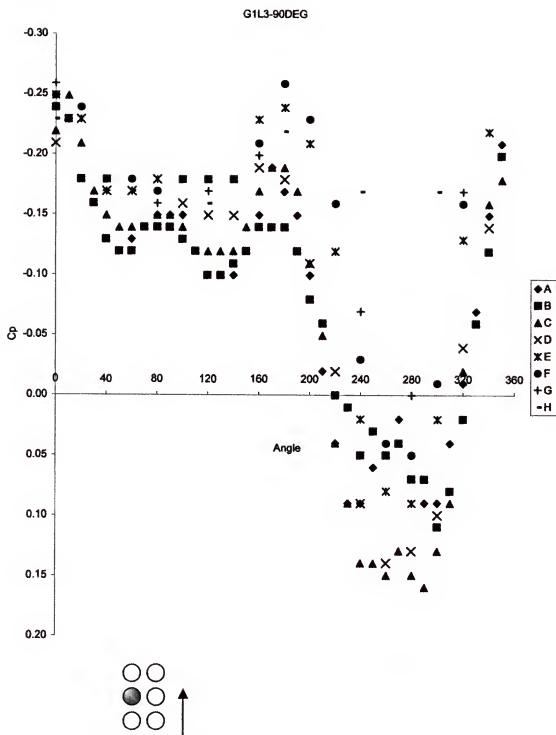


Figure 4-33. Roof mean pressure coefficients (C_p mean) for the first grouping at 90° wind direction (G1-L3, 90 degree).

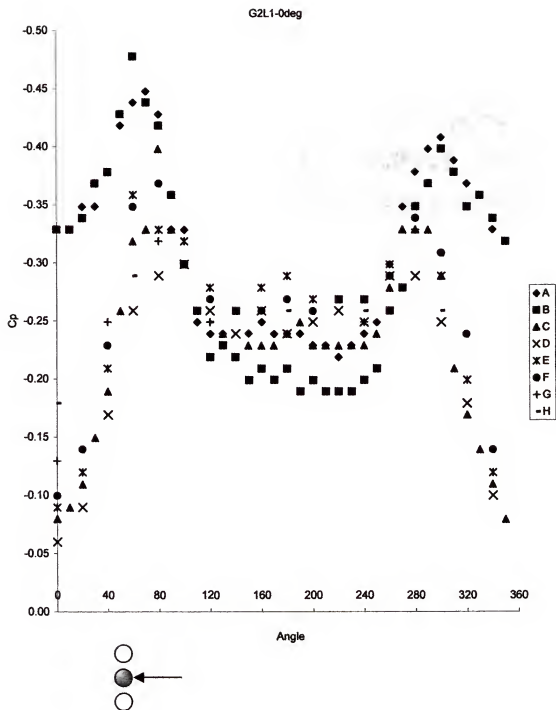


Figure 4-34. Roof mean pressure coefficients (C_p mean) for the second grouping at 0° wind direction (G2-L1, 0 degree).

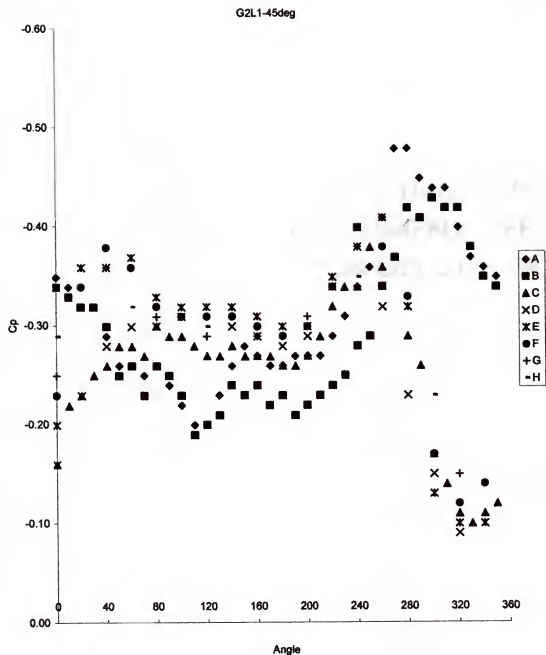


Figure 4-35. Roof mean pressure coefficients (C_p mean) for the second grouping at 45° wind direction (G2-L1, 45 degree).

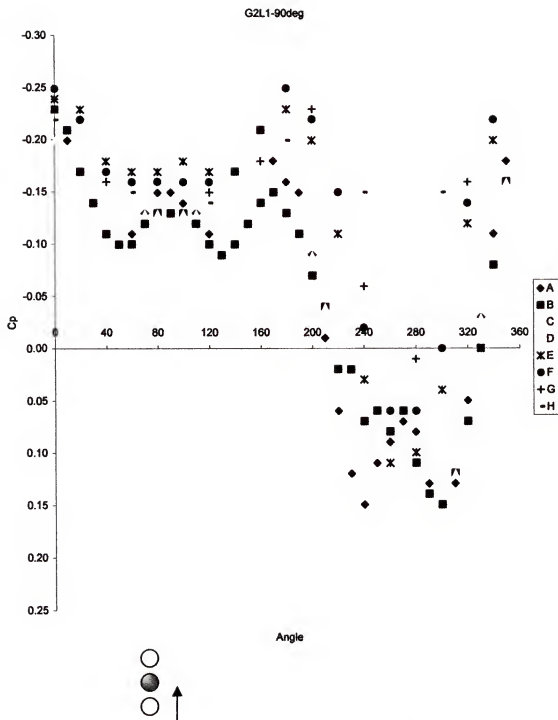


Figure 4-36. Roof mean pressure coefficients (C_p mean) for the second grouping at 90° wind direction (G2-L1, 90 degree).

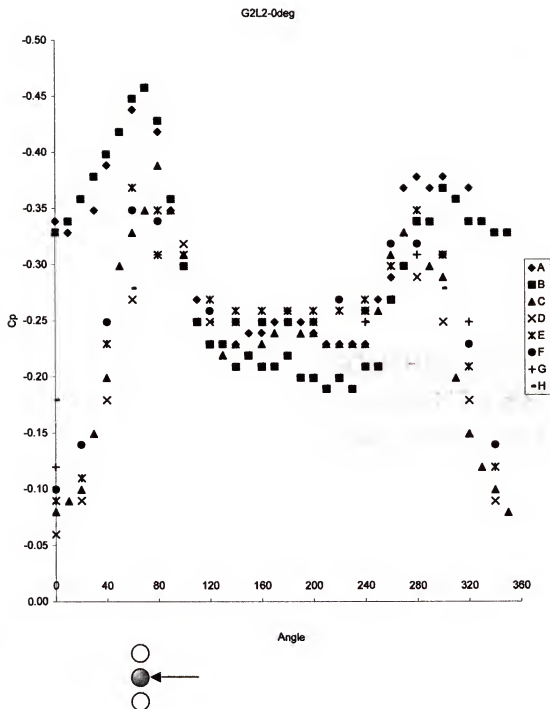


Figure 4-37. Roof mean pressure coefficients (C_p mean) for the second grouping at 0° wind direction (G2-L2, 0 degree).

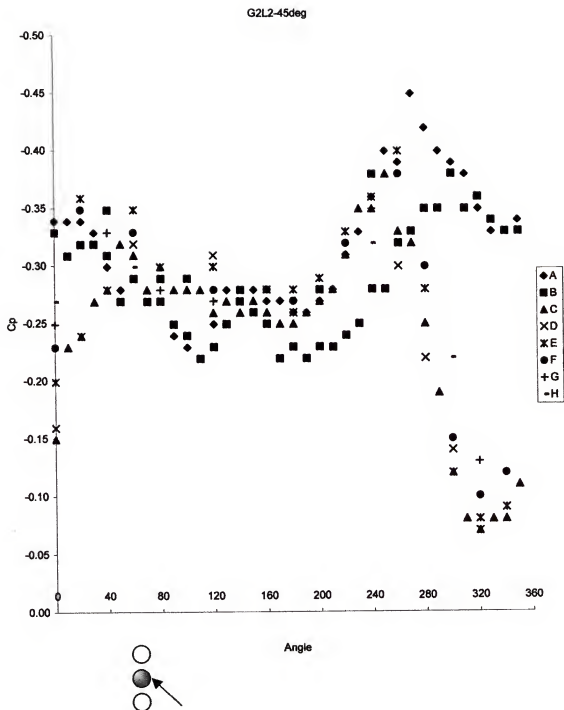


Figure 4-38. Roof mean pressure coefficients (C_p mean) for the second grouping at 45° wind direction (G2-L2, 45 degree).

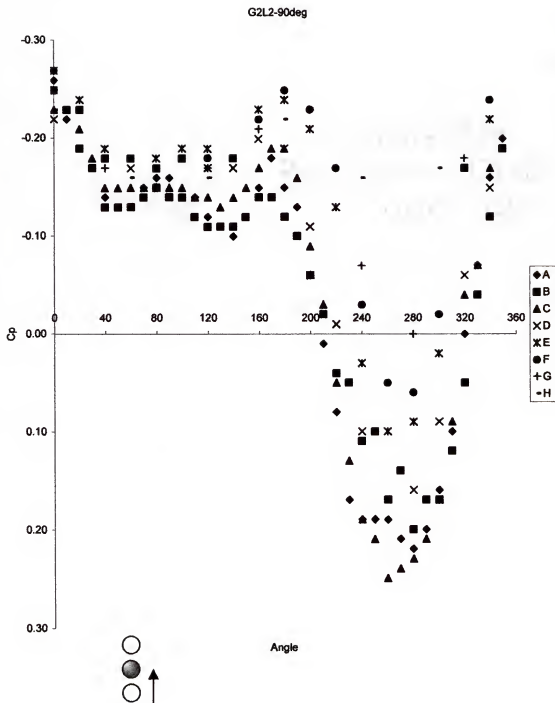


Figure 4-39. Roof mean pressure coefficients (C_p mean) for the second grouping at 90° wind direction (G2-L2, 90 degree).

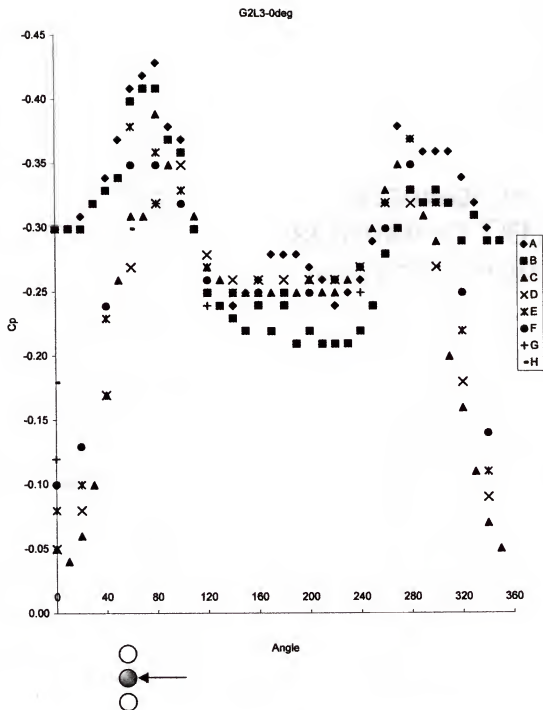


Figure 4-40. Roof mean pressure coefficients (C_p mean) for the second grouping at 0° wind direction (G2-L3, 0 degree).

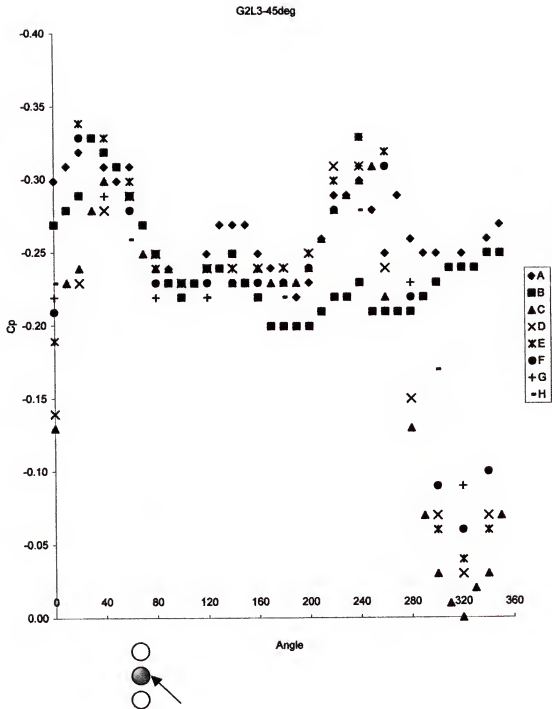


Figure 4-41. Roof mean pressure coefficients (C_p mean) for the second grouping at 45° wind direction (G2-L3, 45 degree).

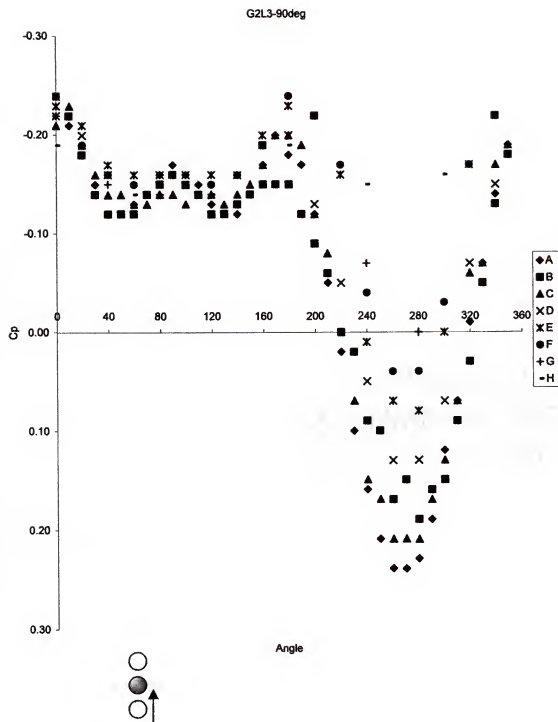


Figure 4-42. Roof mean pressure coefficients (C_p mean) for the second grouping at 90° wind direction (G2-L3, 90 degree).

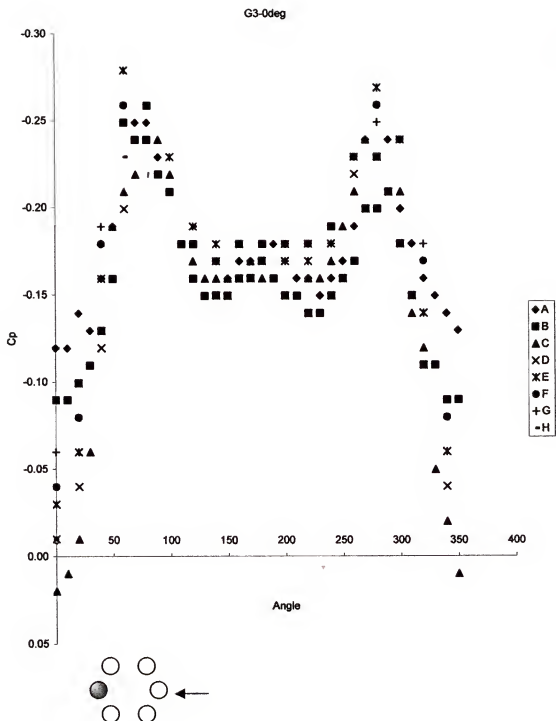


Figure 4-43. Roof mean pressure coefficients (C_p mean) for the third grouping at 0° wind direction (G3, 0 degree).

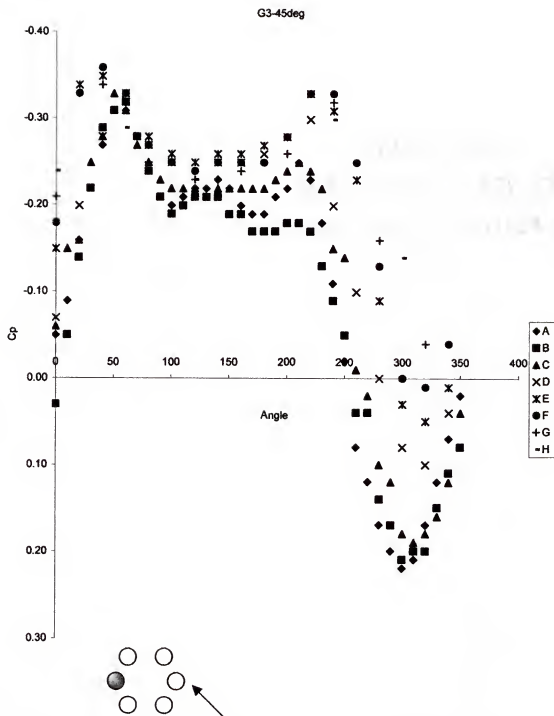


Figure 4-44. Roof mean pressure coefficients (C_p mean) for the third grouping at 45° wind direction (G3, 45 degree).

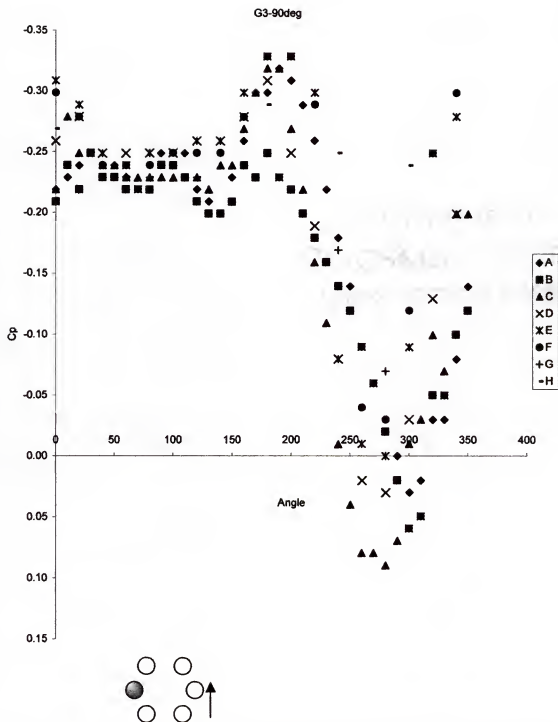


Figure 4-45. Roof mean pressure coefficients (C_p mean) for the third grouping at 90° wind direction (G3, 90 degree).

Full-Scale Tests

Full-scale measurements of the surface pressures on the wall and the roof of a typical grain bin were made under natural wind conditions in Gainesville, Florida. Wind pressure, wind speed, and wind direction data were collected to obtain pressure coefficients that represented the ratio of pressure at a point on the bin wall/roof surfaces divided by the free-stream wind dynamic pressure at the mean roof height of the structure. Wind and pressure data were recorded at 100 samples per second. Pressure coefficient data for each pressure tap point were then derived from wind pressure over 3.0 seconds. This yielded the variation of wind pressure coefficient with wind direction. Hence, it was possible to obtain the wind pressure coefficient for each tap location at any direction angle to the surface from pressure tap data. The measured mean wind directions were typically within a range of typically $\pm 20^\circ$ during a 15 minute recording period while wind velocities were in the range of 2 m/s to 16 m/s. Average turbulence intensity for the full-scale tests were 0.38, and average Reynolds number was in the order of 7×10^5 .

As discussed in detail in Chapter 3 of this dissertation, wind speed and wind direction were recorded in 15-minute segments, and then the data were filtered based on the average speeds recorded during tests. Typical wind speed and wind direction data obtained in one of the experiments for a 15-minute interval are shown in Figures 4-46 and 47, respectively. These figures were obtained by converting the raw data at 100 data points per second to 1 sample per second (average of each 100 data points). Wind direction angle was given with respect to north (compass north direction), assuming clockwise direction positive (+). These wind speed and data were then used for pressure coefficient calculations.

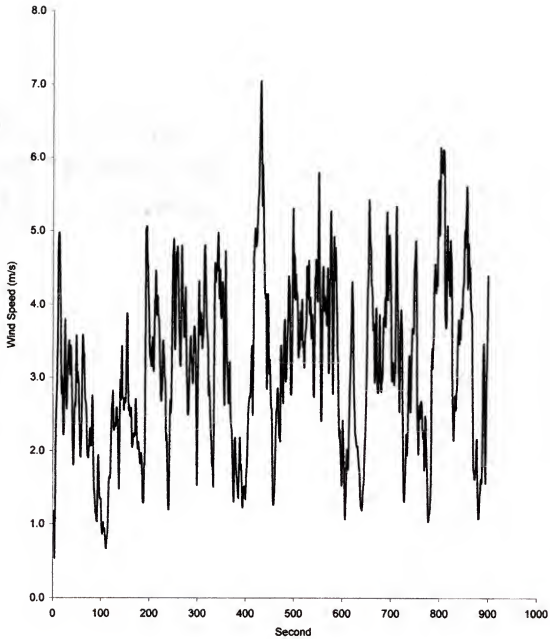


Figure 4-46. A sample of 15-minute wind speed data obtained under natural wind conditions at the field.

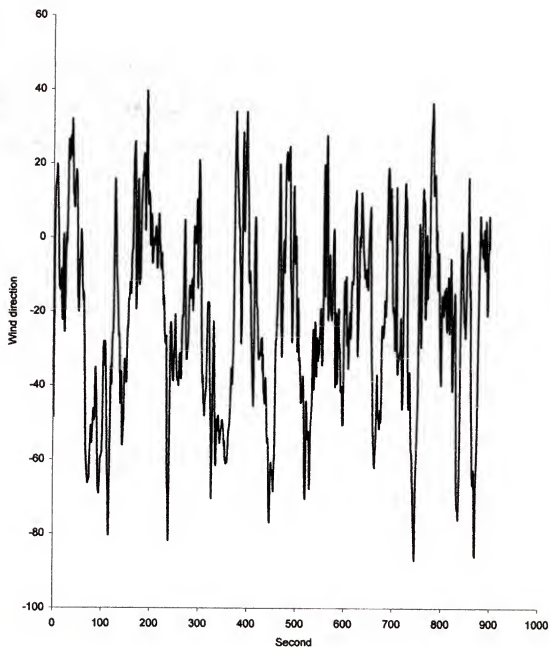


Figure 4 47. A sample of 15-minute wind direction data obtained under natural wind conditions at the field.

Wall Pressure Coefficients

Mean wall pressure coefficients were determined for nine pressure taps located at the mid-height of the wall at 40° apart from each other around the circumference. All the pressure coefficients were normalized based on the velocity pressure at mean sidewall height. The raw C_p mean values obtained from the tests (data segments that were included in the analysis) for the bin wall are presented in Table 4-2. It should be noted that these C_p mean values were not adjusted to the normal (north direction) representing the angle attack of wind with respect to compass north. However, the C_p mean values were later adjusted to normal with respect to their tap location, and then those were averaged to have the representation of the final C_p mean values on the wall (Figure 4-48). As seen in Figure 4-48, the C_p mean values were measured all in the positive (+) range around the circumference while those were recorded as positive for only 1/3 of the wall circumference of the model bins in wind tunnel experiments. This might be attributed to the differences in flow conditions, and the difference of roughness elements on the model walls. The wall of the full-scale bin was constructed from galvanized steel sheet with 101.6 mm (4") wide and 11.1 mm deep (7/16") corrugation pattern. Full-scale bin wall corrugations were horizontal to the ground. However, vertically placed ridges that were also accounted for wall stiffeners achieved the model bin wall surface roughness. These surface differences can affect the flow around the structure and Reynolds number. The highest C_p mean on the wall was approximately 1.05 at both 40° and 200° of the circumference with respect to normal while the smallest C_p mean was approximately 0.60 at 120° and 280° of the wall circumference. Furthermore, the highest positive pressure

Table 4-2. Mean wall pressure coefficients for the full-scale bin.

Wind Angle	Tap 1	Tap 2	Tap 3	Tap 4	Tap 5	Tap 6	Tap 7	Tap 8	Tap 9
58.909	0.735	0.862	1.086	0.906	0.710	0.780	1.168	0.738	0.656
60.831	0.938	1.048	1.317	1.134	0.918	0.961	1.440	0.925	0.836
60.977	0.486	0.616	0.815	0.674	0.458	0.548	0.850	0.499	0.421
62.804	0.720	0.864	1.114	0.921	0.694	0.780	1.176	0.731	0.662
63.935	1.009	1.119	1.427	1.247	0.971	1.038	1.566	0.996	0.906
66.376	0.441	0.577	0.766	0.616	0.411	0.514	0.785	0.455	0.385
67.126	0.754	0.831	1.091	0.977	0.749	0.761	1.191	0.744	0.655
71.138	0.622	0.755	0.965	0.797	0.603	0.686	1.019	0.632	0.571
72.065	0.815	1.054	1.276	1.026	0.747	0.940	1.390	0.796	0.669
73.363	0.526	0.667	0.871	0.724	0.508	0.603	0.921	0.543	0.377
73.722	0.932	1.238	1.588	1.287	0.882	1.107	1.675	0.977	0.854
74.756	0.497	0.661	0.873	0.699	0.463	0.584	0.909	0.527	0.441
75.448	0.528	0.655	0.896	0.757	0.495	0.586	0.929	0.552	0.453
75.482	0.697	0.840	1.040	0.849	0.683	0.765	1.117	0.712	0.637
76.817	0.737	0.890	1.131	0.946	0.704	0.804	1.221	0.734	0.663
82.664	0.510	0.632	0.838	0.700	0.486	0.558	0.883	0.526	0.401
83.391	0.651	0.861	1.078	0.834	0.604	0.763	1.127	0.671	0.610
83.446	0.541	0.777	0.956	0.722	0.503	0.666	0.995	0.583	0.678
94.050	0.464	0.608	0.793	0.634	0.432	0.537	0.823	0.485	0.381
96.069	0.961	1.137	1.371	1.147	0.924	1.034	1.517	0.953	0.870
116.955	0.652	0.916	1.111	0.867	0.559	0.809	1.204	0.654	0.641
164.097	0.791	1.081	1.198	0.918	0.631	0.936	1.326	0.707	0.670
204.553	0.904	0.938	0.981	0.881	0.815	0.912	1.213	0.867	0.932
206.856	0.991	1.167	1.223	1.044	0.958	1.105	1.541	1.008	0.883
208.717	1.012	1.184	1.252	1.065	1.005	1.120	1.551	1.044	0.919
210.342	0.853	1.014	1.066	0.905	0.846	0.955	1.340	0.895	0.774
211.843	0.816	0.970	1.026	0.871	0.834	0.909	1.268	0.878	0.788
213.353	0.869	1.046	1.103	0.935	0.879	0.966	1.364	0.942	0.810
214.830	0.885	1.047	1.103	0.944	0.884	0.984	1.375	0.938	0.841
219.268	1.040	1.226	1.292	1.101	1.044	1.133	1.593	1.091	0.957
261.540	0.572	1.104	1.100	0.723	0.318	0.848	1.247	0.507	0.621
275.755	0.499	0.987	1.003	0.659	0.228	0.764	1.135	0.443	0.563
278.360	0.444	0.754	0.761	0.502	0.295	0.580	0.844	0.398	0.439
309.135	0.823	0.960	0.942	0.842	0.825	0.814	1.088	0.855	0.817
309.948	0.914	1.134	1.076	0.923	0.925	0.899	1.242	0.961	0.958
312.382	0.892	1.040	1.032	0.907	0.889	0.890	1.178	0.937	0.956
315.011	0.959	1.145	1.086	0.960	0.945	0.943	1.266	0.971	0.967
320.876	0.803	0.988	0.961	0.822	0.807	0.804	1.088	0.845	0.856

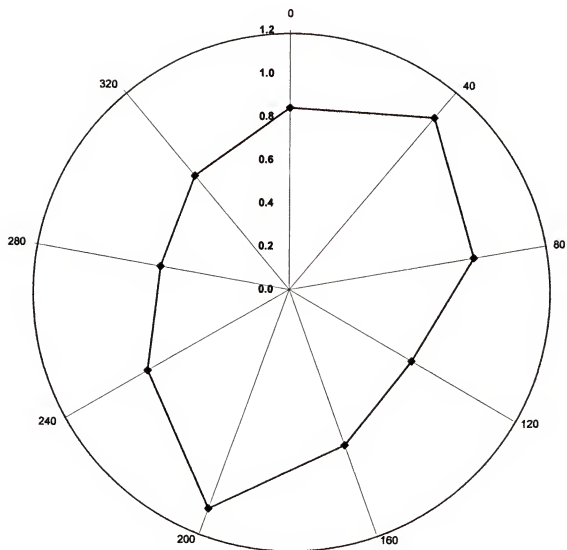


Figure 4-48. Mean wall pressure coefficients (C_p mean) for the full-scale bin.

was observed at around 0° on the model bin, which was in the range of 0.4 for both rough and smooth walls. The differences in magnitude might be due to the fact that all wind tunnel data were converted to ASCE-7 recommended 3-sec gust speed by dividing the original values by 2.34.

Roof Pressure Coefficients

Roof pressure coefficients for the full-scale bin were measured at three levels on the 30° conical roof. A total of 24 pressure taps were placed on the roof; six of the taps at the top level, nine taps at the mean roof height, and nine taps at the bottom level. The same data analysis procedure as for the wall pressure coefficients was repeated for the roof pressure coefficients. The raw mean pressure coefficients (not adjusted to the normal wind direction) obtained from the selected portions of wind pressure and speed data were presented in Tables 4-3 through 4-5; for top, middle, and bottom levels, respectively. These pressures were derived based on the dynamic velocity pressures at mean roof height of the full-scale bin.

After obtaining the raw mean roof pressure coefficients, C_p mean values were then averaged and normalized to the wind direction and tap locations for each tap level. Figure 4-49 shows the mean pressure coefficients at three levels of the full-scale roof averaged from 38 sets of wind pressure, speed, and direction data. As it can be seen in Figure 4-49, the pressure distribution showed similar behavior at bottom and middle height levels of the full-scale bin roof, while those were slightly different at the top level. The highest magnitudes of mean pressure coefficients were measured at 40° and 240° around the roof for the bottom and the middle levels. However, for the top level, highest magnitudes of mean pressure coefficients were measured at 120° on the roof.

Furthermore, middle level C_p mean values were bigger than those for the bottom and top levels of the bin roof. This can be attributed to the wind flow on the roof being less turbulent on the edges causing less suction effect while higher suction might occur at the middle of the roof.

Contour maps of mean pressure coefficient data ($C_{p,mean}$) were plotted for the full-scale 30° roof. This contour plot is presented in Appendix A along with the other roof data obtained from wind tunnel experiments.

The pressure coefficient results obtained from full-scale tests were higher than those obtained from the 30° conical roof model bin. The magnitudes of C_p mean values were almost doubled in full-scale bin results. However, it should be considered that the wind tunnel presented here were converted to 3-sec gust wind speed system dividing the original C_p values by 2.34, a procedure recommended by ASCE-7 (ASCE 1998) for wind tunnel experiments. Ignoring the conversion factor would bring the wind tunnel C_p values in close range to the full-scale ones. It was assumed that the speed-average time conversion factor can be applied to the wind tunnel experiments, but the results from full-scale experiments suggested that the original values obtained based on mean wind speeds were closer to the real situations. In addition, the number of pressure taps on the roof, flow conditions, and surface material were also different for two test procedures.

Table 4-3. Mean roof pressure coefficients at the top level of the full-scale bin.

Wind Angle	Tap 1	Tap 2	Tap 3	Tap 4	Tap 5	Tap 6
48.909	-0.613	-0.456	-0.604	-0.728	-0.598	-0.656
50.831	-0.773	-0.569	-0.744	-0.904	-0.750	-0.832
50.977	-0.429	-0.280	-0.467	-0.530	-0.597	-0.430
52.804	-0.602	-0.443	-0.621	-0.723	-0.597	-0.646
53.935	-0.839	-0.598	-0.821	-0.976	-0.807	-0.878
56.376	-0.394	-0.259	-0.427	-0.486	-0.552	-0.394
57.126	-0.629	-0.435	-0.644	-0.746	-0.829	-0.652
61.138	-0.518	-0.382	-0.534	-0.628	-0.516	-0.556
62.065	-0.723	-0.462	-0.720	-0.895	-0.955	-0.670
63.363	-0.470	-0.318	-0.494	-0.570	-0.628	-0.470
63.722	-0.880	-0.521	-0.917	-1.036	-1.155	-0.806
64.756	-0.463	-0.308	-0.491	-0.552	-0.619	-0.434
65.448	-0.480	-0.310	-0.518	-0.569	-0.636	-0.463
65.482	-0.588	-0.451	-0.572	-0.693	-0.573	-0.631
66.817	-0.626	-0.433	-0.637	-0.757	-0.619	-0.647
72.664	-0.457	-0.306	-0.477	-0.541	-0.603	-0.447
73.391	-0.563	-0.417	-0.574	-0.684	-0.562	-0.582
73.446	-0.518	-0.367	-0.514	-0.614	-0.687	-0.487
84.050	-0.419	-0.289	-0.441	-0.497	-0.557	-0.406
86.069	-0.805	-0.591	-0.767	-0.947	-0.778	-0.836
106.955	-0.637	-0.363	-0.668	-0.781	-0.848	-0.496
154.097	-0.737	-0.410	-0.702	-0.902	-0.973	-0.574
194.553	-0.751	-0.455	-0.570	-0.790	-0.634	-0.708
196.856	-0.803	-0.609	-0.678	-0.964	-0.912	-1.019
198.717	-0.807	-0.630	-0.686	-0.965	-0.843	-0.998
200.342	-0.677	-0.531	-0.580	-0.806	-0.719	-0.845
201.843	-0.663	-0.518	-0.560	-0.787	-0.698	-0.848
203.353	-0.692	-0.540	-0.597	-0.829	-0.726	-0.877
204.830	-0.723	-0.554	-0.609	-0.864	-0.799	-0.935
209.268	-0.834	-0.649	-0.711	-0.995	-0.873	-1.057
251.540	-0.670	-0.244	-0.787	-0.812	-0.942	-0.248
265.755	-0.605	-0.189	-0.730	-0.736	-0.861	-0.193
268.360	-0.541	-0.229	-0.475	-0.534	-0.609	-0.237
299.135	-0.782	-0.628	-0.650	-0.824	-0.742	-0.775
299.948	-0.736	-0.626	-0.615	-0.785	-0.714	-0.744
302.382	-0.860	-0.688	-0.709	-0.897	-0.802	-0.835
305.011	-0.903	-0.739	-0.746	-0.948	-0.854	-0.871
310.876	-0.759	-0.646	-0.642	-0.813	-0.737	-0.764

Table 4-4. Mean roof pressure coefficients at the middle level of the full-scale bin.

Wind angle	Tap 1	Tap 2	Tap 3	Tap 4	Tap 5	Tap 6	Tap 7	Tap 8	Tap 9
48.909	-0.608	-0.582	-0.725	-0.982	-0.719	-0.389	-0.920	-0.721	-0.814
50.831	-0.766	-0.716	-0.902	-1.200	-0.884	-0.505	-1.129	-0.901	-1.011
50.977	-0.403	-0.431	-0.507	-0.772	-0.554	-0.197	-0.888	-0.507	-0.589
52.804	-0.599	-0.579	-0.732	-1.007	-0.733	-0.364	-0.936	-0.717	-0.812
53.935	-0.808	-0.764	-0.965	-1.316	-0.970	-0.513	-1.239	-0.973	-1.093
56.376	-0.370	-0.400	-0.466	-0.713	-0.507	-0.180	-0.825	-0.464	-0.540
57.126	-0.598	-0.569	-0.730	-1.025	-0.756	-0.346	-1.015	-0.726	-0.825
61.138	-0.515	-0.504	-0.632	-0.871	-0.632	-0.312	-0.808	-0.619	-0.704
62.065	-0.669	-0.775	-0.787	-1.234	-0.868	-0.340	-1.478	-0.823	-0.972
63.363	-0.432	-0.453	-0.552	-0.817	-0.585	-0.226	-0.932	-0.550	-0.638
63.722	-0.771	-0.845	-0.966	-1.520	-1.106	-0.348	-1.770	-1.001	-1.175
64.756	-0.402	-0.446	-0.531	-0.811	-0.578	-0.191	-0.949	-0.533	-0.627
65.448	-0.430	-0.449	-0.549	-0.838	-0.603	-0.202	-0.956	-0.551	-0.642
65.482	-0.581	-0.553	-0.702	-0.932	-0.676	-0.390	-0.867	-0.691	-0.781
66.817	-0.610	-0.621	-0.731	-1.054	-0.765	-0.347	-1.011	-0.736	-0.840
72.664	-0.416	-0.436	-0.525	-0.785	-0.561	-0.209	-0.899	-0.527	-0.615
73.391	-0.545	-0.576	-0.676	-0.967	-0.687	-0.322	-0.933	-0.670	-0.770
73.446	-0.442	-0.512	-0.583	-0.879	-0.608	-0.245	-1.041	-0.596	-0.700
84.050	-0.377	-0.405	-0.483	-0.732	-0.519	-0.189	-0.837	-0.484	-0.567
86.069	-0.780	-0.773	-0.923	-1.264	-0.911	-0.509	-1.203	-0.938	-1.063
106.955	-0.514	-0.689	-0.628	-1.117	-0.768	-0.191	-1.385	-0.693	-0.837
154.097	-0.617	-0.832	-0.680	-1.207	-0.833	-0.247	-1.545	-0.767	-0.940
194.553	-0.726	-0.755	-0.647	-0.984	-0.728	-0.466	-1.134	-0.727	-0.954
196.856	-0.791	-0.829	-0.914	-1.145	-0.834	-0.657	-1.376	-0.981	-1.066
198.717	-0.819	-0.840	-0.903	-1.155	-0.841	-0.688	-1.347	-0.991	-1.047
200.342	-0.687	-0.717	-0.762	-0.983	-0.709	-0.589	-1.164	-0.855	-0.890
201.843	-0.666	-0.681	-0.744	-0.941	-0.691	-0.569	-1.106	-0.822	-0.872
203.353	-0.700	-0.736	-0.773	-1.011	-0.735	-0.593	-1.192	-0.873	-0.914
204.830	-0.713	-0.738	-0.818	-1.022	-0.746	-0.603	-1.215	-0.888	-0.962
209.268	-0.848	-0.870	-0.934	-1.193	-0.873	-0.703	-1.395	-1.023	-1.093
251.540	-0.405	-0.904	-0.434	-1.267	-0.814	0.113	-1.810	-0.639	-0.871
265.755	-0.335	-0.809	-0.349	-1.157	-0.735	0.136	-1.672	-0.561	-0.773
268.360	-0.321	-0.569	-0.344	-0.811	-0.526	-0.020	-1.093	-0.438	-0.592
299.135	-0.808	-0.802	-0.853	-0.985	-0.800	-0.645	-1.004	-0.809	-0.949
299.948	-0.776	-0.772	-0.854	-0.940	-0.765	-0.616	-0.960	-0.774	-0.904
302.382	-0.874	-0.881	-0.904	-1.079	-0.873	-0.692	-1.105	-0.881	-1.053
305.011	-0.928	-0.940	-0.962	-1.143	-0.923	-0.729	-1.168	-0.933	-1.100
310.876	-0.792	-0.793	-0.863	-0.984	-0.792	-0.633	-0.994	-0.808	-0.934

Table 4-5. Mean roof pressure coefficients at the bottom level of the full-scale bin.

Wind Angle	Tap 1	Tap 2	Tap 3	Tap 4	Tap 5	Tap 6	Tap 7	Tap 8	Tap 9
48.909	-0.586	-0.619	-0.664	-0.756	-0.519	-0.506	-0.576	-0.589	-0.672
50.831	-0.752	-0.758	-0.793	-0.943	-0.649	-0.644	-0.711	-0.931	-0.819
50.977	-0.362	-0.452	-0.595	-0.582	-0.358	-0.305	-0.406	-0.627	-0.509
52.804	-0.564	-0.620	-0.707	-0.770	-0.518	-0.487	-0.575	-0.586	-0.682
53.935	-0.798	-0.823	-0.897	-1.038	-0.709	-0.674	-0.764	-1.033	-0.892
56.376	-0.325	-0.419	-0.546	-0.533	-0.327	-0.287	-0.375	-0.579	-0.472
57.126	-0.586	-0.608	-0.720	-0.807	-0.544	-0.465	-0.569	-0.851	-0.681
61.138	-0.487	-0.543	-0.616	-0.664	-0.444	-0.422	-0.494	-0.505	-0.591
62.065	-0.588	-0.775	-0.959	-0.937	-0.562	-0.564	-0.673	-1.042	-0.844
63.363	-0.413	-0.487	-0.605	-0.622	-0.390	-0.341	-0.432	-0.667	-0.538
63.722	-0.696	-0.877	-1.201	-1.184	-0.696	-0.587	-0.804	-1.218	-0.987
64.756	-0.385	-0.494	-0.643	-0.623	-0.377	-0.325	-0.429	-0.662	-0.540
65.448	-0.406	-0.492	-0.637	-0.641	-0.395	-0.325	-0.438	-0.678	-0.550
65.482	-0.574	-0.608	-0.620	-0.727	-0.498	-0.499	-0.548	-0.564	-0.639
66.817	-0.555	-0.649	-0.772	-0.799	-0.519	-0.495	-0.594	-0.771	-0.715
72.664	-0.399	-0.467	-0.591	-0.604	-0.375	-0.326	-0.419	-0.640	-0.519
73.391	-0.497	-0.614	-0.717	-0.723	-0.466	-0.464	-0.547	-0.706	-0.663
73.446	-0.433	-0.570	-0.693	-0.680	-0.414	-0.390	-0.470	-0.728	-0.593
84.050	-0.360	-0.446	-0.555	-0.561	-0.347	-0.297	-0.386	-0.593	-0.485
86.069	-0.763	-0.831	-0.871	-0.984	-0.669	-0.668	-0.743	-0.769	-0.874
106.955	-0.409	-0.698	-0.982	-0.841	-0.461	-0.434	-0.571	-0.936	-0.754
154.097	-0.460	-0.773	-1.033	-0.905	-0.494	-0.528	-0.661	-1.060	-0.858
194.553	-0.670	-0.758	-0.669	-0.787	-0.542	-0.639	-0.632	-0.803	-0.795
196.856	-0.844	-0.858	-0.915	-0.924	-0.634	-0.796	-0.776	-1.022	-0.831
198.717	-0.822	-0.853	-0.871	-0.921	-0.644	-0.810	-0.786	-1.026	-0.844
200.342	-0.699	-0.732	-0.746	-0.785	-0.542	-0.691	-0.674	-0.882	-0.718
201.843	-0.693	-0.706	-0.707	-0.763	-0.538	-0.674	-0.650	-0.850	-0.692
203.353	-0.708	-0.748	-0.770	-0.810	-0.566	-0.710	-0.694	-0.911	-0.750
204.830	-0.768	-0.771	-0.794	-0.832	-0.577	-0.725	-0.701	-0.925	-0.752
209.268	-0.860	-0.887	-0.899	-0.957	-0.675	-0.834	-0.811	-1.066	-0.884
251.540	-0.148	-0.829	-1.136	-0.922	-0.376	-0.316	-0.566	-1.069	-0.873
265.755	-0.191	-0.762	-1.151	-0.832	-0.321	-0.268	-0.501	-0.975	-0.808
268.360	-0.191	-0.550	-0.826	-0.592	-0.276	-0.254	-0.384	-0.679	-0.577
299.135	-0.746	-0.837	-0.742	-0.831	-0.644	-0.706	-0.713	-0.727	-0.810
299.948	-0.723	-0.808	-0.704	-0.786	-0.615	-0.670	-0.691	-0.708	-0.781
302.382	-0.805	-0.930	-0.839	-0.917	-0.707	-0.772	-0.771	-0.787	-0.888
305.011	-0.853	-0.982	-0.876	-0.963	-0.745	-0.813	-0.822	-0.826	-0.944
310.876	-0.733	-0.828	-0.744	-0.818	-0.635	-0.694	-0.704	-0.724	0.803

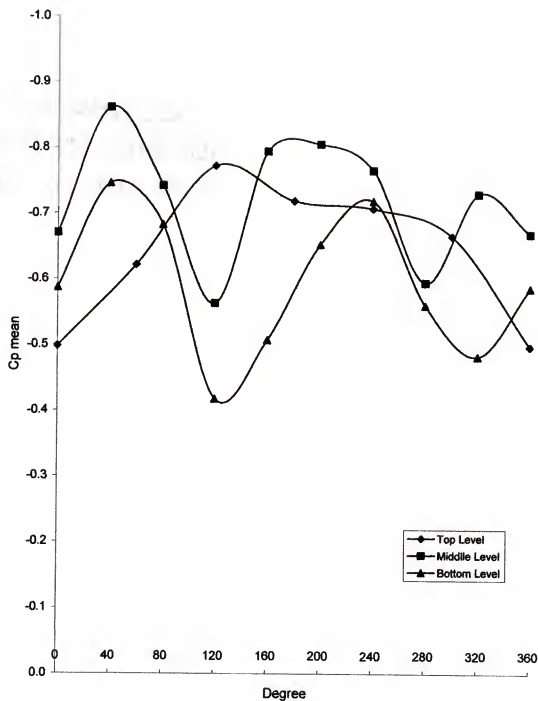


Figure 4-49. Mean roof pressure coefficients (C_p mean) for the full-scale bin.

CHAPTER 5

SUMMARY AND CONCLUSIONS

An experimental study was conducted to determine the effects of wind-induced pressures on the walls and the roofs of grain bin structures. The main objective of this research was to establish wind pressure distributions and thus pressure coefficients due to wind loading for grain bins with conical roofs. To achieve this goal, a series of wind tunnel experiments were conducted with model bins with various sloped roofs and aspect ratios. In addition, the effects of bin groupings were also investigated by running experiments with various types of bin grouping configurations and different wind flow directions. A full-scale bin was constructed in the field and the wind pressure measurements were implemented with necessary instrumentation under natural wind flow conditions. At the end of experiments, pressure coefficient data (C_p) were available for the walls and conical roofs of both model and full-scale bins.

Based on the data collected and analyzed during wind tunnel model and full-scale field experiments, the following summarized results and conclusions were drawn from this study.

Model bins:

1. Wall pressure coefficients for the single model bin with smooth and rough surfaces obtained from wind tunnel experiments show that the type of surface affected the pressure distribution on the roof. However, in spite of the fact that they were statistically different, pressure distributions showed similar behavior for

both surfaces. As expected for a round shape, flow separation points were more pronounced on the smooth surface wall than the rough wall. Both positive and negative mean pressure coefficients (C_p) were measured on both wall surfaces of a single unit. Only a 80° portion of the wall was in the positive pressure region while negative pressure coefficients were measured on the remaining part. ASCE-7 adjusted pressure coefficients (original values divided by 2.34 to reach 3-sec gust speed base) were in the range of -0.75 to $+0.40$.

2. Roof pressure coefficients for the single grain bin were determined for various roof slopes in a boundary layer wind tunnel. Contour plots showing pressure distribution on the roof were plotted. The C_p values were calculated for 25° , 30° , 35° , and 40° conical roofs at eight different height levels on both smooth and rough roof surfaces. It has been observed that the pressure distribution and pressure coefficients were affected by the roof surface. In addition, the pressure coefficients changed with different roof slopes. Changes in conical roof slope had significant effect on pressure distribution and behavior on the roof surface, which resulted in different C_p values for each conical roof slope. Roof surface changes affected flow separation zones, which resulted in differences among the roof tap location levels. Furthermore, the magnitudes of C_p mean values were higher on smooth surface roofs than those on rough surface roofs. As the roof slope increased from 25° to 40° , higher negative (-) C_p values were observed. The slope increase resulted in positive (+) pressure zones on the small portions of the roof. The C_p mean values changed from -0.5 to $+0.1$ for the conical roofs.

3. To determine the effects of aspect ratio (H/D) changes of the bin, further wind tunnel experiments were conducted with a single bin unit. Pressure ratios were determined on a 30° roof with aspect ratios of 1.0, 1.5, and 2.5. C_p values were only measured at the roof level, and for two different roof surfaces; smooth and rough. It has been observed that the changes in aspect ratio of a bin have significant effects on the pressure distribution on the roof. Thus, different C_p values were measured on the conical roofs of three different aspect ratio bins.
4. Grain bins usually are built within groups of other storage bins. It is known that the surrounding bins affect the flow and pressure distribution on a bin. Therefore, additional wind tunnel experiments were conducted to determine the effects of grouping. For this purpose, three different bin-grouping geometries that were believed to represent most closely real bin groupings were chosen, and wind pressure measurements were taken for 30° conical roof and bin wall. The first bin-grouping configuration consisted of six bins that were placed in two rows of three bins in-line. The second grouping was similar to the first one, but with only one row of three in-line bins. The last bin grouping consisted of six bins placed in a circular shaped configuration. Bin grouping configurations were also varied based on the spacing between bins within the groups. Moreover, each bin group configuration was tested under three different wind directions; 0° , 45° and 90° . The C_p values for the walls and the roofs of each bin configuration were calculated, and contour plots of C_p mean values were obtained for each bin roof. It was observed that the bin-grouping configuration had significant effects on the C_p values of bin walls and roofs.

5. Wall pressure coefficients were drastically affected by grouping configurations. However, the changes in C_p values were less noticeable with changing bin spacing within each grouping configuration. When wind direction changed from 0 degree to 45, and 45 to 90 degrees within each bin-grouping configuration, statistically significant differences were observed among the C_p values.
6. As for the wall pressure coefficients, the C_p values obtained from 30° conical roof for each bin grouping were remarkably different. In addition, bin spacing effects were also noticeable on the roofs of three bin groupings. However, the differences among bin spacing variations were not statistically different for the first grouping. Wind direction changes resulted in different pressure distributions on the roofs of each grouping. Therefore, different C_p values were obtained for each wind direction.

Full-scale bin:

1. In addition to wind tunnel experiments with model bins, a full-scale grain bin was constructed and instrumented to conduct field measurements under natural wind flow events. A 3.5 m high and 3.5 m in diameter bin with 30° conical roof was used for this experiments. Twenty-four pressure taps on the roof and nine pressure taps on the wall were placed and connected to pressure sensors to determine pressures and pressure distributions on the wall and roof. Wind direction and speed data were also recorded during experiments to calculate wind pressure coefficients of the wall and roof.
2. Wall pressure coefficients obtained from the full-scale bin were all in the positive pressure range (+) while negative pressure zones were recorded on the model bin

wall in wind tunnel experiments. This suggested that flow separation points were almost negligible on the full size bin, which might be due to low Reynolds numbers. The C_p mean values were within the range of + 1.05 to + 0.60 for the full-scale bin.

3. Similar to the behavior of wall pressure coefficients, only negative (-) C_p mean values were measured during full-scale experiments. Although in very small portions, (+) C_p mean values were recorded in wind tunnel experiments. In addition, the magnitudes of C_p values were higher (as on the walls) on full-scale roof than those obtained from model bins in wind tunnel experiments. Roof pressure coefficients were recorded at three height levels on the roof of full-scale bin. The results show that pressure distributions at the bottom and the middle levels were very similar while pressure distributions at the top level were slightly different. The contour plots based on the C_p mean values of the three height levels were drawn for the full-scale bin. The C_p mean values ranged between -0.86 and -0.56 at the middle level of the roof, -0.75 and -0.42 at the bottom level, and -0.77 and -0.50 at the top level.

The C_p mean values recorded during full-scale experiments were much higher than those obtained from wind tunnel experiments. These differences might be attributed to structural differences between model and full-scale bins (geometrical differences), and the differences in wind flow and its behavior. These differences can be summarized as:

1. The model bins with rough surfaces were similar to the stiffened bins because of the ridges placed on the wall and roof surfaces. However, the full-scale bin used in this study was unstiffened bin with corrugated wall sheets. In addition, the roof of full-scale roof had 10 cm overhang at the eave level while the model bins did not have that extension on their roofs.
2. Due to differences in wind speeds between field conditions and wind tunnel conditions, Reynolds number (Re) was also believed to be different in two experiment setups. The test wind velocities were higher in wind tunnel flow than the natural wind flow during full-scale experiments. The wind speed differences cause the Reynolds number change because Re is directly proportional to the wind velocities. Reynolds numbers was 5 times bigger in wind tunnel experiments than the full-scale experiments. Wind flow behavior on round-shaped surfaces is highly sensitive to small changes in Reynolds number. This can also affect the flow separation point and separation angle. In addition, wind velocities were almost constant in wind tunnel while wind flow velocities were changing (scattered) in field experiments. Turbulence intensity for the wind tunnel experiments was in the order of 0.20 (20%) at the mean roof height. For the full-scale tests, measured turbulence intensity was in the order of 0.40 (40%). The difference in turbulence intensities between full-scale and model bin experiments can cause the wind flow act differently on wall and roof surfaces. These flow behavior differences between wind tunnel and full-scale experiments resulted in different pressures on the wall and roof surfaces. Therefore, it was assumed that the differences among C_p values were also caused by these flow behavior effects.

3. It should be noted that the original measured C_p values in wind tunnel were 2.34 times higher than those presented here due to conversion from mean hourly wind speed to 3-second gust speed recommended by ASCE-7 (ASCE 2000). This constant value of wind speed conversion factor is based on the experiments conducted in various wind tunnels and in field conditions. However, each wind tunnel has different flow characteristics that can cause the conversion factor to be different than 2.34.

Comparison of the results obtained from wind tunnel experiments of this study can be made with a number of previously published works. Even though there were modeling differences, similar pressure distribution results for the cylindrical wall were reported by Sabransky and Melbourne (1987) and Macdonald et al. (1988) for a single bin. However, magnitudes of the pressure coefficients around the cylindrical wall were different. Macdonald et al. (1988) reported mean roof pressure distribution and pressure coefficients for a 25° roof with an aspect ratio of 1.0. Their mean pressure coefficients were in the range of +1.2 to -1.6, and positive pressure ratios were observed in the wind direction. The differences in magnitude of the mean pressure coefficients might be attributed to the fact that they used smooth surface models and 50 pressure taps at every 36° around the circumference of the roof. It should also be noted that an aeronautical type wind tunnel with a relatively short test section was used in their experiments.

The pressure coefficients for the cylindrical walls and the conical roofs of grain bins were obtained from the experiments conducted both with 1:60 scale model bins in a boundary layer wind tunnel and with a full-scale grain bin in the field under natural wind

conditions. It is believed that the results obtained from this study will fill the lack of information on the subject of wind loads on grain bins in design standard and codes. The wind pressure coefficients obtained from this study can be used as a guideline during structural design and analysis processes of bins especially in the high-wind-damage risk areas. Future research should focus on the different slopes of conical roof and additional full-scale tests under severe wind flow conditions. In addition, a next phase in wind tunnel experiments should include measuring the forces and overturning moments acting on the bin structure due to wind loading. It is also recommended that a complete structural analysis of grain bins under dynamic wind loading with the pressure coefficients obtained from this study should also be performed with a detailed finite element method. If it is planned to construct group(s) of grain bins, these specific bin grouping configurations should also be tested for wind pressure coefficients at least in a wind tunnel, because it was shown that bin grouping geometry had significant effects on pressure distribution and behavior.

Based on all of these results, it can be concluded that there is extensive amount of data on wind pressure coefficients for bin structures. Wind tunnel data with model bins is very extensive and should be the basis of actual design process. These data needs to be the basis in design codes and guides for grain bins. Although the full-scale bin data is qualitative and the pressure distributions were similar, there should be some limitations in actual design application of full-scale data. The full-scale data should not be used for the design applications in high wind velocity areas because C_p values were based on low Reynolds numbers. Wind tunnel data will give better estimation of wind pressures in the high wind velocity design areas.

APPENDIX A CONTOUR PLOTS OF ROOF PRESSURE COEFFICIENTS

The mean pressure coefficients obtained from single unit bin models are presented here as contour plots. The $C_{p\text{mean}}$ data for each roof was first transformed with running average method of 3-D data smoothing process. Then, contour map graphs were plotted with Sigma Plot 7 software. Figures A-1 through A-8 show the $C_{p\text{mean}}$ contour maps of single unit roofs tested in the wind tunnel. Figure A-9 shows the contour map of the roof pressure coefficients obtained from the full-scale experiments.

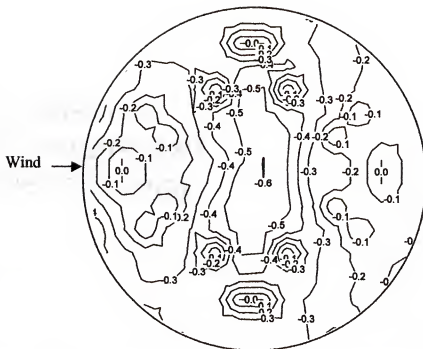


Figure A-1. Contour plot of wind pressure coefficients (C_{pmean}) for 25° smooth roof.

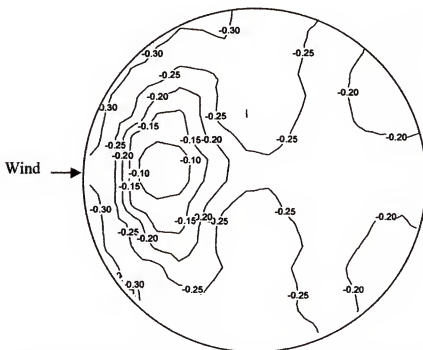


Figure A-2. Contour plot of wind pressure coefficients (C_{pmean}) for 25° rough roof.

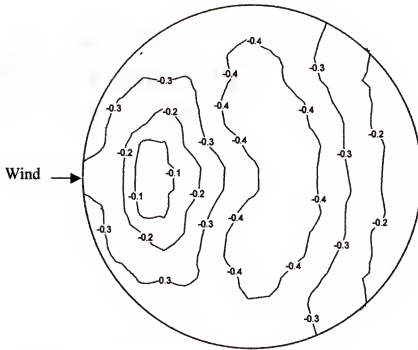


Figure A-3. Contour plot of wind pressure coefficients (C_{pmean}) for 30° smooth roof.

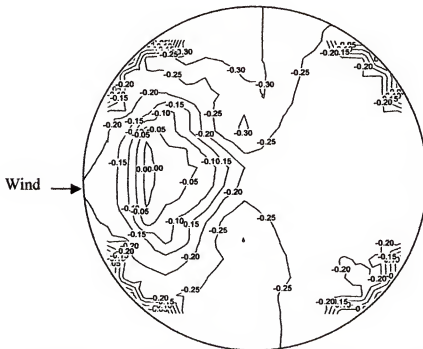


Figure A-4. Contour plot of wind pressure coefficients (C_{pmean}) for 30° rough roof.

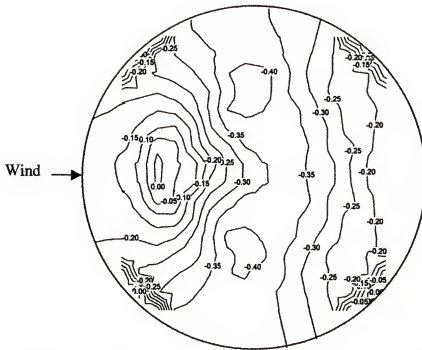


Figure A-5. Contour plot of wind pressure coefficients (C_{pmean}) for 35° smooth roof.

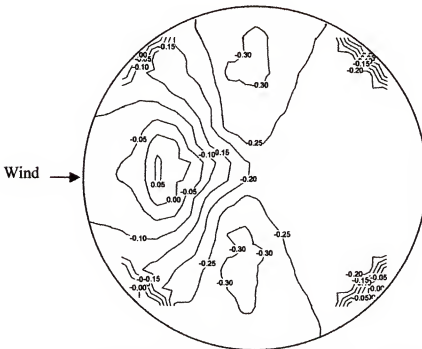


Figure A-6. Contour plot of wind pressure coefficients (C_{pmean}) for 35° rough roof.

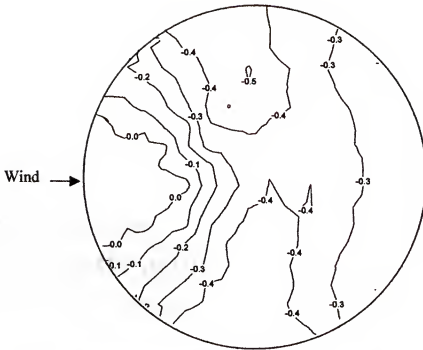


Figure A-7. Contour plot of wind pressure coefficients (C_{pmean}) for 40° smooth roof.

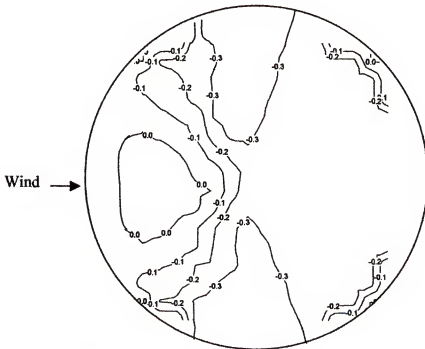


Figure A-8. Contour plot of wind pressure coefficients (C_{pmean}) for 40° rough roof.

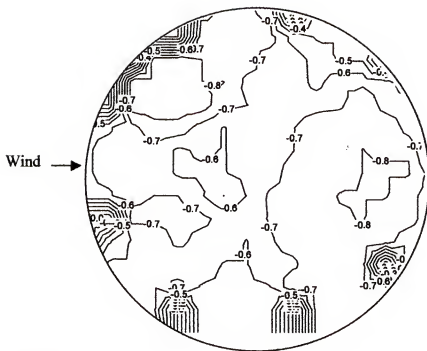


Figure A-9. Contour plot of wind pressure coefficients (C_{pmean}) for full-scale roof.

APPENDIX B PEAK AND RMS PRESSURE COEFFICIENTS

This appendix includes average pressure coefficient data for single bin roofs. The C_p values were averaged from 6-8 data sets conducted during wind tunnel experiments.

Tables B-1 through B-8 show the mean, maximum, minimum, and root-mean-square (rms) values of C_p at each pressure tap location for each roof slope. The first column shows the pressure tap, second column is the angle of wind direction, third through sixth columns show the C_p values after the 3-sec conversion applied based on ASCE 7-98. The remaining columns, seventh through tenth columns, show the C_p values obtained from wind tunnel experiments. In other words, they are the original wind tunnel data converted to the mid-roof height for each conical roof.

Table B-1. Pressure coefficient data obtained from 25° smooth roof.

Pressure tap	Degree	CpMean	CpMin	CpMax	CpRMS	CpMean	CpMin	CpMax	CpRMS
A01	0	-0.45	-1.41	0.27	0.17	-1.04	-3.29	0.64	0.39
A02	10	-0.45	-1.37	0.33	0.16	-1.04	-3.20	0.78	0.38
A03	20	-0.45	-1.32	0.32	0.16	-1.04	-3.08	0.76	0.38
A04	30	-0.44	-1.30	0.42	0.16	-1.02	-3.03	0.97	0.38
A05	40	-0.45	-1.59	0.18	0.15	-1.04	-3.72	0.43	0.36
A06	50	-0.42	-1.36	0.07	0.14	-0.97	-3.18	0.17	0.34
A07	60	-0.40	-1.42	0.06	0.13	-0.95	-3.32	0.14	0.31
A08	70	-0.40	-1.31	-0.02	0.13	-0.95	-3.06	-0.05	0.30
A09	80	-0.37	-1.07	-0.05	0.12	-0.88	-2.51	-0.12	0.28
A10	90	-0.36	-1.09	-0.07	0.12	-0.85	-2.56	-0.17	0.27
A11	100	-0.35	-1.10	-0.03	0.12	-0.83	-2.58	-0.07	0.28
A12	110	-0.31	-1.00	-0.02	0.12	-0.73	-2.35	-0.05	0.28
A13	120	-0.26	-1.02	0.03	0.11	-0.62	-2.39	0.07	0.27
A14	130	-0.19	-0.82	0.09	0.10	-0.45	-1.92	0.21	0.23
A15	140	-0.15	-0.63	0.09	0.07	-0.36	-1.47	0.21	0.16
A16	150	-0.12	-0.54	0.07	0.06	-0.28	-1.26	0.17	0.13
A17	160	-0.11	-0.45	0.07	0.05	-0.26	-1.04	0.17	0.12
A18	170	-0.11	-0.47	0.09	0.05	-0.26	-1.09	0.21	0.11
A19	180	-0.11	-0.46	0.07	0.05	-0.26	-1.07	0.17	0.11
A20	190	-0.11	-0.47	0.09	0.05	-0.26	-1.09	0.21	0.11
A21	200	-0.12	-0.46	0.12	0.05	-0.28	-1.07	0.28	0.13
A22	210	-0.12	-0.60	0.14	0.06	-0.28	-1.40	0.33	0.14
A23	220	-0.14	-0.69	0.12	0.08	-0.33	-1.61	0.28	0.18
A24	230	-0.18	-0.83	0.11	0.09	-0.43	-1.94	0.26	0.22
A25	240	-0.25	-0.87	0.07	0.12	-0.59	-2.04	0.17	0.28
A26	250	-0.30	-1.14	0.04	0.13	-0.71	-2.68	0.09	0.30
A27	260	-0.34	-1.01	-0.01	0.12	-0.81	-2.37	-0.02	0.29
A28	270	-0.35	-0.97	-0.05	0.12	-0.83	-2.27	-0.12	0.28
A29	280	-0.37	-1.04	-0.05	0.12	-0.88	-2.44	-0.12	0.28
A30	290	-0.38	-1.30	-0.02	0.13	-0.90	-3.03	-0.05	0.30
A31	300	-0.40	-1.35	0.05	0.14	-0.95	-3.15	0.12	0.33
A32	310	-0.39	-1.33	0.19	0.15	-0.92	-3.10	0.45	0.35
A33	320	-0.40	-1.51	0.29	0.15	-0.95	-3.53	0.69	0.36
A34	330	-0.44	-1.53	0.44	0.16	-1.02	-3.58	1.02	0.38
A35	340	-0.44	-1.49	0.39	0.17	-1.02	-3.48	0.92	0.40
A36	350	-0.46	-2.01	0.37	0.18	-1.07	-4.72	0.88	0.43
B01	0	-0.47	-1.65	0.34	0.18	-1.09	-3.86	0.81	0.43
B02	10	-0.47	-1.56	0.39	0.18	-1.09	-3.65	0.92	0.43
B03	20	-0.46	-1.85	0.31	0.19	-1.07	-4.34	0.73	0.44
B04	30	-0.46	-1.72	0.30	0.18	-1.07	-4.03	0.71	0.42
B05	40	-0.43	-1.45	0.19	0.17	-1.00	-3.39	0.45	0.41
B06	50	-0.39	-1.58	0.12	0.15	-0.92	-3.70	0.28	0.36
B07	60	-0.38	-1.45	0.00	0.14	-0.90	-3.39	0.00	0.33
B08	70	-0.37	-1.35	0.04	0.13	-0.88	-3.15	0.09	0.29

Table B-1. —continued.

Pressure tap	Degree	CpMean	CpMin	CpMax	CpRMS	CpMean	CpMin	CpMax	CpRMS
B09	80	-0.38	-1.24	-0.04	0.12	-0.90	-2.89	-0.09	0.29
B10	90	-0.35	-1.04	-0.07	0.11	-0.83	-2.44	-0.17	0.27
B11	100	-0.34	-0.92	-0.02	0.12	-0.81	-2.16	-0.05	0.29
B12	110	-0.32	-0.99	-0.01	0.12	-0.76	-2.32	-0.02	0.28
B13	120	-0.26	-1.12	0.05	0.11	-0.62	-2.63	0.12	0.26
B14	130	-0.20	-0.74	0.05	0.09	-0.47	-1.73	0.12	0.22
B15	140	-0.16	-0.67	0.11	0.07	-0.38	-1.56	0.26	0.18
B16	150	-0.13	-0.47	0.09	0.06	-0.31	-1.09	0.21	0.14
B17	160	-0.12	-0.46	0.10	0.05	-0.28	-1.07	0.24	0.13
B18	170	-0.11	-0.43	0.12	0.05	-0.26	-1.00	0.28	0.12
B19	180	-0.11	-0.42	0.10	0.05	-0.26	-0.97	0.24	0.12
B20	190	-0.11	-0.52	0.10	0.05	-0.26	-1.21	0.24	0.12
B21	200	-0.12	-0.44	0.12	0.05	-0.28	-1.02	0.28	0.13
B22	210	-0.12	-0.51	0.10	0.06	-0.28	-1.18	0.24	0.13
B23	220	-0.15	-0.53	0.09	0.07	-0.36	-1.23	0.21	0.15
B24	230	-0.18	-0.66	0.08	0.08	-0.43	-1.54	0.19	0.19
B25	240	-0.24	-0.78	0.03	0.10	-0.57	-1.82	0.07	0.23
B26	250	-0.29	-1.01	0.02	0.11	-0.69	-2.37	0.05	0.26
B27	260	-0.33	-0.93	-0.02	0.12	-0.78	-2.18	-0.05	0.27
B28	270	-0.34	-1.02	0.00	0.11	-0.81	-2.39	0.00	0.26
B29	280	-0.35	-0.98	0.07	0.12	-0.83	-2.30	0.17	0.27
B30	290	-0.36	-1.40	0.00	0.13	-0.85	-3.27	0.00	0.29
B31	300	-0.37	-1.37	0.06	0.14	-0.88	-3.20	0.14	0.33
B32	310	-0.40	-1.56	0.21	0.16	-0.95	-3.65	0.50	0.38
B33	320	-0.40	-1.42	0.31	0.17	-0.95	-3.32	0.73	0.39
B34	330	-0.44	-1.48	0.25	0.17	-1.02	-3.46	0.59	0.40
B35	340	-0.47	-1.66	0.47	0.18	-1.09	-3.89	1.09	0.43
B36	350	-0.47	-1.74	0.31	0.18	-1.09	-4.08	0.73	0.43
C01	0	-0.18	-1.36	0.44	0.20	-0.43	-3.18	1.02	0.46
C02	10	-0.19	-1.87	0.40	0.20	-0.45	-4.38	0.95	0.47
C03	20	-0.20	-1.56	0.39	0.19	-0.47	-3.65	0.92	0.43
C04	30	-0.22	-1.31	0.30	0.17	-0.52	-3.06	0.71	0.39
C05	40	-0.26	-1.30	0.15	0.15	-0.62	-3.03	0.36	0.34
C06	50	-0.29	-1.31	0.10	0.13	-0.69	-3.06	0.24	0.30
C07	60	-0.32	-1.18	0.06	0.12	-0.76	-2.77	0.14	0.28
C08	70	-0.34	-1.12	-0.06	0.11	-0.81	-2.63	-0.14	0.27
C09	80	-0.35	-0.96	-0.04	0.11	-0.83	-2.25	-0.09	0.26
C10	90	-0.35	-0.21	0.03	0.04	-0.21	-0.50	0.07	0.09
C11	100	-0.36	-1.03	-0.03	0.12	-0.85	-2.42	-0.07	0.28
C12	110	-0.32	-0.89	-0.02	0.11	-0.76	-2.09	-0.05	0.27
C13	120	-0.27	-0.84	0.00	0.10	-0.64	-1.97	0.00	0.24
C14	130	-0.23	-0.94	0.04	0.09	-0.55	-2.20	0.09	0.21
C15	140	-0.19	-0.58	0.06	0.07	-0.45	-1.35	0.14	0.17
C16	150	-0.17	-0.18	0.07	0.04	-0.12	-0.43	0.17	0.10
C17	160	-0.14	-0.51	0.07	0.06	-0.33	-1.18	0.17	0.13
C18	170	-0.12	-0.44	0.14	0.05	-0.28	-1.02	0.33	0.12
C19	180	-0.11	-0.47	0.13	0.05	-0.26	-1.09	0.31	0.12

Table B-1. —continued.

Pressure tap	Degree	CpMean	CpMin	CpMax	CpRMS	CpMean	CpMin	CpMax	CpRMS
C20	190	-0.12	-0.45	0.10	0.05	-0.28	-1.04	0.24	0.12
C21	200	-0.13	-0.42	0.09	0.05	-0.31	-0.97	0.21	0.12
C22	210	-0.15	-0.58	0.08	0.06	-0.36	-1.35	0.19	0.14
C23	220	-0.18	-0.61	0.05	0.07	-0.43	-1.42	0.12	0.16
C24	230	-0.22	-0.75	0.06	0.09	-0.52	-1.75	0.14	0.21
C25	240	-0.27	-0.80	0.01	0.10	-0.64	-1.87	0.02	0.24
C26	250	-0.31	-0.85	-0.03	0.11	-0.73	-1.99	-0.07	0.26
C27	260	-0.34	-0.94	-0.04	0.11	-0.81	-2.20	-0.09	0.27
C28	270	-0.36	-0.95	-0.05	0.11	-0.85	-2.23	-0.12	0.27
C29	280	-0.36	-0.97	-0.06	0.11	-0.85	-2.27	-0.14	0.26
C30	290	-0.34	-0.97	-0.03	0.11	-0.81	-2.27	-0.07	0.26
C31	300	-0.32	-1.42	0.03	0.11	-0.76	-3.32	0.07	0.27
C32	310	-0.29	-1.20	0.09	0.12	-0.69	-2.82	0.21	0.28
C33	320	-0.25	-1.17	0.22	0.14	-0.59	-2.75	0.52	0.32
C34	330	-0.24	-1.93	0.25	0.17	-0.57	-4.53	0.59	0.39
C35	340	-0.20	-1.38	0.33	0.18	-0.47	-3.22	0.78	0.42
C36	350	-0.18	-1.29	0.48	0.18	-0.43	-3.01	1.11	0.43
D01	0	-0.10	-0.51	0.23	0.06	-0.24	-1.18	0.55	0.14
D02	20	-0.14	-0.71	0.22	0.06	-0.33	-1.66	0.52	0.15
D03	40	-0.22	-0.94	0.06	0.08	-0.52	-2.20	0.14	0.19
D04	60	-0.31	-0.79	0.03	0.10	-0.73	-1.85	0.07	0.23
D05	80	-0.39	-1.03	-0.07	0.12	-0.92	-2.42	-0.17	0.28
D06	100	-0.43	-0.98	-0.07	0.14	-1.00	-2.30	-0.17	0.32
D07	120	-0.34	-0.93	-0.05	0.12	-0.81	-2.18	-0.12	0.28
D08	140	-0.26	-0.76	0.00	0.09	-0.62	-1.78	0.00	0.22
D09	160	-0.19	-0.68	0.02	0.07	-0.45	-1.59	0.05	0.16
D10	180	-0.17	-0.76	0.04	0.06	-0.40	-1.78	0.09	0.14
D11	200	-0.19	-0.76	0.09	0.07	-0.45	-1.78	0.21	0.16
D12	220	-0.25	-0.76	0.04	0.09	-0.59	-1.78	0.09	0.21
D13	240	-0.33	-0.95	-0.03	0.11	-0.78	-2.23	-0.07	0.27
D14	260	-0.38	-1.03	-0.08	0.13	-0.90	-2.42	-0.19	0.30
D15	280	-0.39	-0.99	-0.09	0.13	-0.92	-2.32	-0.21	0.30
D16	300	-0.32	-0.87	-0.05	0.11	-0.76	-2.04	-0.12	0.25
D17	320	-0.23	-0.86	0.08	0.09	-0.55	-2.01	0.19	0.21
D18	340	-0.13	-0.57	0.19	0.07	-0.31	-1.33	0.45	0.15
E01	0	-0.19	-0.58	0.11	0.07	-0.45	-1.35	0.26	0.16
E02	20	-0.21	-0.61	0.06	0.08	-0.50	-1.42	0.14	0.18
E03	40	-0.30	-0.82	0.01	0.10	-0.71	-1.92	0.02	0.24
E04	60	-0.42	-1.15	-0.08	0.14	-0.97	-2.70	-0.19	0.32
E05	80	-0.50	-1.26	-0.11	0.17	-1.16	-2.94	-0.26	0.39
E06	100	-0.51	-1.35	-0.12	0.17	-1.18	-3.15	-0.28	0.39
E07	120	-0.46	-1.39	-0.07	0.16	-1.07	-3.25	-0.17	0.37
E08	140	-0.37	-1.05	-0.01	0.13	-0.88	-2.46	-0.02	0.31
E09	160	-0.29	-0.96	0.02	0.11	-0.69	-2.25	0.05	0.25
E10	180	-0.27	-0.87	0.06	0.10	-0.64	-2.04	0.14	0.23
E11	200	-0.29	-0.96	0.01	0.10	-0.69	-2.25	0.02	0.24
E12	220	-0.37	-1.03	0.00	0.13	-0.88	-2.42	0.00	0.31

Table B-1. —continued.

Pressure tap	Degree	CpMean	CpMin	CpMax	CpRMS	CpMean	CpMin	CpMax	CpRMS
E13	240	-0.45	-1.28	-0.07	0.15	-1.04	-2.99	-0.17	0.36
E14	260	-0.50	-1.19	-0.12	0.17	-1.16	-2.80	-0.28	0.40
E15	280	-0.51	-1.27	-0.11	0.17	-1.18	-2.96	-0.26	0.40
E16	300	-0.44	-1.67	-0.03	0.15	-1.02	-3.91	-0.07	0.35
E17	320	-0.31	-0.99	0.00	0.11	-0.73	-2.32	0.00	0.26
E18	340	-0.23	-0.72	0.14	0.08	-0.55	-1.68	0.33	0.19
F01	0	-0.26	-0.85	0.07	0.08	-0.62	-1.99	0.17	0.19
F02	20	-0.30	-0.87	0.03	0.10	-0.71	-2.04	0.07	0.24
F03	40	-0.37	-1.10	-0.02	0.13	-0.88	-2.58	-0.05	0.31
F04	60	-0.49	-1.49	-0.11	0.17	-1.14	-3.48	-0.26	0.40
F05	80	-0.56	-1.61	-0.14	0.20	-1.30	-3.77	-0.33	0.46
F06	100	-0.56	-1.46	-0.11	0.20	-1.30	-3.41	-0.26	0.46
F07	120	-0.54	-1.36	-0.04	0.19	-1.26	-3.18	-0.09	0.44
F08	140	-0.50	-1.56	-0.07	0.17	-1.16	-3.65	-0.17	0.40
F09	160	-0.45	-1.19	-0.06	0.15	-1.04	-2.80	-0.14	0.35
F10	180	-0.43	-1.21	-0.04	0.13	-1.00	-2.84	-0.09	0.31
F11	200	-0.46	-1.30	-0.05	0.15	-1.07	-3.03	-0.12	0.35
F12	220	-0.51	-1.38	-0.03	0.17	-1.18	-3.22	-0.07	0.41
F13	240	-0.55	-1.40	-0.11	0.19	-1.28	-3.27	-0.26	0.45
F14	260	-0.58	-1.56	-0.13	0.21	-1.35	-3.65	-0.31	0.49
F15	280	-0.58	-1.68	-0.11	0.20	-1.35	-3.93	-0.26	0.47
F16	300	-0.52	-1.57	-0.09	0.18	-1.21	-3.67	-0.21	0.41
F17	320	-0.40	-1.34	-0.04	0.15	-0.95	-3.13	-0.09	0.34
F18	340	-0.30	-0.95	-0.02	0.10	-0.71	-2.23	-0.05	0.24
G01	0	-0.33	-0.96	-0.01	0.11	-0.78	-2.25	-0.02	0.25
G02	40	-0.45	-1.25	-0.08	0.16	-1.04	-2.91	-0.19	0.37
G03	80	-0.62	-1.89	-0.11	0.24	-1.45	-4.43	-0.26	0.55
G04	120	-0.57	-1.78	-0.11	0.21	-1.33	-4.17	-0.26	0.50
G05	160	-0.58	-1.43	-0.10	0.21	-1.35	-3.34	-0.24	0.49
G06	200	-0.55	-1.50	-0.07	0.20	-1.28	-3.51	-0.17	0.46
G07	240	-0.57	-1.72	-0.10	0.21	-1.33	-4.03	-0.24	0.49
G08	280	-0.63	-2.02	-0.12	0.24	-1.47	-4.74	-0.28	0.55
G09	320	-0.47	-1.36	-0.04	0.17	-1.09	-3.18	-0.09	0.39
H01	0	-0.47	-1.38	-0.10	0.17	-1.09	-3.22	-0.24	0.39
H02	60	-0.66	-1.99	-0.13	0.26	-1.54	-4.67	-0.31	0.61
H03	120	-0.62	-2.55	-0.11	0.26	-1.45	-5.97	-0.26	0.61
H04	180	-0.62	-1.80	-0.08	0.25	-1.45	-4.22	-0.19	0.58
H05	240	-0.63	-1.84	-0.13	0.26	-1.47	-4.31	-0.31	0.60
H06	300	-0.68	-1.94	-0.13	0.27	-1.59	-4.55	-0.31	0.63

Table B-2. Pressure coefficient data obtained from 25° rough roof.

Pressure tap	Degree	CpMean	CpMin	CpMax	CpRMS	CpMean	CpMin	CpMax	CpRMS
A01	0	-0.33	-1.14	0.46	0.14	-0.32	-1.13	0.45	0.14
A02	10	-0.33	-1.12	0.48	0.14	-0.32	-1.10	0.47	0.14
A03	20	-0.32	-1.07	0.38	0.13	-0.32	-1.06	0.38	0.13
A04	30	-0.33	-1.13	0.33	0.13	-0.32	-1.12	0.32	0.13
A05	40	-0.34	-1.10	0.29	0.13	-0.33	-1.09	0.28	0.13
A06	50	-0.33	-1.07	0.25	0.12	-0.33	-1.06	0.24	0.12
A07	60	-0.32	-1.09	0.19	0.12	-0.32	-1.07	0.19	0.11
A08	70	-0.32	-0.99	0.12	0.11	-0.31	-0.97	0.12	0.11
A09	80	-0.31	-0.94	0.09	0.10	-0.30	-0.93	0.09	0.10
A10	90	-0.30	-0.93	-0.02	0.09	-0.30	-0.92	-0.02	0.09
A11	100	-0.28	-0.78	-0.03	0.09	-0.27	-0.77	-0.03	0.09
A12	110	-0.25	-0.74	0.02	0.09	-0.25	-0.73	0.02	0.08
A13	120	-0.22	-0.77	0.03	0.08	-0.22	-0.76	0.03	0.08
A14	130	-0.20	-0.68	0.04	0.08	-0.19	-0.67	0.04	0.08
A15	140	-0.18	-0.72	0.06	0.07	-0.18	-0.72	0.06	0.07
A16	150	-0.18	-0.79	0.08	0.08	-0.18	-0.78	0.08	0.07
A17	160	-0.20	-0.89	0.07	0.08	-0.20	-0.88	0.07	0.08
A18	170	-0.21	-0.83	0.05	0.09	-0.21	-0.82	0.05	0.09
A19	180	-0.22	-0.89	0.04	0.09	-0.21	-0.88	0.04	0.09
A20	190	-0.21	-0.82	0.04	0.09	-0.21	-0.81	0.04	0.09
A21	200	-0.20	-0.97	0.09	0.09	-0.20	-0.95	0.09	0.09
A22	210	-0.19	-0.88	0.10	0.09	-0.19	-0.87	0.10	0.08
A23	220	-0.18	-0.82	0.11	0.08	-0.18	-0.81	0.10	0.08
A24	230	-0.19	-0.75	0.08	0.08	-0.19	-0.74	0.08	0.08
A25	240	-0.21	-0.74	0.08	0.08	-0.21	-0.73	0.08	0.08
A26	250	-0.24	-0.83	0.05	0.09	-0.24	-0.82	0.05	0.09
A27	260	-0.28	-0.87	0.02	0.10	-0.28	-0.86	0.02	0.10
A28	270	-0.29	-0.88	0.01	0.09	-0.28	-0.87	0.01	0.09
A29	280	-0.31	-1.04	0.10	0.10	-0.30	-1.03	0.10	0.10
A30	290	-0.29	-1.05	0.22	0.11	-0.29	-1.04	0.21	0.11
A31	300	-0.28	-1.15	0.26	0.12	-0.28	-1.14	0.26	0.12
A32	310	-0.33	-1.19	0.36	0.14	-0.32	-1.18	0.35	0.14
A33	320	-0.31	-1.13	0.44	0.14	-0.31	-1.11	0.44	0.14
A34	330	-0.32	-1.27	0.46	0.14	-0.32	-1.26	0.45	0.14
A35	340	-0.32	-1.18	0.52	0.15	-0.32	-1.16	0.51	0.14
A36	350	-0.32	-1.23	0.58	0.15	-0.32	-1.21	0.57	0.15
B01	0	-0.34	-1.28	0.51	0.16	-0.33	-1.26	0.50	0.15
B02	10	-0.33	-1.21	0.52	0.15	-0.33	-1.19	0.51	0.15
B03	20	-0.33	-1.24	0.51	0.16	-0.32	-1.22	0.50	0.16
B04	30	-0.33	-1.18	0.47	0.15	-0.33	-1.17	0.47	0.15
B05	40	-0.32	-1.28	0.49	0.16	-0.32	-1.26	0.48	0.16
B06	50	-0.30	-1.19	0.39	0.15	-0.30	-1.18	0.39	0.15
B07	60	-0.29	-1.24	0.34	0.13	-0.29	-1.23	0.34	0.13
B08	70	-0.32	-1.10	0.24	0.11	-0.31	-1.09	0.23	0.11

Table B-2. —continued.

Pressure tap	Degree	CpMean	CpMin	CpMax	CpRMS	CpMean	CpMin	CpMax	CpRMS
B09	80	-0.29	-0.94	0.14	0.10	-0.69	-2.20	0.34	0.23
B10	90	-0.28	-0.93	0.04	0.09	-0.66	-2.18	0.09	0.21
B11	100	-0.27	-0.77	0.00	0.09	-0.63	-1.80	-0.01	0.21
B12	110	-0.25	-0.74	0.02	0.09	-0.58	-1.73	0.04	0.20
B13	120	-0.22	-0.72	0.04	0.08	-0.52	-1.69	0.09	0.19
B14	130	-0.19	-0.66	0.09	0.08	-0.45	-1.55	0.20	0.18
B15	140	-0.18	-0.72	0.12	0.08	-0.43	-1.70	0.28	0.18
B16	150	-0.18	-0.74	0.13	0.08	-0.42	-1.74	0.31	0.18
B17	160	-0.19	-0.81	0.13	0.08	-0.44	-1.89	0.31	0.20
B18	170	-0.20	-0.85	0.11	0.09	-0.47	-2.00	0.27	0.21
B19	180	-0.21	-0.86	0.13	0.09	-0.49	-2.01	0.30	0.21
B20	190	-0.21	-0.84	0.13	0.09	-0.48	-1.97	0.29	0.21
B21	200	-0.19	-0.83	0.14	0.09	-0.46	-1.95	0.33	0.20
B22	210	-0.19	-0.83	0.17	0.08	-0.43	-1.94	0.39	0.19
B23	220	-0.18	-0.80	0.13	0.08	-0.42	-1.87	0.31	0.18
B24	230	-0.19	-0.67	0.11	0.08	-0.44	-1.56	0.25	0.18
B25	240	-0.21	-0.63	0.08	0.08	-0.49	-1.47	0.19	0.18
B26	250	-0.24	-0.80	0.05	0.08	-0.56	-1.87	0.12	0.20
B27	260	-0.27	-0.82	0.00	0.09	-0.64	-1.93	0.01	0.21
B28	270	-0.28	-0.85	0.03	0.09	-0.65	-1.99	0.08	0.21
B29	280	-0.29	-0.96	0.10	0.10	-0.68	-2.26	0.23	0.23
B30	290	-0.26	-1.07	0.26	0.12	-0.61	-2.50	0.61	0.27
B31	300	-0.24	-1.13	0.41	0.14	-0.57	-2.64	0.95	0.33
B32	310	-0.29	-1.25	0.50	0.17	-0.68	-2.93	1.17	0.39
B33	320	-0.29	-1.33	0.56	0.17	-0.69	-3.11	1.30	0.40
B34	330	-0.31	-1.11	0.42	0.15	-0.73	-2.61	0.98	0.35
B35	340	-0.33	-1.20	0.40	0.15	-0.77	-2.81	0.94	0.35
B36	350	-0.33	-1.12	0.44	0.15	-0.78	-2.63	1.03	0.34
C01	0	-0.15	-1.16	0.50	0.18	-0.34	-2.71	1.17	0.42
C02	10	-0.15	-1.20	0.47	0.18	-0.35	-2.81	1.09	0.42
C03	20	-0.15	-1.10	0.47	0.17	-0.36	-2.58	1.10	0.40
C04	30	-0.16	-1.14	0.46	0.16	-0.38	-2.68	1.08	0.37
C05	40	-0.19	-1.12	0.42	0.14	-0.44	-2.63	0.98	0.32
C06	50	-0.22	-1.07	0.23	0.11	-0.52	-2.51	0.54	0.26
C07	60	-0.24	-0.96	0.16	0.10	-0.57	-2.25	0.37	0.24
C08	70	-0.31	-0.96	0.03	0.10	-0.72	-2.25	0.07	0.23
C09	80	-0.28	-0.84	0.02	0.09	-0.67	-1.98	0.06	0.21
C10	90	-0.22	-0.34	-0.11	0.03	-0.53	-0.80	-0.26	0.08
C11	100	-0.27	-0.75	-0.01	0.09	-0.63	-1.75	-0.01	0.20
C12	110	-0.25	-0.73	0.00	0.08	-0.59	-1.72	0.01	0.19
C13	120	-0.22	-0.64	0.04	0.08	-0.52	-1.51	0.09	0.18
C14	130	-0.21	-0.72	0.07	0.08	-0.48	-1.67	0.16	0.18
C15	140	-0.20	-0.70	0.12	0.07	-0.46	-1.64	0.29	0.17
C16	150	-0.12	-0.22	-0.01	0.03	-0.27	-0.52	-0.03	0.07
C17	160	-0.20	-0.77	0.14	0.08	-0.46	-1.80	0.32	0.18
C18	170	-0.20	-0.76	0.11	0.08	-0.47	-1.78	0.26	0.18
C19	180	-0.20	-0.72	0.09	0.07	-0.47	-1.68	0.21	0.17

Table B-2. —continued.

Pressure tap	Degree	CpMean	CpMin	CpMax	CpRMS	CpMean	CpMin	CpMax	CpRMS
C20	190	-0.20	-0.69	0.11	0.08	-0.47	-1.61	0.26	0.18
C21	200	-0.20	-0.76	0.14	0.08	-0.47	-1.79	0.32	0.18
C22	210	-0.20	-0.77	0.12	0.08	-0.46	-1.80	0.28	0.18
C23	220	-0.20	-0.77	0.11	0.08	-0.46	-1.80	0.26	0.18
C24	230	-0.20	-0.67	0.05	0.07	-0.48	-1.56	0.11	0.17
C25	240	-0.22	-0.66	0.02	0.07	-0.51	-1.54	0.06	0.18
C26	250	-0.23	-0.67	0.03	0.08	-0.55	-1.56	0.07	0.18
C27	260	-0.27	-0.76	0.00	0.09	-0.63	-1.78	-0.01	0.20
C28	270	-0.27	-0.81	0.00	0.09	-0.64	-1.91	0.01	0.20
C29	280	-0.26	-0.86	0.08	0.08	-0.61	-2.00	0.19	0.20
C30	290	-0.28	-0.96	0.06	0.09	-0.65	-2.26	0.14	0.22
C31	300	-0.19	-1.02	0.27	0.10	-0.45	-2.38	0.64	0.23
C32	310	-0.20	-1.10	0.29	0.11	-0.47	-2.57	0.67	0.25
C33	320	-0.16	-1.10	0.43	0.13	-0.38	-2.58	1.01	0.30
C34	330	-0.14	-1.07	0.46	0.15	-0.34	-2.49	1.08	0.35
C35	340	-0.15	-1.18	0.44	0.16	-0.35	-2.77	1.03	0.38
C36	350	-0.15	-1.11	0.49	0.17	-0.34	-2.61	1.14	0.40
D01	0	-0.04	-0.60	0.35	0.06	-0.09	-1.41	0.81	0.15
D02	20	-0.07	-0.54	0.29	0.06	-0.16	-1.27	0.68	0.14
D03	40	-0.13	-0.59	0.16	0.06	-0.31	-1.39	0.38	0.13
D04	60	-0.19	-0.65	0.09	0.06	-0.44	-1.53	0.20	0.15
D05	80	-0.28	-0.81	0.01	0.09	-0.66	-1.89	0.02	0.21
D06	100	-0.28	-0.75	-0.03	0.08	-0.65	-1.75	-0.07	0.20
D07	120	-0.24	-0.68	0.02	0.08	-0.57	-1.59	0.05	0.18
D08	140	-0.22	-0.70	0.08	0.07	-0.52	-1.64	0.18	0.17
D09	160	-0.22	-0.73	0.07	0.08	-0.53	-1.71	0.17	0.18
D10	180	-0.22	-0.69	0.02	0.07	-0.52	-1.61	0.05	0.16
D11	200	-0.23	-0.76	0.09	0.08	-0.54	-1.79	0.21	0.18
D12	220	-0.23	-0.70	0.07	0.07	-0.53	-1.63	0.15	0.18
D13	240	-0.24	-0.64	0.03	0.08	-0.56	-1.51	0.07	0.18
D14	260	-0.28	-0.75	-0.01	0.09	-0.66	-1.76	-0.03	0.21
D15	280	-0.28	-0.78	0.01	0.09	-0.65	-1.82	0.02	0.22
D16	300	-0.20	-0.63	0.09	0.07	-0.47	-1.47	0.21	0.16
D17	320	-0.13	-0.59	0.18	0.06	-0.31	-1.38	0.43	0.14
D18	340	-0.07	-0.60	0.33	0.06	-0.17	-1.41	0.77	0.15
E01	0	-0.07	-0.43	0.29	0.06	-0.15	-1.00	0.67	0.13
E02	20	-0.09	-0.56	0.27	0.07	-0.21	-1.31	0.63	0.15
E03	40	-0.20	-0.70	0.19	0.10	-0.48	-1.64	0.43	0.22
E04	60	-0.29	-0.76	0.05	0.09	-0.68	-1.77	0.12	0.21
E05	80	-0.33	-0.86	-0.02	0.10	-0.76	-2.02	-0.04	0.23
E06	100	-0.30	-0.86	0.01	0.10	-0.71	-2.02	0.03	0.22
E07	120	-0.25	-0.74	0.04	0.08	-0.59	-1.72	0.08	0.20
E08	140	-0.23	-0.74	0.06	0.08	-0.53	-1.74	0.15	0.18
E09	160	-0.23	-0.70	0.03	0.07	-0.53	-1.63	0.08	0.17
E10	180	-0.22	-0.69	0.02	0.07	-0.52	-1.62	0.05	0.17
E11	200	-0.23	-0.69	0.02	0.07	-0.54	-1.61	0.05	0.17
E12	220	-0.23	-0.70	0.05	0.08	-0.53	-1.64	0.12	0.18

Table B-2. —continued.

Pressure tap	Degree	CpMean	CpMin	CpMax	CpRMS	CpMean	CpMin	CpMax	CpRMS
E13	240	-0.25	-0.72	0.03	0.08	-0.58	-1.69	0.08	0.19
E14	260	-0.30	-0.79	-0.02	0.09	-0.70	-1.85	-0.05	0.21
E15	280	-0.31	-0.79	-0.01	0.09	-0.73	-1.85	-0.02	0.21
E16	300	-0.30	-0.77	0.02	0.09	-0.70	-1.81	0.05	0.21
E17	320	-0.19	-0.65	0.18	0.09	-0.45	-1.52	0.42	0.21
E18	340	-0.09	-0.55	0.26	0.07	-0.21	-1.30	0.61	0.16
F01	0	-0.10	-0.46	0.20	0.05	-0.23	-1.08	0.48	0.12
F02	20	-0.13	-0.50	0.16	0.06	-0.31	-1.16	0.38	0.15
F03	40	-0.22	-0.67	0.07	0.08	-0.53	-1.56	0.15	0.18
F04	60	-0.30	-0.75	-0.02	0.09	-0.69	-1.76	-0.06	0.21
F05	80	-0.33	-0.87	-0.05	0.10	-0.78	-2.03	-0.12	0.23
F06	100	-0.30	-0.81	-0.01	0.09	-0.70	-1.89	-0.03	0.22
F07	120	-0.24	-0.71	0.01	0.08	-0.56	-1.66	0.02	0.18
F08	140	-0.21	-0.64	0.02	0.07	-0.50	-1.50	0.04	0.16
F09	160	-0.21	-0.63	0.00	0.07	-0.50	-1.48	0.01	0.16
F10	180	-0.21	-0.60	0.02	0.07	-0.50	-1.40	0.05	0.15
F11	200	-0.22	-0.62	0.01	0.07	-0.51	-1.44	0.02	0.16
F12	220	-0.22	-0.67	0.01	0.07	-0.52	-1.56	0.03	0.17
F13	240	-0.24	-0.72	0.02	0.08	-0.57	-1.69	0.06	0.19
F14	260	-0.29	-0.82	-0.02	0.09	-0.68	-1.92	-0.05	0.22
F15	280	-0.31	-0.82	-0.02	0.10	-0.74	-1.91	-0.04	0.23
F16	300	-0.29	-0.79	0.00	0.09	-0.69	-1.86	0.01	0.21
F17	320	-0.22	-0.67	0.11	0.08	-0.51	-1.57	0.26	0.18
F18	340	-0.13	-0.54	0.22	0.07	-0.31	-1.27	0.52	0.16
G01	0	-0.14	-0.44	0.13	0.05	-0.32	-1.03	0.29	0.11
G02	40	-0.24	-0.65	0.00	0.07	-0.57	-1.53	0.01	0.18
G03	80	-0.31	-0.82	-0.04	0.09	-0.73	-1.92	-0.09	0.22
G04	120	-0.23	-0.69	0.00	0.08	-0.55	-1.60	0.00	0.18
G05	160	-0.21	-0.61	0.00	0.06	-0.48	-1.44	0.01	0.15
G06	200	-0.21	-0.62	-0.01	0.06	-0.49	-1.45	-0.02	0.15
G07	240	-0.24	-0.73	0.01	0.08	-0.55	-1.70	0.03	0.18
G08	280	-0.30	-0.79	-0.03	0.09	-0.71	-1.84	-0.06	0.21
G09	320	-0.23	-0.65	0.04	0.07	-0.55	-1.52	0.09	0.18
H01	0	-0.22	-0.57	-0.02	0.06	-0.52	-1.33	-0.04	0.14
H02	60	-0.29	-0.74	-0.04	0.09	-0.67	-1.72	-0.09	0.20
H03	120	-0.25	-0.72	-0.01	0.08	-0.58	-1.69	-0.02	0.19
H04	180	-0.22	-0.66	-0.01	0.07	-0.51	-1.55	-0.02	0.16
H05	240	-0.24	-0.69	0.00	0.07	-0.56	-1.61	0.00	0.17
H06	300	-0.29	-0.81	-0.03	0.09	-0.68	-1.90	-0.08	0.21

Table B-3. Pressure coefficient data obtained from 30° smooth roof.

Pressure tap	Degree	CpMean	CpMin	CpMax	CpRMS	CpMean	CpMin	CpMax	CpRMS
A01	0	-0.30	-1.25	0.39	0.15	-0.71	-2.92	0.92	0.36
A02	10	-0.31	-1.16	0.54	0.16	-0.73	-2.70	1.27	0.37
A03	20	-0.31	-1.05	0.41	0.16	-0.73	-2.47	0.96	0.36
A04	30	-0.33	-1.33	0.33	0.15	-0.78	-3.10	0.78	0.34
A05	40	-0.34	-1.34	0.21	0.14	-0.80	-3.13	0.49	0.32
A06	50	-0.36	-1.25	0.11	0.13	-0.85	-2.92	0.26	0.31
A07	60	-0.38	-1.36	0.08	0.13	-0.89	-3.17	0.19	0.30
A08	70	-0.39	-1.10	-0.07	0.12	-0.92	-2.59	-0.16	0.28
A09	80	-0.39	-1.10	-0.08	0.12	-0.92	-2.59	-0.19	0.28
A10	90	-0.39	-1.20	-0.06	0.14	-0.92	-2.80	-0.14	0.32
A11	100	-0.35	-1.11	-0.05	0.13	-0.82	-2.61	-0.12	0.30
A12	110	-0.33	-1.32	0.02	0.14	-0.78	-3.08	0.05	0.33
A13	120	-0.26	-0.94	0.05	0.12	-0.61	-2.21	0.12	0.29
A14	130	-0.20	-0.81	0.06	0.10	-0.47	-1.90	0.14	0.24
A15	140	-0.17	-0.82	0.07	0.08	-0.40	-1.93	0.16	0.20
A16	150	-0.15	-0.83	0.09	0.07	-0.35	-1.95	0.21	0.17
A17	160	-0.15	-0.72	0.11	0.07	-0.35	-1.69	0.26	0.17
A18	170	-0.14	-0.81	0.10	0.07	-0.33	-1.90	0.24	0.17
A19	180	-0.14	-0.82	0.10	0.08	-0.33	-1.93	0.24	0.18
A20	190	-0.15	-0.79	0.13	0.08	-0.35	-1.86	0.31	0.18
A21	200	-0.15	-1.04	0.13	0.09	-0.35	-2.45	0.31	0.20
A22	210	-0.15	-0.84	0.12	0.08	-0.35	-1.97	0.28	0.18
A23	220	-0.17	-0.87	0.10	0.09	-0.40	-2.05	0.24	0.20
A24	230	-0.20	-0.93	0.09	0.10	-0.47	-2.19	0.21	0.23
A25	240	-0.27	-1.05	0.04	0.13	-0.63	-2.47	0.09	0.30
A26	250	-0.32	-1.00	0.00	0.13	-0.75	-2.35	0.00	0.30
A27	260	-0.36	-1.07	-0.03	0.13	-0.85	-2.52	-0.07	0.31
A28	270	-0.38	-1.22	-0.05	0.13	-0.89	-2.84	-0.12	0.30
A29	280	-0.39	-1.26	-0.05	0.13	-0.92	-2.94	-0.12	0.30
A30	290	-0.38	-1.17	0.02	0.12	-0.89	-2.73	0.05	0.29
A31	300	-0.37	-1.08	0.16	0.13	-0.87	-2.54	0.38	0.29
A32	310	-0.34	-1.13	0.23	0.14	-0.80	-2.66	0.54	0.32
A33	320	-0.34	-1.31	0.40	0.15	-0.80	-3.06	0.94	0.36
A34	330	-0.32	-1.45	0.46	0.16	-0.75	-3.39	1.08	0.38
A35	340	-0.32	-1.17	0.55	0.17	-0.75	-2.73	1.29	0.39
A36	350	-0.31	-1.30	0.71	0.17	-0.73	-3.03	1.67	0.40
B01	0	-0.30	-1.27	0.60	0.19	-0.71	-2.96	1.41	0.43
B02	10	-0.32	-1.17	0.62	0.18	-0.75	-2.73	1.46	0.43
B03	20	-0.32	-1.45	0.39	0.18	-0.75	-3.39	0.92	0.42
B04	30	-0.33	-1.54	0.37	0.17	-0.78	-3.60	0.87	0.40
B05	40	-0.34	-1.44	0.22	0.15	-0.80	-3.36	0.52	0.36
B06	50	-0.36	-1.16	0.18	0.14	-0.85	-2.70	0.42	0.34
B07	60	-0.36	-1.82	0.09	0.13	-0.85	-4.26	0.21	0.30
B08	70	-0.39	-1.47	-0.05	0.13	-0.92	-3.43	-0.12	0.30

Table B-3. —continued.

Pressure tap	Degree	CpMean	CpMin	CpMax	CpRMS	CpMean	CpMin	CpMax	CpRMS
B09	80	-0.40	-0.97	-0.04	0.13	-0.94	-2.28	-0.09	0.30
B10	90	-0.40	-1.15	-0.03	0.13	-0.94	-2.68	-0.07	0.31
B11	100	-0.36	-1.15	-0.03	0.13	-0.85	-2.68	-0.07	0.31
B12	110	-0.31	-0.86	0.00	0.12	-0.73	-2.02	0.00	0.28
B13	120	-0.25	-0.82	0.04	0.11	-0.59	-1.93	0.09	0.25
B14	130	-0.19	-0.76	0.04	0.08	-0.45	-1.79	0.09	0.19
B15	140	-0.18	-0.68	0.07	0.08	-0.42	-1.60	0.16	0.18
B16	150	-0.15	-0.64	0.06	0.06	-0.35	-1.50	0.14	0.14
B17	160	-0.15	-0.79	0.05	0.07	-0.35	-1.86	0.12	0.16
B18	170	-0.14	-0.62	0.07	0.06	-0.33	-1.46	0.16	0.13
B19	180	-0.15	-0.58	0.07	0.06	-0.35	-1.36	0.16	0.14
B20	190	-0.15	-0.61	0.03	0.05	-0.35	-1.43	0.07	0.12
B21	200	-0.15	-0.56	0.05	0.05	-0.35	-1.32	0.12	0.13
B22	210	-0.16	-0.55	0.03	0.05	-0.38	-1.29	0.07	0.12
B23	220	-0.17	-0.53	0.02	0.06	-0.40	-1.25	0.05	0.13
B24	230	-0.18	-0.56	0.00	0.06	-0.42	-1.32	0.00	0.14
B25	240	-0.23	-0.71	-0.01	0.08	-0.54	-1.67	-0.02	0.19
B26	250	-0.26	-0.69	-0.03	0.08	-0.61	-1.62	-0.07	0.19
B27	260	-0.32	-0.85	-0.05	0.10	-0.75	-2.00	-0.12	0.23
B28	270	-0.32	-0.79	-0.07	0.10	-0.75	-1.86	-0.16	0.22
B29	280	-0.35	-0.94	-0.08	0.10	-0.82	-2.21	-0.19	0.24
B30	290	-0.34	-0.95	-0.01	0.10	-0.80	-2.23	-0.02	0.24
B31	300	-0.35	-1.33	0.13	0.12	-0.82	-3.10	0.31	0.28
B32	310	-0.34	-1.17	0.20	0.13	-0.80	-2.73	0.47	0.31
B33	320	-0.33	-1.33	0.34	0.16	-0.78	-3.10	0.80	0.39
B34	330	-0.32	-1.32	0.32	0.16	-0.75	-3.08	0.75	0.38
B35	340	-0.30	-1.21	0.44	0.17	-0.71	-2.82	1.03	0.39
B36	350	-0.31	-1.23	0.40	0.17	-0.73	-2.87	0.94	0.40
C01	0	-0.01	-0.72	0.48	0.10	-0.02	-1.69	1.13	0.24
C02	10	-0.03	-1.25	0.50	0.10	-0.07	-2.92	1.18	0.23
C03	20	-0.07	-0.96	0.45	0.10	-0.16	-2.26	1.06	0.23
C04	30	-0.12	-0.85	0.28	0.09	-0.28	-2.00	0.66	0.22
C05	40	-0.18	-0.96	0.23	0.09	-0.42	-2.26	0.54	0.21
C06	50	-0.24	-0.92	0.13	0.09	-0.56	-2.16	0.31	0.22
C07	60	-0.30	-0.92	0.09	0.10	-0.71	-2.16	0.21	0.24
C08	70	-0.36	-1.16	-0.02	0.12	-0.85	-2.70	-0.05	0.28
C09	80	-0.40	-1.05	-0.08	0.12	-0.94	-2.47	-0.19	0.29
C10	90	-0.40	-1.05	-0.09	0.13	-0.94	-2.47	-0.21	0.30
C11	100	-0.39	-1.11	-0.05	0.13	-0.92	-2.61	-0.12	0.31
C12	110	-0.34	-1.06	0.01	0.12	-0.80	-2.49	0.02	0.29
C13	120	-0.31	-0.96	0.17	0.12	-0.73	-2.26	0.40	0.29
C14	130	-0.25	-0.92	0.11	0.10	-0.59	-2.16	0.26	0.24
C15	140	-0.24	-1.18	0.15	0.11	-0.56	-2.75	0.35	0.27
C16	150	-0.22	-1.34	0.20	0.11	-0.52	-3.13	0.47	0.26
C17	160	-0.20	-1.42	0.18	0.11	-0.47	-3.32	0.42	0.25
C18	170	-0.19	-0.87	0.22	0.10	-0.45	-2.05	0.52	0.23
C19	180	-0.18	-0.89	0.20	0.09	-0.42	-2.09	0.47	0.22

Table B-3. —continued.

Pressure tap	Degree	CpMean	CpMin	CpMax	CpRMS	CpMean	CpMin	CpMax	CpRMS
C20	190	-0.18	-1.17	0.19	0.09	-0.42	-2.73	0.45	0.22
C21	200	-0.20	-1.04	0.17	0.10	-0.47	-2.45	0.40	0.24
C22	210	-0.22	-1.55	0.20	0.11	-0.52	-3.62	0.47	0.26
C23	220	-0.25	-1.18	0.17	0.11	-0.59	-2.75	0.40	0.27
C24	230	-0.27	-1.09	0.05	0.11	-0.63	-2.56	0.12	0.26
C25	240	-0.30	-0.98	0.03	0.11	-0.71	-2.30	0.07	0.25
C26	250	-0.35	-1.08	-0.02	0.12	-0.82	-2.54	-0.05	0.29
C27	260	-0.37	-0.99	-0.06	0.12	-0.87	-2.33	-0.14	0.29
C28	270	-0.39	-1.05	-0.09	0.12	-0.92	-2.47	-0.21	0.29
C29	280	-0.38	-0.95	-0.09	0.12	-0.89	-2.23	-0.21	0.28
C30	290	-0.35	-0.89	-0.06	0.11	-0.82	-2.09	-0.14	0.27
C31	300	-0.30	-0.90	0.06	0.11	-0.71	-2.12	0.14	0.25
C32	310	-0.24	-0.77	0.12	0.10	-0.56	-1.81	0.28	0.23
C33	320	-0.18	-0.93	0.22	0.10	-0.42	-2.19	0.52	0.23
C34	330	-0.11	-0.80	0.39	0.10	-0.26	-1.88	0.92	0.23
C35	340	-0.06	-1.06	0.41	0.10	-0.14	-2.49	0.96	0.23
C36	350	-0.02	-0.91	0.53	0.10	-0.05	-2.14	1.25	0.24
D01	0	-0.06	-0.47	0.33	0.07	-0.14	-1.11	0.78	0.16
D02	20	-0.11	-0.68	0.31	0.07	-0.26	-1.60	0.73	0.16
D03	40	-0.23	-0.71	0.09	0.09	-0.54	-1.67	0.21	0.21
D04	60	-0.38	-1.00	-0.05	0.12	-0.89	-2.35	-0.12	0.29
D05	80	-0.44	-1.10	-0.11	0.14	-1.03	-2.59	-0.26	0.32
D06	100	-0.43	-1.25	-0.05	0.14	-1.01	-2.92	-0.12	0.33
D07	120	-0.36	-1.02	0.05	0.13	-0.85	-2.40	0.12	0.30
D08	140	-0.33	-1.31	0.26	0.14	-0.78	-3.06	0.61	0.32
D09	160	-0.28	-1.31	0.09	0.12	-0.66	-3.06	0.21	0.28
D10	180	-0.28	-1.17	0.09	0.12	-0.66	-2.73	0.21	0.28
D11	200	-0.30	-1.33	0.16	0.13	-0.71	-3.10	0.38	0.31
D12	220	-0.33	-1.81	0.14	0.14	-0.78	-4.23	0.33	0.32
D13	240	-0.37	-1.01	0.08	0.13	-0.87	-2.37	0.19	0.32
D14	260	-0.42	-1.12	-0.09	0.14	-0.99	-2.63	-0.21	0.33
D15	280	-0.42	-1.10	-0.11	0.13	-0.99	-2.59	-0.26	0.30
D16	300	-0.35	-1.00	-0.03	0.12	-0.82	-2.35	-0.07	0.28
D17	320	-0.23	-0.75	0.20	0.10	-0.54	-1.76	0.47	0.23
D18	340	-0.11	-0.60	0.37	0.08	-0.26	-1.41	0.87	0.18
E01	0	-0.13	-0.46	0.28	0.07	-0.31	-1.08	0.66	0.16
E02	20	-0.18	-0.60	0.19	0.08	-0.42	-1.41	0.45	0.19
E03	40	-0.31	-0.91	0.03	0.12	-0.73	-2.14	0.07	0.27
E04	60	-0.40	-1.28	-0.08	0.14	-0.94	-2.99	-0.19	0.33
E05	80	-0.49	-1.60	-0.06	0.17	-1.15	-3.74	-0.14	0.41
E06	100	-0.46	-1.33	0.02	0.16	-1.08	-3.10	0.05	0.38
E07	120	-0.45	-1.49	0.05	0.17	-1.06	-3.48	0.12	0.40
E08	140	-0.41	-1.55	0.15	0.17	-0.96	-3.62	0.35	0.39
E09	160	-0.39	-1.51	0.08	0.15	-0.92	-3.53	0.19	0.36
E10	180	-0.38	-1.27	0.07	0.14	-0.89	-2.96	0.16	0.32
E11	200	-0.40	-1.60	0.14	0.16	-0.94	-3.74	0.33	0.36
E12	220	-0.42	-1.60	0.18	0.17	-0.99	-3.74	0.42	0.40

Table B-3. —continued.

Pressure tap	Degree	CpMean	CpMin	CpMax	CpRMS	CpMean	CpMin	CpMax	CpRMS
E13	240	-0.45	-1.53	0.05	0.17	-1.06	-3.57	0.12	0.41
E14	260	-0.46	-1.44	-0.04	0.17	-1.08	-3.36	-0.09	0.39
E15	280	-0.46	-1.40	-0.11	0.15	-1.08	-3.27	-0.26	0.35
E16	300	-0.41	-1.20	-0.05	0.14	-0.96	-2.80	-0.12	0.33
E17	320	-0.27	-0.87	0.07	0.10	-0.63	-2.05	0.16	0.24
E18	340	-0.17	-0.78	0.28	0.08	-0.40	-1.83	0.66	0.18
F01	0	-0.17	-0.54	0.13	0.07	-0.40	-1.27	0.31	0.16
F02	20	-0.23	-0.76	0.12	0.09	-0.54	-1.79	0.28	0.21
F03	40	-0.35	-1.01	-0.01	0.12	-0.82	-2.37	-0.02	0.28
F04	60	-0.46	-1.53	-0.09	0.16	-1.08	-3.57	-0.21	0.38
F05	80	-0.46	-1.54	-0.09	0.16	-1.08	-3.60	-0.21	0.39
F06	100	-0.46	-1.37	-0.05	0.17	-1.08	-3.20	-0.12	0.41
F07	120	-0.46	-1.34	0.02	0.18	-1.08	-3.13	0.05	0.42
F08	140	-0.46	-1.53	-0.02	0.18	-1.08	-3.57	-0.05	0.43
F09	160	-0.43	-1.77	0.01	0.17	-1.01	-4.14	0.02	0.39
F10	180	-0.42	-1.53	-0.03	0.15	-0.99	-3.57	-0.07	0.35
F11	200	-0.42	-1.46	0.02	0.16	-0.99	-3.41	0.05	0.37
F12	220	-0.43	-1.35	-0.01	0.17	-1.01	-3.15	-0.02	0.39
F13	240	-0.44	-1.38	0.00	0.16	-1.03	-3.22	0.00	0.38
F14	260	-0.45	-1.39	-0.06	0.17	-1.06	-3.24	-0.14	0.39
F15	280	-0.47	-1.39	-0.08	0.17	-1.11	-3.24	-0.19	0.40
F16	300	-0.45	-1.43	-0.08	0.16	-1.06	-3.34	-0.19	0.38
F17	320	-0.34	-1.10	0.02	0.13	-0.80	-2.59	0.05	0.30
F18	340	-0.22	-0.85	0.13	0.09	-0.52	-2.00	0.31	0.21
G01	0	-0.23	-0.78	0.15	0.08	-0.54	-1.83	0.35	0.18
G02	40	-0.38	-1.29	-0.06	0.14	-0.89	-3.01	-0.14	0.33
G03	80	-0.47	-1.66	-0.04	0.19	-1.11	-3.88	-0.09	0.45
G04	120	-0.43	-1.51	-0.06	0.17	-1.01	-3.53	-0.14	0.41
G05	160	-0.44	-1.52	-0.07	0.16	-1.03	-3.55	-0.16	0.38
G06	200	-0.43	-1.53	-0.04	0.17	-1.01	-3.57	-0.09	0.39
G07	240	-0.44	-1.69	-0.04	0.19	-1.03	-3.95	-0.09	0.43
G08	280	-0.44	-1.53	-0.08	0.18	-1.03	-3.57	-0.19	0.43
G09	320	-0.40	-1.25	-0.04	0.15	-0.94	-2.92	-0.09	0.36
H01	0	-0.32	-0.89	-0.02	0.12	-0.75	-2.09	-0.05	0.28
H02	60	-0.46	-1.75	-0.09	0.20	-1.08	-4.09	-0.21	0.46
H03	120	-0.40	-1.74	-0.05	0.18	-0.94	-4.07	-0.12	0.43
H04	180	-0.40	-1.71	-0.05	0.17	-0.94	-4.00	-0.12	0.41
H05	240	-0.40	-1.81	-0.06	0.17	-0.94	-4.23	-0.14	0.40
H06	300	-0.47	-1.72	-0.08	0.20	-1.11	-4.02	-0.19	0.46

Table B-4. Pressure coefficient data obtained from 30° rough roof.

Pressure tap	Degree	CpMean	CpMin	CpMax	CpRMS	CpMean	CpMin	CpMax	CpRMS
A01	0	-0.19	-0.95	0.54	0.14	-0.46	-2.23	1.27	0.33
A02	10	-0.20	-0.97	0.58	0.14	-0.47	-2.27	1.35	0.33
A03	20	-0.21	-0.96	0.54	0.14	-0.48	-2.24	1.26	0.33
A04	30	-0.22	-0.99	0.45	0.13	-0.51	-2.32	1.06	0.31
A05	40	-0.24	-1.02	0.42	0.13	-0.56	-2.38	0.99	0.30
A06	50	-0.27	-1.03	0.37	0.13	-0.63	-2.41	0.87	0.29
A07	60	-0.33	-1.04	0.26	0.13	-0.78	-2.43	0.62	0.29
A08	70	-0.33	-0.95	0.13	0.11	-0.76	-2.22	0.30	0.25
A09	80	-0.33	-0.92	0.05	0.11	-0.77	-2.15	0.12	0.25
A10	90	-0.31	-0.85	-0.03	0.10	-0.72	-1.99	-0.07	0.23
A11	100	-0.31	-0.92	-0.01	0.10	-0.72	-2.14	-0.02	0.24
A12	110	-0.26	-0.84	0.01	0.09	-0.62	-1.97	0.02	0.22
A13	120	-0.23	-0.77	0.03	0.09	-0.55	-1.79	0.08	0.20
A14	130	-0.21	-0.74	0.05	0.08	-0.49	-1.74	0.11	0.19
A15	140	-0.21	-0.94	0.06	0.08	-0.49	-2.19	0.14	0.20
A16	150	-0.21	-0.92	0.06	0.09	-0.50	-2.15	0.14	0.20
A17	160	-0.23	-0.94	0.08	0.09	-0.53	-2.19	0.18	0.21
A18	170	-0.24	-0.98	0.05	0.09	-0.56	-2.30	0.12	0.22
A19	180	-0.24	-0.95	0.05	0.09	-0.57	-2.23	0.12	0.22
A20	190	-0.24	-0.96	0.03	0.09	-0.56	-2.24	0.08	0.22
A21	200	-0.23	-1.11	0.08	0.10	-0.54	-2.59	0.19	0.23
A22	210	-0.22	-1.09	0.10	0.09	-0.51	-2.55	0.24	0.22
A23	220	-0.21	-0.94	0.09	0.09	-0.48	-2.19	0.22	0.21
A24	230	-0.21	-0.81	0.10	0.09	-0.48	-1.90	0.24	0.20
A25	240	-0.22	-0.81	0.07	0.09	-0.53	-1.90	0.17	0.21
A26	250	-0.25	-0.83	0.06	0.09	-0.59	-1.93	0.14	0.22
A27	260	-0.26	-0.82	0.03	0.09	-0.62	-1.92	0.08	0.21
A28	270	-0.32	-0.95	0.04	0.11	-0.74	-2.21	0.09	0.25
A29	280	-0.29	-1.01	0.11	0.10	-0.68	-2.35	0.25	0.23
A30	290	-0.28	-1.02	0.23	0.11	-0.66	-2.40	0.54	0.25
A31	300	-0.26	-0.99	0.32	0.12	-0.61	-2.32	0.76	0.28
A32	310	-0.25	-0.96	0.40	0.13	-0.58	-2.25	0.94	0.31
A33	320	-0.24	-1.15	0.52	0.15	-0.57	-2.69	1.21	0.35
A34	330	-0.22	-1.04	0.56	0.15	-0.51	-2.43	1.32	0.34
A35	340	-0.20	-0.99	0.61	0.15	-0.47	-2.31	1.42	0.35
A36	350	-0.19	-1.04	0.66	0.15	-0.45	-2.42	1.54	0.36
B01	0	-0.19	-1.09	0.66	0.16	-0.45	-2.56	1.53	0.38
B02	10	-0.20	-1.02	0.61	0.16	-0.46	-2.38	1.43	0.38
B03	20	-0.20	-1.06	0.64	0.16	-0.47	-2.47	1.49	0.38
B04	30	-0.21	-1.07	0.61	0.16	-0.50	-2.51	1.43	0.38
B05	40	-0.23	-1.00	0.54	0.16	-0.53	-2.33	1.28	0.38
B06	50	-0.23	-1.06	0.48	0.15	-0.54	-2.48	1.12	0.35
B07	60	-0.31	-1.10	0.39	0.14	-0.72	-2.58	0.92	0.32
B08	70	-0.31	-1.08	0.20	0.11	-0.73	-2.53	0.48	0.26

Table B-4. —continued.

Pressure tap	Degree	CpMean	CpMin	CpMax	CpRMS	CpMean	CpMin	CpMax	CpRMS
B09	80	-0.32	-1.02	0.09	0.11	-0.76	-2.39	0.21	0.25
B10	90	-0.30	-0.84	0.02	0.10	-0.69	-1.97	0.04	0.22
B11	100	-0.29	-0.84	-0.02	0.10	-0.68	-1.98	-0.04	0.23
B12	110	-0.25	-0.81	0.02	0.09	-0.60	-1.89	0.05	0.21
B13	120	-0.22	-0.70	0.03	0.08	-0.52	-1.64	0.06	0.19
B14	130	-0.20	-0.64	0.03	0.07	-0.47	-1.51	0.06	0.17
B15	140	-0.20	-0.71	0.04	0.07	-0.47	-1.66	0.10	0.17
B16	150	-0.20	-0.70	0.03	0.07	-0.47	-1.64	0.07	0.16
B17	160	-0.21	-0.73	0.03	0.07	-0.49	-1.71	0.07	0.17
B18	170	-0.20	-0.68	-0.01	0.06	-0.47	-1.58	-0.01	0.15
B19	180	-0.20	-0.67	-0.01	0.07	-0.48	-1.57	-0.01	0.16
B20	190	-0.19	-0.62	0.00	0.06	-0.45	-1.45	-0.01	0.13
B21	200	-0.19	-0.63	-0.01	0.06	-0.45	-1.48	-0.02	0.14
B22	210	-0.18	-0.54	0.00	0.05	-0.42	-1.26	-0.01	0.12
B23	220	-0.18	-0.57	0.01	0.06	-0.43	-1.34	0.01	0.13
B24	230	-0.18	-0.51	-0.01	0.05	-0.42	-1.20	-0.01	0.12
B25	240	-0.19	-0.58	-0.01	0.06	-0.45	-1.37	-0.02	0.14
B26	250	-0.20	-0.53	-0.02	0.06	-0.48	-1.24	-0.06	0.13
B27	260	-0.23	-0.65	-0.02	0.07	-0.54	-1.51	-0.06	0.16
B28	270	-0.26	-0.66	-0.03	0.07	-0.60	-1.55	-0.06	0.17
B29	280	-0.25	-0.71	0.07	0.08	-0.60	-1.67	0.16	0.18
B30	290	-0.25	-0.79	0.18	0.09	-0.59	-1.86	0.41	0.20
B31	300	-0.23	-0.88	0.31	0.11	-0.55	-2.06	0.72	0.26
B32	310	-0.21	-0.99	0.34	0.13	-0.50	-2.31	0.80	0.30
B33	320	-0.18	-1.02	0.59	0.16	-0.42	-2.39	1.37	0.39
B34	330	-0.20	-0.95	0.51	0.15	-0.48	-2.21	1.19	0.35
B35	340	-0.19	-0.94	0.60	0.15	-0.45	-2.20	1.41	0.36
B36	350	-0.19	-0.98	0.58	0.15	-0.44	-2.30	1.35	0.36
C01	0	0.03	-0.74	0.63	0.11	0.06	-1.74	1.47	0.27
C02	10	0.02	-0.92	0.61	0.12	0.05	-2.15	1.43	0.27
C03	20	0.00	-0.80	0.55	0.11	0.01	-1.86	1.28	0.27
C04	30	-0.04	-0.84	0.53	0.11	-0.10	-1.97	1.24	0.27
C05	40	-0.12	-0.84	0.37	0.10	-0.28	-1.96	0.87	0.24
C06	50	-0.21	-0.85	0.22	0.09	-0.48	-1.98	0.51	0.22
C07	60	-0.25	-0.85	0.14	0.09	-0.59	-1.99	0.32	0.21
C08	70	-0.25	-0.76	0.09	0.09	-0.58	-1.79	0.21	0.20
C09	80	-0.32	-0.84	-0.03	0.10	-0.74	-1.97	-0.07	0.23
C10	90	-0.31	-0.83	0.02	0.10	-0.71	-1.94	0.04	0.22
C11	100	-0.30	-0.87	-0.01	0.10	-0.71	-2.05	-0.02	0.24
C12	110	-0.26	-0.74	0.02	0.09	-0.60	-1.74	0.06	0.21
C13	120	-0.23	-0.77	0.04	0.08	-0.54	-1.81	0.10	0.20
C14	130	-0.22	-0.75	0.09	0.08	-0.51	-1.76	0.20	0.19
C15	140	-0.21	-0.86	0.09	0.08	-0.50	-2.01	0.22	0.19
C16	150	-0.21	-0.92	0.11	0.08	-0.50	-2.15	0.26	0.19
C17	160	-0.22	-0.82	0.12	0.08	-0.51	-1.92	0.27	0.19
C18	170	-0.22	-0.83	0.07	0.08	-0.51	-1.95	0.16	0.18
C19	180	-0.21	-0.76	0.06	0.08	-0.50	-1.77	0.14	0.18

Table B-4. —continued.

Pressure tap	Degree	CpMean	CpMin	CpMax	CpRMS	CpMean	CpMin	CpMax	CpRMS
C20	190	-0.21	-0.79	0.09	0.08	-0.50	-1.85	0.21	0.18
C21	200	-0.22	-0.84	0.09	0.08	-0.51	-1.97	0.21	0.19
C22	210	-0.21	-0.81	0.10	0.08	-0.50	-1.89	0.23	0.19
C23	220	-0.21	-0.90	0.09	0.08	-0.50	-2.11	0.20	0.19
C24	230	-0.21	-0.78	0.07	0.08	-0.50	-1.82	0.16	0.18
C25	240	-0.22	-0.73	0.03	0.08	-0.52	-1.71	0.08	0.18
C26	250	-0.25	-0.77	0.01	0.08	-0.58	-1.80	0.03	0.20
C27	260	-0.27	-0.77	0.01	0.09	-0.63	-1.81	0.01	0.21
C28	270	-0.29	-0.82	-0.02	0.09	-0.68	-1.93	-0.04	0.21
C29	280	-0.28	-0.82	0.08	0.09	-0.65	-1.93	0.18	0.21
C30	290	-0.25	-0.78	0.13	0.09	-0.59	-1.82	0.30	0.20
C31	300	-0.24	-0.81	0.18	0.09	-0.56	-1.89	0.43	0.22
C32	310	-0.15	-0.80	0.28	0.09	-0.34	-1.88	0.66	0.21
C33	320	-0.12	-0.79	0.37	0.10	-0.29	-1.85	0.87	0.24
C34	330	-0.05	-0.76	0.52	0.11	-0.11	-1.79	1.21	0.25
C35	340	-0.01	-0.76	0.56	0.11	-0.02	-1.78	1.32	0.27
C36	350	0.02	-0.87	0.61	0.12	0.05	-2.03	1.42	0.27
D01	0	0.00	-0.35	0.41	0.07	0.00	-0.81	0.96	0.16
D02	20	-0.04	-0.39	0.37	0.07	-0.09	-0.91	0.87	0.16
D03	40	-0.13	-0.49	0.21	0.06	-0.31	-1.14	0.50	0.14
D04	60	-0.22	-0.67	0.09	0.07	-0.53	-1.58	0.22	0.17
D05	80	-0.28	-0.81	0.00	0.09	-0.67	-1.90	0.01	0.21
D06	100	-0.30	-0.89	-0.02	0.10	-0.71	-2.07	-0.04	0.23
D07	120	-0.24	-0.71	0.04	0.08	-0.56	-1.65	0.09	0.19
D08	140	-0.22	-0.82	0.06	0.08	-0.52	-1.92	0.14	0.18
D09	160	-0.22	-0.85	0.05	0.07	-0.52	-1.98	0.12	0.17
D10	180	-0.22	-0.69	0.00	0.07	-0.52	-1.63	0.01	0.16
D11	200	-0.22	-0.78	0.06	0.08	-0.53	-1.82	0.13	0.18
D12	220	-0.22	-0.83	0.05	0.08	-0.53	-1.95	0.12	0.18
D13	240	-0.23	-0.70	0.07	0.08	-0.55	-1.63	0.16	0.19
D14	260	-0.28	-0.77	-0.01	0.09	-0.65	-1.80	-0.01	0.21
D15	280	-0.28	-0.78	0.01	0.09	-0.66	-1.83	0.02	0.21
D16	300	-0.22	-0.65	0.09	0.07	-0.52	-1.51	0.21	0.17
D17	320	-0.13	-0.51	0.22	0.07	-0.31	-1.20	0.52	0.15
D18	340	-0.05	-0.42	0.39	0.07	-0.11	-0.98	0.91	0.17
E01	0	-0.03	-0.35	0.39	0.07	-0.07	-0.81	0.92	0.15
E02	20	-0.06	-0.54	0.37	0.08	-0.13	-1.27	0.86	0.18
E03	40	-0.19	-0.68	0.28	0.10	-0.43	-1.60	0.65	0.23
E04	60	-0.33	-0.89	0.03	0.10	-0.77	-2.09	0.07	0.24
E05	80	-0.31	-0.87	-0.02	0.10	-0.73	-2.03	-0.04	0.23
E06	100	-0.29	-0.89	0.01	0.10	-0.68	-2.09	0.03	0.24
E07	120	-0.23	-0.73	0.05	0.08	-0.54	-1.72	0.12	0.19
E08	140	-0.22	-0.79	0.04	0.08	-0.51	-1.85	0.09	0.18
E09	160	-0.22	-0.75	0.02	0.07	-0.51	-1.75	0.06	0.17
E10	180	-0.22	-0.73	0.01	0.07	-0.51	-1.71	0.02	0.16
E11	200	-0.22	-0.74	0.04	0.07	-0.51	-1.73	0.09	0.17
E12	220	-0.22	-0.78	0.05	0.08	-0.51	-1.83	0.12	0.18

Table B-4. —continued.

Pressure tap	Degree	CpMean	CpMin	CpMax	CpRMS	CpMean	CpMin	CpMax	CpRMS
E13	240	-0.23	-0.78	0.04	0.08	-0.54	-1.82	0.09	0.19
E14	260	-0.27	-0.75	0.00	0.09	-0.64	-1.76	0.00	0.21
E15	280	-0.32	-0.87	-0.03	0.10	-0.76	-2.03	-0.07	0.23
E16	300	-0.28	-0.73	0.08	0.09	-0.65	-1.72	0.20	0.21
E17	320	-0.17	-0.66	0.26	0.10	-0.40	-1.54	0.62	0.22
E18	340	-0.07	-0.54	0.31	0.08	-0.16	-1.26	0.73	0.18
F01	0	-0.05	-0.42	0.33	0.06	-0.11	-0.97	0.76	0.14
F02	20	-0.09	-0.50	0.31	0.07	-0.20	-1.17	0.73	0.17
F03	40	-0.20	-0.65	0.15	0.08	-0.47	-1.52	0.36	0.19
F04	60	-0.30	-0.80	-0.03	0.09	-0.71	-1.88	-0.07	0.22
F05	80	-0.31	-0.84	-0.04	0.10	-0.73	-1.97	-0.08	0.23
F06	100	-0.27	-0.85	0.00	0.10	-0.64	-1.98	0.01	0.23
F07	120	-0.22	-0.69	0.02	0.08	-0.52	-1.63	0.06	0.18
F08	140	-0.21	-0.72	0.03	0.07	-0.49	-1.69	0.06	0.16
F09	160	-0.21	-0.66	0.01	0.07	-0.49	-1.53	0.03	0.16
F10	180	-0.21	-0.64	0.01	0.07	-0.49	-1.50	0.02	0.16
F11	200	-0.21	-0.64	0.02	0.07	-0.49	-1.50	0.06	0.16
F12	220	-0.21	-0.66	0.02	0.07	-0.49	-1.54	0.05	0.17
F13	240	-0.22	-0.74	0.03	0.08	-0.52	-1.73	0.07	0.18
F14	260	-0.27	-0.81	0.01	0.09	-0.62	-1.90	0.01	0.21
F15	280	-0.31	-0.86	-0.03	0.10	-0.73	-2.01	-0.06	0.23
F16	300	-0.28	-0.80	0.03	0.09	-0.65	-1.87	0.06	0.21
F17	320	-0.20	-0.64	0.18	0.08	-0.47	-1.50	0.42	0.19
F18	340	-0.10	-0.61	0.31	0.08	-0.23	-1.43	0.73	0.19
G01	0	-0.08	-0.42	0.24	0.05	-0.18	-0.98	0.56	0.13
G02	40	-0.21	-0.63	0.08	0.07	-0.48	-1.48	0.19	0.17
G03	80	-0.28	-0.79	-0.02	0.09	-0.66	-1.84	-0.04	0.21
G04	120	-0.21	-0.67	0.03	0.07	-0.49	-1.57	0.07	0.16
G05	160	-0.20	-0.62	0.00	0.06	-0.47	-1.45	0.00	0.15
G06	200	-0.20	-0.60	0.01	0.07	-0.47	-1.41	0.02	0.15
G07	240	-0.21	-0.66	0.00	0.07	-0.50	-1.53	0.01	0.17
G08	280	-0.29	-0.81	-0.02	0.09	-0.69	-1.89	-0.04	0.22
G09	320	-0.21	-0.69	0.09	0.08	-0.50	-1.62	0.20	0.18
H01	0	-0.13	-0.45	0.13	0.05	-0.31	-1.05	0.30	0.11
H02	60	-0.25	-0.73	-0.02	0.08	-0.59	-1.72	-0.05	0.18
H03	120	-0.22	-0.64	0.00	0.07	-0.51	-1.51	-0.01	0.16
H04	180	-0.20	-0.59	0.00	0.06	-0.47	-1.38	0.00	0.15
H05	240	-0.22	-0.68	0.00	0.07	-0.51	-1.60	-0.01	0.16
H06	300	-0.23	-0.71	-0.01	0.07	-0.53	-1.66	-0.02	0.17

Table B-5. Pressure coefficient data obtained from 35° smooth roof.

Pressure tap	Degree	CpMean	CpMin	CpMax	CpRMS	CpMean	CpMin	CpMax	CpRMS
A01	0	-0.18	-0.88	0.56	0.15	-0.42	-2.05	1.31	0.35
A02	10	-0.18	-0.93	0.81	0.16	-0.42	-2.17	1.89	0.36
A03	20	-0.20	-0.93	0.54	0.14	-0.47	-2.17	1.26	0.33
A04	30	-0.22	-0.98	0.45	0.14	-0.51	-2.29	1.05	0.31
A05	40	-0.24	-0.88	0.46	0.12	-0.56	-2.05	1.07	0.27
A06	50	-0.29	-1.03	0.20	0.12	-0.68	-2.40	0.47	0.27
A07	60	-0.31	-0.82	0.10	0.10	-0.72	-1.91	0.23	0.23
A08	70	-0.36	-0.93	0.10	0.11	-0.84	-2.17	0.23	0.26
A09	80	-0.34	-0.93	-0.08	0.10	-0.79	-2.17	-0.19	0.23
A10	90	-0.37	-1.03	-0.07	0.12	-0.86	-2.40	-0.16	0.28
A11	100	-0.34	-1.04	-0.04	0.11	-0.79	-2.43	-0.09	0.27
A12	110	-0.32	-1.06	-0.02	0.13	-0.75	-2.47	-0.05	0.30
A13	120	-0.26	-0.88	0.03	0.11	-0.61	-2.05	0.07	0.26
A14	130	-0.22	-0.88	0.08	0.10	-0.51	-2.05	0.19	0.24
A15	140	-0.19	-1.05	0.14	0.09	-0.44	-2.45	0.33	0.22
A16	150	-0.19	-0.88	0.12	0.10	-0.44	-2.05	0.28	0.23
A17	160	-0.19	-0.89	0.15	0.10	-0.44	-2.08	0.35	0.24
A18	170	-0.19	-1.03	0.08	0.11	-0.44	-2.40	0.19	0.25
A19	180	-0.18	-0.92	0.12	0.10	-0.42	-2.15	0.28	0.24
A20	190	-0.18	-0.82	0.10	0.09	-0.42	-1.91	0.23	0.22
A21	200	-0.19	-1.20	0.20	0.11	-0.44	-2.80	0.47	0.26
A22	210	-0.20	-1.18	0.19	0.12	-0.47	-2.75	0.44	0.27
A23	220	-0.20	-1.20	0.17	0.11	-0.47	-2.80	0.40	0.25
A24	230	-0.21	-1.30	0.12	0.11	-0.49	-3.03	0.28	0.26
A25	240	-0.25	-0.96	0.07	0.12	-0.58	-2.24	0.16	0.28
A26	250	-0.31	-1.04	0.08	0.13	-0.72	-2.43	0.19	0.31
A27	260	-0.37	-1.17	0.01	0.14	-0.86	-2.73	0.02	0.32
A28	270	-0.39	-1.26	-0.07	0.13	-0.91	-2.94	-0.16	0.31
A29	280	-0.40	-1.09	-0.02	0.14	-0.93	-2.54	-0.05	0.31
A30	290	-0.38	-1.03	0.04	0.12	-0.89	-2.40	0.09	0.28
A31	300	-0.35	-1.11	0.09	0.12	-0.82	-2.59	0.21	0.29
A32	310	-0.30	-1.12	0.36	0.13	-0.70	-2.61	0.84	0.30
A33	320	-0.27	-1.11	0.35	0.14	-0.63	-2.59	0.82	0.32
A34	330	-0.23	-1.03	0.49	0.15	-0.54	-2.40	1.14	0.34
A35	340	-0.21	-1.11	0.60	0.16	-0.49	-2.59	1.40	0.37
A36	350	-0.18	-1.03	0.64	0.16	-0.42	-2.40	1.49	0.38
B01	0	-0.13	-1.07	0.64	0.19	-0.30	-2.50	1.49	0.44
B02	10	-0.14	-0.98	0.66	0.18	-0.33	-2.29	1.54	0.43
B03	20	-0.15	-0.99	0.48	0.17	-0.35	-2.31	1.12	0.40
B04	30	-0.18	-1.21	0.52	0.16	-0.42	-2.82	1.21	0.38
B05	40	-0.22	-1.02	0.50	0.14	-0.51	-2.38	1.17	0.32
B06	50	-0.28	-0.99	0.23	0.13	-0.65	-2.31	0.54	0.30
B07	60	-0.32	-1.04	0.13	0.12	-0.75	-2.43	0.30	0.28
B08	70	-0.37	-1.09	-0.04	0.12	-0.86	-2.54	-0.09	0.29

Table B-5. —continued.

Pressure tap	Degree	CpMean	CpMin	CpMax	CpRMS	CpMean	CpMin	CpMax	CpRMS
B09	80	-0.38	-0.99	-0.09	0.12	-0.89	-2.31	-0.21	0.28
B10	90	-0.37	-0.96	-0.06	0.12	-0.86	-2.24	-0.14	0.27
B11	100	-0.37	-1.04	0.00	0.13	-0.86	-2.43	0.00	0.31
B12	110	-0.34	-1.02	0.05	0.13	-0.79	-2.38	0.12	0.31
B13	120	-0.28	-1.00	0.07	0.12	-0.65	-2.33	0.16	0.28
B14	130	-0.23	-0.99	0.09	0.11	-0.54	-2.31	0.21	0.25
B15	140	-0.21	-0.99	0.14	0.10	-0.49	-2.31	0.33	0.24
B16	150	-0.20	-1.04	0.16	0.10	-0.47	-2.43	0.37	0.24
B17	160	-0.19	-1.29	0.15	0.10	-0.44	-3.01	0.35	0.24
B18	170	-0.18	-0.88	0.16	0.10	-0.42	-2.05	0.37	0.23
B19	180	-0.18	-1.16	0.19	0.10	-0.42	-2.71	0.44	0.24
B20	190	-0.19	-0.95	0.16	0.10	-0.44	-2.22	0.37	0.24
B21	200	-0.19	-1.03	0.16	0.10	-0.44	-2.40	0.37	0.24
B22	210	-0.19	-1.08	0.16	0.10	-0.44	-2.52	0.37	0.24
B23	220	-0.20	-1.11	0.18	0.10	-0.47	-2.59	0.42	0.24
B24	230	-0.23	-1.06	0.14	0.11	-0.54	-2.47	0.33	0.25
B25	240	-0.26	-0.98	0.07	0.11	-0.61	-2.29	0.16	0.26
B26	250	-0.31	-0.94	0.05	0.12	-0.72	-2.19	0.12	0.29
B27	260	-0.36	-1.32	0.04	0.12	-0.84	-3.08	0.09	0.29
B28	270	-0.37	-0.99	-0.02	0.12	-0.86	-2.31	-0.05	0.29
B29	280	-0.39	-0.93	-0.01	0.12	-0.91	-2.17	-0.02	0.28
B30	290	-0.37	-1.05	-0.01	0.12	-0.86	-2.45	-0.02	0.27
B31	300	-0.34	-1.17	0.09	0.12	-0.79	-2.73	0.21	0.29
B32	310	-0.29	-0.98	0.31	0.13	-0.68	-2.29	0.72	0.29
B33	320	-0.24	-1.16	0.31	0.14	-0.56	-2.71	0.72	0.33
B34	330	-0.20	-1.34	0.63	0.15	-0.47	-3.13	1.47	0.36
B35	340	-0.17	-1.01	0.54	0.17	-0.40	-2.36	1.26	0.39
B36	350	-0.15	-0.94	0.86	0.18	-0.35	-2.19	2.01	0.42
C01	0	0.04	-0.52	0.58	0.10	0.09	-1.21	1.35	0.23
C02	10	0.03	-0.66	0.54	0.10	0.07	-1.54	1.26	0.23
C03	20	-0.01	-0.48	0.48	0.10	-0.02	-1.12	1.12	0.22
C04	30	-0.07	-0.54	0.40	0.09	-0.16	-1.26	0.93	0.22
C05	40	-0.14	-0.66	0.34	0.09	-0.33	-1.54	0.79	0.21
C06	50	-0.21	-0.96	0.26	0.10	-0.49	-2.24	0.61	0.22
C07	60	-0.30	-0.88	0.05	0.10	-0.70	-2.05	0.12	0.23
C08	70	-0.35	-1.07	0.09	0.11	-0.82	-2.50	0.21	0.26
C09	80	-0.40	-1.15	-0.05	0.13	-0.93	-2.68	-0.12	0.31
C10	90	-0.42	-1.00	-0.04	0.13	-0.98	-2.33	-0.09	0.30
C11	100	-0.40	-1.08	-0.04	0.14	-0.93	-2.52	-0.09	0.32
C12	110	-0.35	-1.10	0.05	0.13	-0.82	-2.57	0.12	0.30
C13	120	-0.31	-1.13	0.08	0.12	-0.72	-2.64	0.19	0.28
C14	130	-0.28	-1.38	0.26	0.13	-0.65	-3.20	0.61	0.29
C15	140	-0.27	-1.30	0.17	0.13	-0.63	-3.03	0.40	0.31
C16	150	-0.25	-2.18	0.21	0.13	-0.58	-5.06	0.49	0.31
C17	160	-0.25	-1.95	0.22	0.13	-0.58	-4.52	0.51	0.29
C18	170	-0.22	-0.93	0.16	0.11	-0.51	-2.17	0.37	0.25
C19	180	-0.22	-1.13	0.14	0.10	-0.51	-2.64	0.33	0.24

Table B-5. —continued.

Pressure tap	Degree	CpMean	CpMin	CpMax	CpRMS	CpMean	CpMin	CpMax	CpRMS
C20	190	-0.23	-1.03	0.15	0.11	-0.54	-2.40	0.35	0.25
C21	200	-0.25	-1.25	0.20	0.12	-0.58	-2.92	0.47	0.28
C22	210	-0.26	-1.30	0.25	0.13	-0.61	-3.03	0.58	0.30
C23	220	-0.26	-1.28	0.20	0.12	-0.61	-2.99	0.47	0.29
C24	230	-0.28	-1.30	0.14	0.13	-0.65	-3.03	0.33	0.30
C25	240	-0.31	-1.00	0.17	0.12	-0.72	-2.33	0.40	0.29
C26	250	-0.35	-1.01	0.08	0.12	-0.82	-2.36	0.19	0.29
C27	260	-0.36	-0.92	-0.02	0.13	-0.84	-2.15	-0.05	0.30
C28	270	-0.39	-1.14	-0.05	0.13	-0.91	-2.66	-0.12	0.31
C29	280	-0.39	-1.00	-0.09	0.13	-0.91	-2.33	-0.21	0.29
C30	290	-0.37	-1.02	-0.06	0.12	-0.86	-2.38	-0.14	0.28
C31	300	-0.31	-0.91	0.12	0.11	-0.72	-2.12	0.28	0.26
C32	310	-0.25	-0.89	0.19	0.11	-0.58	-2.08	0.44	0.26
C33	320	-0.17	-0.68	0.22	0.10	-0.40	-1.59	0.51	0.23
C34	330	-0.09	-0.95	0.33	0.10	-0.21	-2.22	0.77	0.23
C35	340	-0.03	-0.66	0.61	0.09	-0.07	-1.54	1.42	0.22
C36	350	0.02	-0.68	0.46	0.10	0.05	-1.59	1.07	0.22
D01	0	-0.02	-0.36	0.52	0.08	-0.05	-0.84	1.21	0.18
D02	20	-0.06	-0.45	0.36	0.08	-0.14	-1.05	0.84	0.17
D03	40	-0.19	-0.70	0.38	0.09	-0.44	-1.63	0.89	0.21
D04	60	-0.35	-0.99	-0.03	0.12	-0.82	-2.31	-0.07	0.27
D05	80	-0.44	-1.05	-0.07	0.14	-1.03	-2.45	-0.16	0.31
D06	100	-0.41	-1.07	0.01	0.14	-0.96	-2.50	0.02	0.34
D07	120	-0.35	-1.27	0.18	0.13	-0.82	-2.96	0.42	0.31
D08	140	-0.33	-1.50	0.21	0.14	-0.77	-3.48	0.49	0.32
D09	160	-0.31	-1.30	0.26	0.13	-0.72	-3.03	0.61	0.31
D10	180	-0.30	-0.95	0.10	0.12	-0.70	-2.22	0.23	0.27
D11	200	-0.31	-1.42	0.19	0.13	-0.72	-3.29	0.44	0.30
D12	220	-0.33	-1.37	0.17	0.14	-0.77	-3.17	0.40	0.33
D13	240	-0.34	-1.06	0.19	0.13	-0.79	-2.47	0.44	0.31
D14	260	-0.39	-1.12	0.03	0.13	-0.91	-2.61	0.07	0.31
D15	280	-0.43	-1.39	-0.08	0.14	-1.00	-3.22	-0.19	0.32
D16	300	-0.37	-1.02	0.02	0.13	-0.86	-2.38	0.05	0.30
D17	320	-0.22	-0.74	0.19	0.10	-0.51	-1.73	0.44	0.23
D18	340	-0.08	-0.58	0.40	0.08	-0.19	-1.35	0.93	0.19
E01	0	-0.08	-0.47	0.33	0.08	-0.19	-1.10	0.77	0.17
E02	20	-0.12	-0.56	0.26	0.08	-0.28	-1.31	0.61	0.18
E03	40	-0.24	-0.96	0.17	0.10	-0.56	-2.24	0.40	0.23
E04	60	-0.39	-1.28	-0.04	0.14	-0.91	-2.99	-0.09	0.32
E05	80	-0.42	-1.26	0.00	0.16	-0.98	-2.94	0.00	0.37
E06	100	-0.39	-1.31	0.01	0.15	-0.91	-3.06	0.02	0.35
E07	120	-0.38	-1.29	0.14	0.15	-0.89	-3.01	0.33	0.35
E08	140	-0.36	-1.42	0.09	0.15	-0.84	-3.29	0.21	0.36
E09	160	-0.36	-1.45	0.12	0.15	-0.84	-3.36	0.28	0.34
E10	180	-0.36	-1.10	0.07	0.14	-0.84	-2.57	0.16	0.31
E11	200	-0.37	-1.53	0.15	0.14	-0.86	-3.55	0.35	0.33
E12	220	-0.36	-1.56	0.15	0.16	-0.84	-3.62	0.35	0.36

Table B-5. —continued.

Pressure tap	Degree	CpMean	CpMin	CpMax	CpRMS	CpMean	CpMin	CpMax	CpRMS
E13	240	-0.37	-1.33	0.24	0.15	-0.86	-3.10	0.56	0.35
E14	260	-0.39	-1.31	0.00	0.15	-0.91	-3.06	0.00	0.34
E15	280	-0.43	-1.32	-0.05	0.15	-1.00	-3.08	-0.12	0.34
E16	300	-0.41	-1.24	-0.06	0.14	-0.96	-2.89	-0.14	0.32
E17	320	-0.29	-0.89	0.11	0.11	-0.68	-2.08	0.26	0.27
E18	340	-0.14	-0.69	0.32	0.08	-0.33	-1.61	0.75	0.19
F01	0	-0.12	-0.50	0.21	0.07	-0.28	-1.17	0.49	0.16
F02	20	-0.17	-0.65	0.22	0.08	-0.40	-1.52	0.51	0.19
F03	40	-0.29	-0.86	0.07	0.11	-0.68	-2.01	0.16	0.26
F04	60	-0.40	-1.27	-0.08	0.14	-0.93	-2.96	-0.19	0.33
F05	80	-0.40	-1.55	-0.03	0.16	-0.93	-3.59	-0.07	0.38
F06	100	-0.37	-1.44	0.01	0.15	-0.86	-3.34	0.02	0.35
F07	120	-0.36	-1.28	0.00	0.15	-0.84	-2.99	0.00	0.34
F08	140	-0.35	-1.41	0.00	0.15	-0.82	-3.27	0.00	0.34
F09	160	-0.37	-1.36	0.04	0.15	-0.86	-3.15	0.09	0.34
F10	180	-0.37	-1.42	0.02	0.14	-0.86	-3.29	0.05	0.32
F11	200	-0.37	-1.26	0.06	0.14	-0.86	-2.94	0.14	0.34
F12	220	-0.36	-1.37	0.04	0.15	-0.84	-3.17	0.09	0.35
F13	240	-0.36	-1.26	0.02	0.15	-0.84	-2.94	0.05	0.35
F14	260	-0.37	-1.23	0.07	0.14	-0.86	-2.87	0.16	0.33
F15	280	-0.39	-1.41	-0.05	0.16	-0.91	-3.27	-0.12	0.36
F16	300	-0.40	-1.50	-0.03	0.15	-0.93	-3.48	-0.07	0.35
F17	320	-0.33	-1.38	0.06	0.14	-0.77	-3.20	0.14	0.32
F18	340	-0.19	-0.79	0.19	0.09	-0.44	-1.84	0.44	0.21
G01	0	-0.17	-0.71	0.13	0.07	-0.40	-1.66	0.30	0.17
G02	40	-0.33	-1.48	0.02	0.12	-0.77	-3.43	0.05	0.28
G03	80	-0.37	-1.71	-0.02	0.17	-0.86	-3.96	-0.05	0.40
G04	120	-0.36	-1.47	-0.02	0.15	-0.84	-3.41	-0.05	0.34
G05	160	-0.36	-1.34	-0.03	0.15	-0.84	-3.13	-0.07	0.35
G06	200	-0.34	-1.58	-0.02	0.14	-0.79	-3.66	-0.05	0.33
G07	240	-0.34	-1.33	-0.03	0.14	-0.79	-3.10	-0.07	0.32
G08	280	-0.35	-1.58	-0.05	0.16	-0.82	-3.66	-0.12	0.36
G09	320	-0.35	-1.09	-0.01	0.13	-0.82	-2.54	-0.02	0.31
H01	0	-0.25	-0.91	0.01	0.10	-0.58	-2.12	0.02	0.23
H02	60	-0.38	-1.79	-0.01	0.17	-0.89	-4.15	-0.02	0.38
H03	120	-0.33	-1.80	-0.04	0.14	-0.77	-4.17	-0.09	0.34
H04	180	-0.32	-1.30	-0.01	0.14	-0.75	-3.03	-0.02	0.32
H05	240	-0.32	-1.31	-0.03	0.14	-0.75	-3.06	-0.07	0.33
H06	300	-0.37	-1.50	-0.03	0.15	-0.86	-3.48	-0.07	0.36

Table B-6. Pressure coefficient data obtained from 35° rough roof.

Pressure tap	Degree	CpMean	CpMin	CpMax	CpRMS	CpMean	CpMin	CpMax	CpRMS
A01	0	-0.09	-0.84	0.69	0.14	-0.22	-1.97	1.61	0.34
A02	10	-0.10	-0.78	0.65	0.14	-0.22	-1.83	1.53	0.34
A03	20	-0.12	-0.84	0.64	0.14	-0.28	-1.98	1.49	0.32
A04	30	-0.14	-0.77	0.55	0.13	-0.33	-1.80	1.28	0.31
A05	40	-0.18	-0.76	0.45	0.12	-0.42	-1.77	1.06	0.29
A06	50	-0.22	-0.83	0.40	0.12	-0.52	-1.94	0.93	0.28
A07	60	-0.21	-0.73	0.24	0.09	-0.49	-1.70	0.56	0.20
A08	70	-0.26	-0.87	0.15	0.10	-0.61	-2.04	0.35	0.23
A09	80	-0.28	-0.82	0.02	0.09	-0.66	-1.92	0.04	0.20
A10	90	-0.30	-0.82	-0.04	0.09	-0.70	-1.93	-0.10	0.22
A11	100	-0.30	-0.85	-0.03	0.10	-0.70	-2.00	-0.06	0.23
A12	110	-0.27	-0.84	-0.01	0.09	-0.63	-1.98	-0.01	0.22
A13	120	-0.23	-0.75	0.01	0.08	-0.55	-1.75	0.03	0.19
A14	130	-0.22	-0.81	0.02	0.08	-0.52	-1.88	0.06	0.20
A15	140	-0.22	-0.92	0.03	0.08	-0.51	-2.15	0.07	0.20
A16	150	-0.23	-0.96	0.05	0.09	-0.54	-2.24	0.13	0.21
A17	160	-0.24	-0.99	0.03	0.09	-0.56	-2.31	0.07	0.22
A18	170	-0.25	-1.02	0.07	0.09	-0.59	-2.39	0.17	0.22
A19	180	-0.25	-1.00	0.04	0.10	-0.59	-2.33	0.10	0.22
A20	190	-0.25	-1.02	0.02	0.09	-0.58	-2.38	0.04	0.22
A21	200	-0.24	-1.11	0.07	0.10	-0.56	-2.60	0.17	0.24
A22	210	-0.23	-1.15	0.07	0.10	-0.55	-2.69	0.17	0.23
A23	220	-0.23	-0.96	0.12	0.10	-0.53	-2.26	0.29	0.23
A24	230	-0.23	-1.03	0.11	0.09	-0.53	-2.40	0.25	0.22
A25	240	-0.24	-0.95	0.07	0.09	-0.55	-2.23	0.17	0.22
A26	250	-0.26	-0.84	0.07	0.10	-0.60	-1.97	0.16	0.23
A27	260	-0.29	-0.89	0.02	0.10	-0.68	-2.08	0.06	0.23
A28	270	-0.31	-0.90	0.00	0.10	-0.72	-2.11	0.00	0.24
A29	280	-0.31	-0.97	0.11	0.10	-0.73	-2.27	0.25	0.25
A30	290	-0.29	-0.93	0.22	0.11	-0.67	-2.18	0.52	0.26
A31	300	-0.26	-0.99	0.31	0.12	-0.60	-2.32	0.73	0.28
A32	310	-0.23	-1.00	0.40	0.13	-0.54	-2.35	0.95	0.31
A33	320	-0.20	-0.92	0.53	0.15	-0.46	-2.16	1.24	0.34
A34	330	-0.14	-0.86	0.66	0.14	-0.33	-2.01	1.54	0.34
A35	340	-0.12	-0.93	0.76	0.16	-0.29	-2.17	1.77	0.36
A36	350	-0.09	-0.85	0.85	0.16	-0.21	-1.98	1.98	0.37
B01	0	-0.07	-0.83	0.72	0.16	-0.15	-1.95	1.67	0.38
B02	10	-0.07	-0.87	0.70	0.16	-0.16	-2.04	1.64	0.38
B03	20	-0.07	-0.87	0.74	0.17	-0.16	-2.03	1.72	0.39
B04	30	-0.06	-0.88	0.67	0.16	-0.13	-2.07	1.56	0.38
B05	40	-0.10	-1.03	0.66	0.17	-0.24	-2.42	1.54	0.40
B06	50	-0.16	-0.95	0.53	0.15	-0.38	-2.22	1.24	0.36
B07	60	-0.17	-0.87	0.37	0.11	-0.40	-2.05	0.87	0.26
B08	70	-0.26	-0.90	0.25	0.12	-0.62	-2.11	0.58	0.27

Table B-6. —continued.

Pressure tap	Degree	CpMean	CpMin	CpMax	CpRMS	CpMean	CpMin	CpMax	CpRMS
B09	80	-0.32	-0.98	0.09	0.11	-0.74	-2.29	0.21	0.25
B10	90	-0.29	-0.90	0.02	0.10	-0.69	-2.10	0.04	0.23
B11	100	-0.31	-0.94	-0.01	0.11	-0.73	-2.20	-0.02	0.25
B12	110	-0.26	-0.87	0.02	0.09	-0.60	-2.03	0.06	0.21
B13	120	-0.24	-0.79	0.04	0.09	-0.56	-1.84	0.08	0.21
B14	130	-0.22	-0.80	0.06	0.09	-0.51	-1.88	0.14	0.20
B15	140	-0.22	-0.85	0.08	0.09	-0.50	-1.99	0.18	0.20
B16	150	-0.23	-0.92	0.08	0.09	-0.53	-2.16	0.19	0.21
B17	160	-0.23	-0.92	0.10	0.09	-0.54	-2.15	0.23	0.21
B18	170	-0.24	-1.02	0.07	0.09	-0.56	-2.39	0.17	0.21
B19	180	-0.24	-0.89	0.02	0.09	-0.55	-2.09	0.06	0.21
B20	190	-0.24	-0.96	0.07	0.09	-0.56	-2.26	0.15	0.21
B21	200	-0.24	-1.00	0.09	0.09	-0.55	-2.35	0.21	0.21
B22	210	-0.23	-0.87	0.12	0.09	-0.54	-2.04	0.29	0.21
B23	220	-0.22	-0.85	0.11	0.09	-0.52	-1.99	0.25	0.21
B24	230	-0.22	-0.90	0.08	0.09	-0.50	-2.10	0.18	0.20
B25	240	-0.23	-0.78	0.05	0.08	-0.53	-1.83	0.12	0.20
B26	250	-0.26	-0.81	0.02	0.09	-0.61	-1.89	0.05	0.21
B27	260	-0.28	-0.80	0.03	0.09	-0.65	-1.87	0.07	0.22
B28	270	-0.30	-0.88	0.01	0.10	-0.70	-2.06	0.02	0.23
B29	280	-0.30	-0.84	0.08	0.10	-0.70	-1.98	0.18	0.23
B30	290	-0.27	-0.90	0.20	0.10	-0.63	-2.11	0.46	0.24
B31	300	-0.21	-0.89	0.34	0.12	-0.50	-2.09	0.79	0.28
B32	310	-0.16	-0.86	0.51	0.14	-0.37	-2.02	1.18	0.32
B33	320	-0.10	-0.87	0.64	0.16	-0.22	-2.04	1.50	0.37
B34	330	-0.08	-0.86	0.55	0.15	-0.19	-2.02	1.29	0.36
B35	340	-0.07	-0.79	0.65	0.16	-0.16	-1.84	1.53	0.37
B36	350	-0.06	-0.88	0.66	0.16	-0.15	-2.06	1.53	0.37
C01	0	0.08	-0.52	0.62	0.11	0.18	-1.21	1.45	0.25
C02	10	0.07	-0.61	0.66	0.11	0.17	-1.43	1.53	0.25
C03	20	0.04	-0.63	0.60	0.11	0.08	-1.46	1.41	0.27
C04	30	-0.02	-0.63	0.55	0.11	-0.05	-1.47	1.28	0.25
C05	40	-0.13	-0.67	0.41	0.10	-0.30	-1.58	0.96	0.23
C06	50	-0.18	-0.69	0.27	0.09	-0.42	-1.61	0.62	0.20
C07	60	-0.19	-0.70	0.23	0.09	-0.45	-1.64	0.54	0.21
C08	70	-0.34	-0.96	0.00	0.11	-0.79	-2.26	0.00	0.25
C09	80	-0.29	-0.78	0.00	0.09	-0.69	-1.83	0.00	0.22
C10	90	-0.32	-0.86	-0.03	0.10	-0.74	-2.02	-0.07	0.23
C11	100	-0.31	-0.87	-0.02	0.10	-0.73	-2.04	-0.05	0.24
C12	110	-0.27	-0.79	0.01	0.09	-0.62	-1.85	0.03	0.21
C13	120	-0.24	-0.78	0.05	0.09	-0.56	-1.82	0.12	0.20
C14	130	-0.23	-0.82	0.05	0.08	-0.53	-1.92	0.12	0.20
C15	140	-0.23	-0.86	0.09	0.08	-0.53	-2.02	0.21	0.20
C16	150	-0.23	-0.88	0.07	0.08	-0.53	-2.06	0.17	0.19
C17	160	-0.23	-0.88	0.06	0.08	-0.53	-2.07	0.14	0.19
C18	170	-0.23	-0.86	0.04	0.08	-0.53	-2.02	0.09	0.18
C19	180	-0.22	-0.75	0.07	0.07	-0.51	-1.75	0.17	0.17

Table B-6. —continued.

Pressure tap	Degree	CpMean	CpMin	CpMax	CpRMS	CpMean	CpMin	CpMax	CpRMS
C20	190	-0.22	-0.79	0.04	0.08	-0.52	-1.84	0.10	0.18
C21	200	-0.23	-0.85	0.08	0.08	-0.53	-1.99	0.18	0.19
C22	210	-0.23	-0.89	0.06	0.08	-0.53	-2.08	0.15	0.19
C23	220	-0.23	-0.86	0.07	0.08	-0.53	-2.02	0.16	0.20
C24	230	-0.22	-0.81	0.05	0.08	-0.52	-1.89	0.11	0.19
C25	240	-0.23	-0.81	0.07	0.08	-0.54	-1.89	0.16	0.19
C26	250	-0.26	-0.82	0.00	0.09	-0.61	-1.91	0.01	0.21
C27	260	-0.29	-0.89	0.01	0.10	-0.68	-2.09	0.02	0.23
C28	270	-0.31	-0.90	-0.02	0.10	-0.72	-2.10	-0.05	0.23
C29	280	-0.32	-0.85	-0.02	0.10	-0.75	-1.99	-0.04	0.24
C30	290	-0.32	-0.88	0.00	0.10	-0.75	-2.07	0.00	0.24
C31	300	-0.25	-0.87	0.18	0.10	-0.58	-2.03	0.41	0.23
C32	310	-0.20	-0.70	0.20	0.09	-0.46	-1.64	0.47	0.21
C33	320	-0.11	-0.59	0.43	0.10	-0.25	-1.39	1.02	0.22
C34	330	-0.03	-0.58	0.56	0.11	-0.07	-1.36	1.30	0.25
C35	340	0.03	-0.52	0.59	0.11	0.07	-1.23	1.38	0.25
C36	350	0.07	-0.63	0.64	0.11	0.16	-1.46	1.49	0.25
D01	0	0.03	-0.29	0.51	0.08	0.07	-0.69	1.19	0.19
D02	20	-0.01	-0.29	0.42	0.07	-0.02	-0.69	0.99	0.17
D03	40	-0.11	-0.49	0.30	0.07	-0.25	-1.14	0.70	0.16
D04	60	-0.20	-0.61	0.16	0.07	-0.46	-1.42	0.38	0.16
D05	80	-0.30	-0.84	0.00	0.10	-0.71	-1.96	-0.01	0.23
D06	100	-0.29	-0.80	-0.02	0.09	-0.68	-1.87	-0.06	0.22
D07	120	-0.24	-0.71	0.02	0.08	-0.56	-1.65	0.04	0.19
D08	140	-0.23	-0.84	0.03	0.08	-0.53	-1.97	0.07	0.18
D09	160	-0.23	-0.82	0.00	0.07	-0.53	-1.91	0.00	0.17
D10	180	-0.23	-0.77	0.00	0.07	-0.53	-1.79	0.00	0.16
D11	200	-0.23	-0.83	0.01	0.07	-0.54	-1.95	0.02	0.17
D12	220	-0.23	-0.80	0.03	0.08	-0.53	-1.87	0.07	0.18
D13	240	-0.23	-0.72	0.04	0.08	-0.55	-1.68	0.09	0.18
D14	260	-0.28	-0.83	0.00	0.09	-0.66	-1.95	0.00	0.22
D15	280	-0.33	-0.93	-0.04	0.11	-0.76	-2.18	-0.09	0.25
D16	300	-0.22	-0.80	0.14	0.08	-0.52	-1.88	0.32	0.20
D17	320	-0.12	-0.51	0.29	0.07	-0.28	-1.18	0.69	0.17
D18	340	-0.02	-0.41	0.47	0.07	-0.05	-0.96	1.11	0.18
E01	0	0.00	-0.37	0.48	0.07	0.00	-0.87	1.11	0.17
E02	20	-0.03	-0.50	0.40	0.08	-0.07	-1.18	0.95	0.19
E03	40	-0.19	-0.74	0.28	0.11	-0.44	-1.73	0.65	0.26
E04	60	-0.29	-0.80	0.08	0.09	-0.68	-1.87	0.20	0.22
E05	80	-0.33	-0.93	-0.03	0.10	-0.77	-2.17	-0.07	0.24
E06	100	-0.27	-0.83	0.02	0.09	-0.64	-1.94	0.05	0.22
E07	120	-0.23	-0.71	0.03	0.08	-0.54	-1.66	0.07	0.19
E08	140	-0.22	-0.70	0.05	0.07	-0.51	-1.64	0.11	0.18
E09	160	-0.22	-0.75	0.02	0.07	-0.50	-1.74	0.05	0.17
E10	180	-0.22	-0.69	-0.01	0.07	-0.50	-1.60	-0.02	0.16
E11	200	-0.22	-0.70	0.00	0.07	-0.51	-1.63	0.01	0.17
E12	220	-0.22	-0.78	0.04	0.08	-0.51	-1.83	0.08	0.18

Table B-6. —continued.

Pressure tap	Degree	CpMean	CpMin	CpMax	CpRMS	CpMean	CpMin	CpMax	CpRMS
E13	240	-0.23	-0.74	0.03	0.08	-0.53	-1.73	0.07	0.19
E14	260	-0.27	-0.82	-0.01	0.09	-0.63	-1.93	-0.02	0.21
E15	280	-0.32	-0.86	-0.04	0.10	-0.75	-2.01	-0.09	0.23
E16	300	-0.33	-0.88	0.05	0.11	-0.78	-2.07	0.12	0.25
E17	320	-0.19	-0.77	0.26	0.11	-0.43	-1.80	0.60	0.26
E18	340	-0.04	-0.58	0.37	0.09	-0.10	-1.35	0.86	0.20
F01	0	-0.03	-0.40	0.36	0.07	-0.07	-0.95	0.85	0.15
F02	20	-0.06	-0.48	0.36	0.08	-0.14	-1.12	0.83	0.18
F03	40	-0.21	-0.63	0.18	0.08	-0.48	-1.46	0.42	0.20
F04	60	-0.28	-0.83	0.01	0.09	-0.67	-1.95	0.03	0.21
F05	80	-0.32	-0.85	-0.03	0.10	-0.74	-1.99	-0.08	0.24
F06	100	-0.27	-0.76	-0.01	0.09	-0.62	-1.79	-0.01	0.21
F07	120	-0.22	-0.69	0.02	0.07	-0.51	-1.61	0.04	0.17
F08	140	-0.21	-0.63	0.02	0.07	-0.49	-1.46	0.04	0.18
F09	160	-0.21	-0.65	0.00	0.07	-0.49	-1.51	0.00	0.16
F10	180	-0.21	-0.68	-0.01	0.07	-0.49	-1.59	-0.02	0.15
F11	200	-0.21	-0.67	-0.01	0.07	-0.49	-1.57	-0.02	0.16
F12	220	-0.21	-0.68	0.01	0.07	-0.49	-1.59	0.03	0.16
F13	240	-0.22	-0.68	0.02	0.07	-0.51	-1.59	0.06	0.17
F14	260	-0.25	-0.78	0.01	0.09	-0.59	-1.82	0.02	0.20
F15	280	-0.30	-0.83	-0.01	0.10	-0.71	-1.95	-0.03	0.23
F16	300	-0.31	-0.87	-0.02	0.10	-0.73	-2.04	-0.05	0.23
F17	320	-0.21	-0.67	0.20	0.09	-0.50	-1.57	0.47	0.20
F18	340	-0.08	-0.53	0.35	0.09	-0.20	-1.25	0.81	0.20
G01	0	-0.06	-0.38	0.27	0.06	-0.14	-0.88	0.63	0.13
G02	40	-0.21	-0.70	0.14	0.08	-0.49	-1.63	0.32	0.18
G03	80	-0.29	-0.84	-0.03	0.09	-0.68	-1.98	-0.07	0.22
G04	120	-0.22	-0.66	0.00	0.07	-0.51	-1.54	0.01	0.16
G05	160	-0.20	-0.63	0.00	0.06	-0.47	-1.47	-0.01	0.15
G06	200	-0.20	-0.59	0.01	0.06	-0.47	-1.37	0.02	0.15
G07	240	-0.21	-0.67	0.00	0.07	-0.49	-1.57	0.00	0.16
G08	280	-0.28	-0.77	-0.02	0.09	-0.65	-1.81	-0.06	0.21
G09	320	-0.22	-0.69	0.11	0.08	-0.51	-1.62	0.25	0.18
H01	0	-0.11	-0.44	0.15	0.05	-0.26	-1.03	0.35	0.12
H02	60	-0.26	-0.76	-0.03	0.08	-0.61	-1.77	-0.08	0.19
H03	120	-0.21	-0.63	-0.01	0.07	-0.49	-1.47	-0.02	0.16
H04	180	-0.21	-0.61	0.00	0.06	-0.48	-1.42	0.00	0.15
H05	240	-0.21	-0.66	0.00	0.07	-0.50	-1.55	0.00	0.16
H06	300	-0.25	-0.70	-0.03	0.08	-0.57	-1.64	-0.06	0.18

Table B-7. Pressure coefficient data obtained from 40° smooth roof.

Pressure tap	Degree	CpMean	CpMin	CpMax	CpRMS	CpMean	CpMin	CpMax	CpRMS
A01	0	-0.03	-1.63	1.84	0.33	-0.07	-3.78	4.24	0.77
A02	10	-0.06	-1.58	1.54	0.32	-0.15	-3.65	3.57	0.75
A03	20	-0.11	-1.49	1.44	0.29	-0.26	-3.44	3.34	0.66
A04	30	-0.17	-1.43	1.06	0.25	-0.40	-3.31	2.45	0.57
A05	40	-0.23	-1.28	0.75	0.21	-0.53	-2.95	1.73	0.49
A06	50	-0.28	-1.32	0.65	0.19	-0.64	-3.04	1.50	0.43
A07	60	-0.41	-1.56	0.49	0.21	-0.95	-3.60	1.12	0.48
A08	70	-0.44	-1.37	0.28	0.17	-1.02	-3.16	0.65	0.38
A09	80	-0.44	-1.34	0.04	0.14	-1.02	-3.10	0.08	0.33
A10	90	-0.42	-1.21	-0.03	0.14	-0.97	-2.80	-0.06	0.31
A11	100	-0.35	-1.09	0.02	0.12	-0.81	-2.51	0.05	0.28
A12	110	-0.32	-1.08	0.07	0.12	-0.75	-2.50	0.15	0.27
A13	120	-0.28	-1.16	0.08	0.11	-0.64	-2.69	0.19	0.25
A14	130	-0.24	-1.01	0.07	0.10	-0.55	-2.34	0.17	0.22
A15	140	-0.22	-1.08	0.08	0.09	-0.50	-2.49	0.18	0.21
A16	150	-0.22	-1.08	0.06	0.09	-0.51	-2.49	0.14	0.21
A17	160	-0.21	-0.90	0.05	0.08	-0.49	-2.09	0.11	0.19
A18	170	-0.21	-0.91	0.04	0.08	-0.48	-2.09	0.08	0.19
A19	180	-0.20	-0.83	0.03	0.08	-0.46	-1.92	0.08	0.18
A20	190	-0.20	-0.95	0.02	0.08	-0.46	-2.20	0.05	0.19
A21	200	-0.21	-1.10	0.07	0.09	-0.48	-2.53	0.16	0.20
A22	210	-0.22	-1.03	0.08	0.09	-0.50	-2.38	0.18	0.20
A23	220	-0.21	-0.90	0.07	0.09	-0.50	-2.07	0.17	0.20
A24	230	-0.23	-1.01	0.08	0.09	-0.53	-2.32	0.18	0.22
A25	240	-0.28	-1.06	0.07	0.11	-0.64	-2.44	0.16	0.26
A26	250	-0.37	-1.24	0.06	0.15	-0.85	-2.86	0.14	0.34
A27	260	-0.44	-1.35	0.05	0.16	-1.01	-3.13	0.11	0.37
A28	270	-0.51	-1.46	-0.01	0.18	-1.18	-3.36	-0.03	0.41
A29	280	-0.43	-1.42	0.17	0.15	-0.99	-3.27	0.39	0.35
A30	290	-0.47	-1.63	0.39	0.18	-1.08	-3.77	0.90	0.42
A31	300	-0.37	-1.48	0.61	0.19	-0.86	-3.42	1.41	0.44
A32	310	-0.27	-1.34	0.83	0.20	-0.62	-3.09	1.92	0.46
A33	320	-0.21	-1.43	1.04	0.23	-0.48	-3.30	2.41	0.54
A34	330	-0.13	-1.60	1.38	0.28	-0.31	-3.71	3.19	0.65
A35	340	-0.07	-1.51	1.56	0.31	-0.17	-3.48	3.61	0.71
A36	350	-0.03	-1.89	1.99	0.36	-0.08	-4.37	4.59	0.82
B01	0	0.13	-1.59	1.81	0.35	0.31	-3.69	4.18	0.81
B02	10	0.14	-1.52	1.66	0.34	0.33	-3.52	3.84	0.78
B03	20	0.12	-1.80	1.80	0.36	0.27	-4.15	4.16	0.82
B04	30	0.06	-2.70	2.32	0.49	0.14	-6.24	5.37	1.13
B05	40	-0.16	-1.81	1.35	0.35	-0.37	-4.19	3.13	0.82
B06	50	-0.28	-1.45	1.00	0.25	-0.64	-3.34	2.31	0.58
B07	60	-0.47	-1.82	0.66	0.24	-1.08	-4.21	1.53	0.55
B08	70	-0.40	-1.29	0.29	0.15	-0.93	-2.98	0.66	0.35

Table B-7. —continued.

Pressure tap	Degree	CpMean	CpMin	CpMax	CpRMS	CpMean	CpMin	CpMax	CpRMS
B09	80	-0.41	-1.21	0.06	0.13	-0.94	-2.79	0.15	0.31
B10	90	-0.42	-1.19	0.01	0.13	-0.97	-2.74	0.03	0.31
B11	100	-0.37	-1.11	0.04	0.13	-0.85	-2.56	0.10	0.29
B12	110	-0.35	-1.23	0.08	0.13	-0.82	-2.84	0.20	0.30
B13	120	-0.29	-1.11	0.10	0.11	-0.66	-2.56	0.23	0.25
B14	130	-0.25	-1.03	0.11	0.10	-0.58	-2.38	0.25	0.23
B15	140	-0.24	-0.99	0.10	0.09	-0.54	-2.30	0.22	0.22
B16	150	-0.22	-1.00	0.08	0.09	-0.52	-2.30	0.18	0.21
B17	160	-0.21	-0.88	0.07	0.08	-0.50	-2.04	0.15	0.19
B18	170	-0.20	-0.78	0.04	0.07	-0.45	-1.81	0.08	0.17
B19	180	-0.20	-0.81	0.05	0.08	-0.45	-1.88	0.12	0.17
B20	190	-0.21	-0.96	0.06	0.08	-0.47	-2.23	0.14	0.19
B21	200	-0.20	-0.89	0.06	0.08	-0.47	-2.05	0.15	0.19
B22	210	-0.21	-0.86	0.11	0.08	-0.48	-1.98	0.26	0.19
B23	220	-0.21	-0.95	0.11	0.09	-0.49	-2.20	0.25	0.20
B24	230	-0.25	-1.09	0.12	0.10	-0.59	-2.52	0.27	0.24
B25	240	-0.29	-1.07	0.10	0.11	-0.66	-2.47	0.24	0.27
B26	250	-0.35	-1.27	0.10	0.14	-0.82	-2.94	0.23	0.32
B27	260	-0.42	-1.28	0.04	0.15	-0.96	-2.97	0.09	0.35
B28	270	-0.48	-1.43	-0.02	0.17	-1.11	-3.31	-0.05	0.38
B29	280	-0.41	-1.22	0.22	0.14	-0.95	-2.82	0.51	0.32
B30	290	-0.51	-1.62	0.39	0.18	-1.19	-3.75	0.91	0.42
B31	300	-0.41	-1.54	0.76	0.22	-0.95	-3.56	1.77	0.51
B32	310	-0.24	-1.76	1.25	0.31	-0.55	-4.07	2.89	0.71
B33	320	-0.06	-2.33	2.17	0.47	-0.14	-5.38	5.01	1.08
B34	330	0.10	-2.04	2.06	0.42	0.23	-4.72	4.77	0.97
B35	340	0.15	-2.17	2.09	0.44	0.34	-5.01	4.83	1.01
B36	350	0.14	-1.81	1.99	0.42	0.32	-4.17	4.60	0.98
C01	0	0.06	-0.20	0.42	0.06	0.14	-0.46	0.96	0.14
C02	10	0.04	-0.18	0.30	0.05	0.09	-0.41	0.69	0.11
C03	20	-0.01	0.14	-0.18	-0.03	-0.01	0.33	-0.42	-0.08
C04	30	-0.21	-2.15	2.05	0.40	-0.48	-4.97	4.74	0.92
C05	40	-0.17	-0.88	0.44	0.12	-0.40	-2.04	1.01	0.27
C06	50	-0.23	-0.90	0.35	0.13	-0.52	-2.08	0.82	0.29
C07	60	-0.47	-1.51	0.26	0.19	-1.08	-3.50	0.60	0.45
C08	70	-0.33	-0.94	0.06	0.11	-0.76	-2.17	0.13	0.26
C09	80	-0.50	-1.30	-0.04	0.16	-1.16	-3.00	-0.10	0.36
C10	90	-0.45	-1.25	-0.01	0.14	-1.04	-2.89	-0.02	0.33
C11	100	-0.40	-1.20	0.05	0.13	-0.91	-2.78	0.11	0.31
C12	110	-0.36	-1.18	0.05	0.13	-0.84	-2.72	0.11	0.29
C13	120	-0.32	-1.19	0.07	0.12	-0.74	-2.76	0.15	0.27
C14	130	-0.31	-1.37	0.09	0.12	-0.71	-3.16	0.21	0.27
C15	140	-0.30	-1.22	0.08	0.11	-0.68	-2.81	0.18	0.26
C16	150	-0.28	-1.26	0.08	0.10	-0.64	-2.91	0.18	0.23
C17	160	-0.27	-1.15	0.06	0.09	-0.63	-2.66	0.14	0.22
C18	170	-0.24	-0.83	0.02	0.08	-0.56	-1.91	0.06	0.18
C19	180	-0.25	-0.91	0.01	0.08	-0.57	-2.10	0.03	0.19

Table B-7. —continued.

Pressure tap	Degree	CpMean	CpMin	CpMax	CpRMS	CpMean	CpMin	CpMax	CpRMS
C20	190	-0.25	-1.04	0.04	0.09	-0.58	-2.40	0.09	0.20
C21	200	-0.27	-1.19	0.06	0.10	-0.63	-2.75	0.14	0.23
C22	210	-0.28	-1.23	0.09	0.10	-0.65	-2.84	0.21	0.24
C23	220	-0.28	-1.20	0.09	0.11	-0.66	-2.77	0.21	0.25
C24	230	-0.31	-1.20	0.06	0.12	-0.72	-2.77	0.14	0.27
C25	240	-0.35	-1.22	0.07	0.13	-0.81	-2.81	0.17	0.30
C26	250	-0.39	-1.33	0.05	0.15	-0.91	-3.08	0.11	0.34
C27	260	-0.40	-1.19	0.02	0.14	-0.93	-2.75	0.04	0.33
C28	270	-0.48	-1.31	-0.04	0.16	-1.10	-3.03	-0.09	0.37
C29	280	-0.41	-1.12	0.05	0.13	-0.94	-2.59	0.12	0.30
C30	290	-0.41	-1.14	0.08	0.13	-0.95	-2.64	0.18	0.30
C31	300	-0.28	-0.99	0.33	0.13	-0.64	-2.29	0.76	0.29
C32	310	-0.22	-0.95	0.45	0.13	-0.52	-2.20	1.03	0.30
C33	320	-0.15	-1.11	0.83	0.17	-0.36	-2.57	1.92	0.39
C34	330	-0.02	-1.85	2.13	0.39	-0.04	-4.28	4.92	0.90
C35	340	-0.08	0.53	-0.80	-0.14	-0.18	1.23	-1.85	-0.32
C36	350	0.03	-0.12	0.23	0.03	0.07	-0.28	0.53	0.08
D01	0	-0.04	0.19	-0.39	-0.06	-0.09	0.44	-0.90	-0.14
D02	20	0.02	-3.98	4.11	0.66	0.04	-9.19	9.49	1.53
D03	40	-0.20	-1.50	0.66	0.17	-0.47	-3.47	1.52	0.38
D04	60	-0.54	-1.93	0.34	0.28	-1.26	-4.46	0.78	0.64
D05	80	-0.56	-1.50	-0.05	0.18	-1.30	-3.47	-0.12	0.42
D06	100	-0.43	-1.32	0.01	0.14	-1.00	-3.06	0.02	0.33
D07	120	-0.36	-1.24	0.09	0.13	-0.84	-2.86	0.20	0.30
D08	140	-0.35	-1.33	0.06	0.12	-0.81	-3.07	0.13	0.28
D09	160	-0.34	-1.33	0.01	0.11	-0.78	-3.07	0.02	0.25
D10	180	-0.32	-1.07	-0.01	0.10	-0.75	-2.46	-0.03	0.24
D11	200	-0.33	-1.29	0.04	0.11	-0.76	-2.98	0.10	0.25
D12	220	-0.35	-1.31	0.08	0.12	-0.80	-3.03	0.19	0.28
D13	240	-0.37	-1.24	0.06	0.13	-0.85	-2.86	0.13	0.30
D14	260	-0.44	-1.34	0.02	0.16	-1.02	-3.10	0.04	0.37
D15	280	-0.45	-1.28	-0.01	0.14	-1.03	-2.96	-0.02	0.33
D16	300	-0.33	-1.42	0.41	0.15	-0.76	-3.27	0.96	0.35
D17	320	-0.15	-0.93	0.75	0.14	-0.35	-2.15	1.74	0.33
D18	340	0.12	-1.32	2.38	0.38	0.27	-3.06	5.49	0.87
E01	0	0.03	-0.36	0.59	0.09	0.07	-0.83	1.37	0.21
E02	20	-0.24	-2.85	1.94	0.46	-0.55	-6.58	4.48	1.07
E03	40	-0.31	-1.11	0.36	0.16	-0.72	-2.56	0.83	0.37
E04	60	-0.48	-1.32	0.05	0.15	-1.12	-3.06	0.12	0.35
E05	80	-0.42	-1.16	-0.01	0.14	-0.98	-2.68	-0.03	0.31
E06	100	-0.41	-1.29	0.04	0.14	-0.94	-2.99	0.09	0.33
E07	120	-0.40	-1.29	0.07	0.14	-0.92	-2.98	0.16	0.32
E08	140	-0.39	-1.45	0.04	0.13	-0.90	-3.34	0.10	0.30
E09	160	-0.40	-1.26	0.01	0.13	-0.92	-2.92	0.03	0.30
E10	180	-0.40	-1.28	0.00	0.12	-0.92	-2.95	0.00	0.29
E11	200	-0.41	-1.48	0.04	0.13	-0.94	-3.41	0.09	0.31
E12	220	-0.40	-1.51	0.05	0.14	-0.91	-3.49	0.11	0.31

Table B-7. —continued.

Pressure tap	Degree	CpMean	CpMin	CpMax	CpRMS	CpMean	CpMin	CpMax	CpRMS
E13	240	-0.41	-1.38	0.08	0.15	-0.94	-3.18	0.19	0.34
E14	260	-0.44	-1.37	-0.01	0.16	-1.03	-3.16	-0.02	0.37
E15	280	-0.44	-1.20	-0.02	0.14	-1.02	-2.78	-0.05	0.32
E16	300	-0.41	-1.13	0.11	0.13	-0.94	-2.60	0.25	0.30
E17	320	-0.23	-1.12	0.61	0.19	-0.52	-2.60	1.41	0.44
E18	340	0.00	-1.72	1.83	0.32	0.01	-3.98	4.22	0.73
F01	0	-0.02	-1.94	2.25	0.35	-0.04	-4.48	5.19	0.81
F02	20	-0.25	-1.62	1.14	0.27	-0.57	-3.74	2.63	0.63
F03	40	-0.35	-1.16	0.33	0.15	-0.81	-2.68	0.77	0.34
F04	60	-0.48	-1.35	-0.05	0.15	-1.12	-3.11	-0.12	0.36
F05	80	-0.39	-1.12	-0.02	0.13	-0.91	-2.58	-0.05	0.29
F06	100	-0.36	-1.26	0.00	0.13	-0.83	-2.90	0.00	0.29
F07	120	-0.38	-1.24	0.05	0.13	-0.88	-2.86	0.12	0.29
F08	140	-0.37	-1.21	0.03	0.12	-0.86	-2.79	0.06	0.29
F09	160	-0.40	-1.21	0.02	0.13	-0.93	-2.80	0.05	0.30
F10	180	-0.41	-1.33	0.04	0.13	-0.94	-3.07	0.09	0.30
F11	200	-0.40	-1.19	0.00	0.13	-0.93	-2.74	0.00	0.29
F12	220	-0.40	-1.23	0.00	0.13	-0.91	-2.84	0.01	0.30
F13	240	-0.40	-1.28	0.03	0.13	-0.93	-2.96	0.07	0.31
F14	260	-0.43	-1.36	0.01	0.15	-1.00	-3.15	0.03	0.35
F15	280	-0.44	-1.27	-0.03	0.15	-1.02	-2.93	-0.07	0.34
F16	300	-0.43	-1.23	0.05	0.13	-0.99	-2.83	0.12	0.30
F17	320	-0.29	-1.08	0.51	0.15	-0.67	-2.50	1.17	0.35
F18	340	-0.09	-1.24	1.08	0.22	-0.20	-2.88	2.49	0.50
G01	0	-0.11	-1.37	1.11	0.21	-0.26	-3.16	2.56	0.48
G02	40	-0.40	-1.29	0.20	0.15	-0.92	-2.98	0.46	0.35
G03	80	-0.37	-1.07	-0.02	0.12	-0.85	-2.48	-0.06	0.28
G04	120	-0.37	-1.10	0.01	0.12	-0.87	-2.54	0.02	0.28
G05	160	-0.39	-1.18	0.01	0.13	-0.91	-2.73	0.03	0.29
G06	200	-0.38	-1.09	0.01	0.12	-0.88	-2.53	0.02	0.28
G07	240	-0.38	-1.24	0.03	0.13	-0.88	-2.87	0.08	0.29
G08	280	-0.41	-1.26	-0.02	0.14	-0.95	-2.91	-0.05	0.32
G09	320	-0.33	-1.17	0.30	0.14	-0.76	-2.69	0.69	0.32
H01	0	-0.57	-1.75	-0.03	0.18	-1.31	-4.05	-0.07	0.41
H02	60	-0.39	-1.26	-0.02	0.13	-0.91	-2.91	-0.05	0.30
H03	120	-0.36	-1.13	0.00	0.11	-0.82	-2.60	-0.01	0.26
H04	180	-0.35	-1.03	0.01	0.11	-0.82	-2.39	0.01	0.26
H05	240	-0.37	-1.16	0.00	0.12	-0.85	-2.69	0.00	0.28
H06	300	-0.43	-1.38	-0.02	0.15	-0.99	-3.20	-0.04	0.34

Table B-8. Pressure coefficient data obtained from 40° smooth roof.

Pressure tap	Degree	CpMean	CpMin	CpMax	CpRMS	CpMean	CpMin	CpMax	CpRMS
A01	0	-0.02	-0.85	0.95	0.17	-0.04	-1.96	2.20	0.40
A02	10	-0.03	-0.84	0.82	0.17	-0.08	-1.93	1.89	0.40
A03	20	-0.07	-0.87	0.85	0.17	-0.15	-2.01	1.96	0.39
A04	30	-0.11	-0.91	0.67	0.16	-0.25	-2.09	1.55	0.36
A05	40	-0.17	-0.94	0.55	0.16	-0.39	-2.18	1.28	0.36
A06	50	-0.21	-1.01	0.50	0.14	-0.49	-2.33	1.15	0.33
A07	60	-0.28	-1.05	0.33	0.14	-0.64	-2.42	0.75	0.32
A08	70	-0.32	-0.98	0.20	0.12	-0.73	-2.26	0.47	0.28
A09	80	-0.37	-1.11	0.03	0.12	-0.84	-2.57	0.07	0.27
A10	90	-0.34	-0.98	-0.02	0.11	-0.79	-2.26	-0.05	0.25
A11	100	-0.30	-0.95	0.02	0.10	-0.70	-2.19	0.04	0.24
A12	110	-0.27	-0.90	0.06	0.10	-0.62	-2.07	0.13	0.23
A13	120	-0.25	-1.04	0.07	0.10	-0.57	-2.40	0.17	0.22
A14	130	-0.24	-1.03	0.07	0.10	-0.55	-2.37	0.17	0.23
A15	140	-0.25	-1.23	0.09	0.10	-0.57	-2.84	0.21	0.24
A16	150	-0.27	-1.30	0.07	0.11	-0.61	-3.01	0.17	0.25
A17	160	-0.27	-1.14	0.06	0.11	-0.62	-2.64	0.14	0.25
A18	170	-0.28	-1.19	0.05	0.11	-0.64	-2.76	0.11	0.26
A19	180	-0.28	-1.16	0.05	0.11	-0.64	-2.67	0.11	0.25
A20	190	-0.28	-1.31	0.03	0.11	-0.64	-3.04	0.06	0.26
A21	200	-0.27	-1.39	0.09	0.11	-0.61	-3.20	0.20	0.26
A22	210	-0.25	-1.19	0.09	0.10	-0.58	-2.76	0.21	0.24
A23	220	-0.24	-1.02	0.08	0.10	-0.56	-2.35	0.19	0.23
A24	230	-0.25	-1.08	0.09	0.10	-0.57	-2.50	0.20	0.24
A25	240	-0.26	-0.99	0.07	0.10	-0.60	-2.29	0.15	0.24
A26	250	-0.30	-1.02	0.05	0.12	-0.70	-2.37	0.11	0.28
A27	260	-0.34	-1.05	0.04	0.12	-0.78	-2.43	0.08	0.28
A28	270	-0.40	-1.15	-0.01	0.14	-0.93	-2.65	-0.02	0.32
A29	280	-0.33	-1.10	0.13	0.12	-0.77	-2.55	0.30	0.28
A30	290	-0.35	-1.23	0.29	0.14	-0.81	-2.83	0.68	0.32
A31	300	-0.27	-1.08	0.44	0.14	-0.63	-2.48	1.03	0.32
A32	310	-0.21	-1.02	0.63	0.15	-0.47	-2.35	1.46	0.35
A33	320	-0.15	-1.03	0.75	0.17	-0.34	-2.38	1.73	0.39
A34	330	-0.08	-0.97	0.84	0.17	-0.19	-2.24	1.93	0.39
A35	340	-0.04	-0.88	0.92	0.18	-0.10	-2.04	2.11	0.42
A36	350	-0.02	-0.96	1.01	0.18	-0.04	-2.22	2.33	0.42
B01	0	0.07	-0.80	0.91	0.18	0.16	-1.86	2.11	0.41
B02	10	0.07	-0.76	0.82	0.17	0.16	-1.75	1.90	0.39
B03	20	0.05	-0.83	0.83	0.17	0.12	-1.92	1.93	0.38
B04	30	0.02	-0.83	0.72	0.15	0.04	-1.93	1.86	0.35
B05	40	-0.08	-0.85	0.64	0.17	-0.17	-1.96	1.47	0.38
B06	50	-0.16	-0.83	0.57	0.14	-0.37	-1.92	1.33	0.33
B07	60	-0.25	-0.96	0.35	0.13	-0.57	-2.22	0.81	0.29
B08	70	-0.29	-0.91	0.20	0.11	-0.66	-2.11	0.47	0.25

Table B-8. —continued.

Pressure tap	Degree	CpMean	CpMin	CpMax	CpRMS	CpMean	CpMin	CpMax	CpRMS
B09	80	-0.34	-1.00	0.05	0.11	-0.78	-2.32	0.12	0.26
B10	90	-0.33	-0.94	0.01	0.11	-0.77	-2.18	0.02	0.25
B11	100	-0.31	-0.93	0.04	0.11	-0.71	-2.15	0.09	0.24
B12	110	-0.27	-0.93	0.06	0.10	-0.62	-2.14	0.15	0.22
B13	120	-0.24	-0.94	0.09	0.09	-0.56	-2.18	0.20	0.21
B14	130	-0.24	-0.98	0.10	0.10	-0.55	-2.26	0.23	0.22
B15	140	-0.24	-1.02	0.10	0.10	-0.55	-2.35	0.23	0.22
B16	150	-0.25	-1.12	0.09	0.10	-0.58	-2.58	0.21	0.23
B17	160	-0.26	-1.07	0.08	0.10	-0.60	-2.47	0.19	0.23
B18	170	-0.26	-1.04	0.05	0.10	-0.60	-2.39	0.11	0.23
B19	180	-0.26	-1.06	0.07	0.10	-0.59	-2.44	0.15	0.23
B20	190	-0.26	-1.21	0.08	0.10	-0.60	-2.79	0.17	0.23
B21	200	-0.25	-1.10	0.08	0.10	-0.58	-2.53	0.18	0.23
B22	210	-0.25	-1.03	0.14	0.10	-0.57	-2.38	0.31	0.23
B23	220	-0.23	-1.05	0.12	0.10	-0.54	-2.42	0.28	0.22
B24	230	-0.24	-1.02	0.11	0.10	-0.55	-2.35	0.25	0.23
B25	240	-0.25	-0.93	0.09	0.10	-0.58	-2.15	0.21	0.23
B26	250	-0.29	-1.06	0.08	0.12	-0.68	-2.44	0.19	0.27
B27	260	-0.32	-0.98	0.03	0.12	-0.74	-2.27	0.07	0.27
B28	270	-0.39	-1.15	-0.02	0.13	-0.89	-2.66	-0.04	0.31
B29	280	-0.31	-0.93	0.17	0.11	-0.72	-2.14	0.39	0.25
B30	290	-0.37	-1.17	0.28	0.13	-0.86	-2.70	0.65	0.30
B31	300	-0.26	-0.96	0.48	0.14	-0.59	-2.22	1.10	0.32
B32	310	-0.13	-0.97	0.68	0.17	-0.30	-2.23	1.58	0.39
B33	320	-0.02	-0.92	0.86	0.18	-0.05	-2.13	1.99	0.43
B34	330	0.04	-0.83	0.84	0.17	0.09	-1.92	1.94	0.39
B35	340	0.06	-0.86	0.83	0.17	0.14	-1.99	1.92	0.40
B36	350	0.06	-0.77	0.84	0.18	0.14	-1.77	1.95	0.41
C01	0	0.11	-0.38	0.81	0.12	0.26	-0.89	1.86	0.28
C02	10	0.09	-0.43	0.73	0.12	0.22	-1.00	1.69	0.27
C03	20	0.02	-0.51	0.64	0.12	0.04	-1.17	1.49	0.28
C04	30	-0.06	-0.61	0.58	0.11	-0.14	-1.41	1.34	0.26
C05	40	-0.16	-0.81	0.40	0.11	-0.37	-1.88	0.93	0.25
C06	50	-0.19	-0.77	0.31	0.11	-0.45	-1.79	0.70	0.25
C07	60	-0.30	-0.97	0.17	0.12	-0.69	-2.24	0.38	0.29
C08	70	-0.32	-0.90	0.06	0.11	-0.73	-2.09	0.13	0.25
C09	80	-0.37	-0.95	-0.03	0.11	-0.85	-2.20	-0.08	0.26
C10	90	-0.34	-0.94	-0.01	0.11	-0.78	-2.18	-0.01	0.25
C11	100	-0.31	-0.93	0.04	0.10	-0.71	-2.16	0.09	0.24
C12	110	-0.27	-0.89	0.04	0.09	-0.63	-2.05	0.08	0.22
C13	120	-0.25	-0.92	0.05	0.09	-0.57	-2.12	0.12	0.21
C14	130	-0.25	-1.10	0.07	0.09	-0.57	-2.53	0.17	0.21
C15	140	-0.25	-1.01	0.07	0.09	-0.57	-2.34	0.15	0.21
C16	150	-0.25	-1.13	0.07	0.09	-0.57	-2.61	0.16	0.21
C17	160	-0.24	-1.03	0.05	0.08	-0.56	-2.39	0.12	0.19
C18	170	-0.25	-0.85	0.03	0.08	-0.57	-1.97	0.06	0.19
C19	180	-0.25	-0.90	0.01	0.08	-0.57	-2.08	0.03	0.19

Table B-8. —continued.

Pressure tap	Degree	CpMean	CpMin	CpMax	CpRMS	CpMean	CpMin	CpMax	CpRMS
C20	190	-0.24	-1.00	0.04	0.08	-0.56	-2.30	0.08	0.19
C21	200	-0.25	-1.08	0.05	0.09	-0.57	-2.49	0.12	0.20
C22	210	-0.24	-1.06	0.08	0.09	-0.56	-2.45	0.18	0.21
C23	220	-0.25	-1.04	0.08	0.09	-0.57	-2.39	0.18	0.21
C24	230	-0.24	-0.94	0.05	0.09	-0.56	-2.18	0.11	0.21
C25	240	-0.26	-0.90	0.05	0.09	-0.60	-2.07	0.12	0.22
C26	250	-0.29	-0.98	0.03	0.11	-0.67	-2.27	0.08	0.25
C27	260	-0.33	-0.96	0.01	0.11	-0.75	-2.21	0.03	0.26
C28	270	-0.37	-1.03	-0.03	0.12	-0.86	-2.37	-0.07	0.29
C29	280	-0.33	-0.92	0.04	0.11	-0.77	-2.13	0.10	0.24
C30	290	-0.35	-0.98	0.07	0.11	-0.81	-2.27	0.15	0.26
C31	300	-0.22	-0.79	0.26	0.10	-0.51	-1.83	0.61	0.23
C32	310	-0.17	-0.74	0.35	0.10	-0.40	-1.71	0.80	0.23
C33	320	-0.10	-0.70	0.53	0.11	-0.23	-1.62	1.21	0.24
C34	330	-0.01	-0.57	0.66	0.12	-0.01	-1.32	1.52	0.28
C35	340	0.07	-0.49	0.74	0.13	0.17	-1.14	1.71	0.30
C36	350	0.11	-0.42	0.79	0.12	0.25	-0.97	1.83	0.27
D01	0	0.06	-0.30	0.62	0.09	0.14	-0.69	1.43	0.22
D02	20	0.00	-0.53	0.54	0.09	0.01	-1.22	1.26	0.20
D03	40	-0.11	-0.85	0.37	0.09	-0.26	-1.96	0.86	0.22
D04	60	-0.30	-1.07	0.19	0.15	-0.70	-2.48	0.43	0.35
D05	80	-0.39	-1.03	-0.04	0.12	-0.89	-2.38	-0.08	0.29
D06	100	-0.31	-0.94	0.01	0.10	-0.71	-2.16	0.02	0.24
D07	120	-0.25	-0.85	0.06	0.09	-0.58	-1.96	0.14	0.20
D08	140	-0.24	-0.91	0.04	0.08	-0.55	-2.11	0.09	0.19
D09	160	-0.24	-0.96	0.01	0.08	-0.56	-2.22	0.01	0.18
D10	180	-0.24	-0.80	-0.01	0.08	-0.56	-1.84	-0.02	0.18
D11	200	-0.24	-0.95	0.03	0.08	-0.56	-2.19	0.07	0.19
D12	220	-0.24	-0.90	0.06	0.08	-0.55	-2.08	0.13	0.19
D13	240	-0.25	-0.85	0.04	0.09	-0.58	-1.95	0.09	0.21
D14	260	-0.32	-0.97	0.01	0.11	-0.74	-2.24	0.03	0.27
D15	280	-0.34	-0.97	-0.01	0.11	-0.78	-2.24	-0.01	0.25
D16	300	-0.20	-0.85	0.25	0.09	-0.46	-1.97	0.57	0.21
D17	320	-0.08	-0.51	0.41	0.08	-0.19	-1.18	0.96	0.18
D18	340	0.03	-0.33	0.59	0.09	0.07	-0.76	1.36	0.22
E01	0	0.03	-0.36	0.59	0.09	0.07	-0.83	1.37	0.21
E02	20	-0.06	-0.71	0.48	0.12	-0.14	-1.63	1.11	0.27
E03	40	-0.25	-0.87	0.28	0.13	-0.57	-2.01	0.66	0.29
E04	60	-0.36	-0.98	0.04	0.11	-0.82	-2.26	0.09	0.26
E05	80	-0.33	-0.91	-0.01	0.11	-0.77	-2.11	-0.03	0.24
E06	100	-0.28	-0.90	0.03	0.10	-0.66	-2.09	0.06	0.23
E07	120	-0.24	-0.78	0.04	0.08	-0.55	-1.79	0.10	0.19
E08	140	-0.24	-0.88	0.03	0.08	-0.54	-2.03	0.06	0.18
E09	160	-0.24	-0.75	0.01	0.08	-0.55	-1.74	0.02	0.18
E10	180	-0.24	-0.76	0.00	0.07	-0.55	-1.76	0.00	0.17
E11	200	-0.24	-0.86	0.02	0.08	-0.55	-2.00	0.05	0.18
E12	220	-0.24	-0.91	0.03	0.08	-0.55	-2.10	0.06	0.19

Table B-8. —continued.

Pressure tap	Degree	CpMean	CpMin	CpMax	CpRMS	CpMean	CpMin	CpMax	CpRMS
E13	240	-0.25	-0.83	0.05	0.09	-0.57	-1.93	0.11	0.21
E14	260	-0.31	-0.94	-0.01	0.11	-0.70	-2.17	-0.01	0.25
E15	280	-0.33	-0.89	-0.02	0.10	-0.76	-2.07	-0.03	0.23
E16	300	-0.33	-0.91	0.09	0.10	-0.76	-2.10	0.21	0.24
E17	320	-0.14	-0.72	0.39	0.12	-0.33	-1.65	0.90	0.28
E18	340	0.00	-0.51	0.54	0.09	0.00	-1.18	1.26	0.22
F01	0	0.00	-0.45	0.52	0.08	-0.01	-1.04	1.20	0.19
F02	20	-0.09	-0.59	0.41	0.10	-0.21	-1.35	0.95	0.23
F03	40	-0.25	-0.82	0.24	0.11	-0.57	-1.89	0.54	0.24
F04	60	-0.34	-0.96	-0.04	0.11	-0.79	-2.21	-0.08	0.25
F05	80	-0.31	-0.88	-0.02	0.10	-0.72	-2.04	-0.04	0.23
F06	100	-0.26	-0.90	0.00	0.09	-0.60	-2.07	0.00	0.21
F07	120	-0.23	-0.74	0.03	0.08	-0.53	-1.72	0.07	0.18
F08	140	-0.23	-0.73	0.02	0.07	-0.52	-1.68	0.04	0.17
F09	160	-0.23	-0.68	0.01	0.07	-0.52	-1.58	0.03	0.17
F10	180	-0.23	-0.75	0.02	0.07	-0.53	-1.73	0.05	0.17
F11	200	-0.23	-0.68	0.00	0.07	-0.53	-1.56	0.00	0.17
F12	220	-0.23	-0.72	0.00	0.08	-0.53	-1.66	0.01	0.18
F13	240	-0.24	-0.77	0.02	0.08	-0.56	-1.78	0.04	0.19
F14	260	-0.29	-0.92	0.01	0.10	-0.68	-2.13	0.02	0.24
F15	280	-0.34	-0.98	-0.03	0.11	-0.79	-2.27	-0.06	0.26
F16	300	-0.33	-0.95	0.04	0.10	-0.77	-2.19	0.10	0.23
F17	320	-0.19	-0.70	0.33	0.10	-0.43	-1.61	0.75	0.22
F18	340	-0.04	-0.55	0.47	0.10	-0.09	-1.26	1.09	0.22
G01	0	-0.04	-0.48	0.39	0.07	-0.09	-1.11	0.90	0.17
G02	40	-0.25	-0.81	0.13	0.09	-0.58	-1.88	0.29	0.22
G03	80	-0.29	-0.84	-0.02	0.09	-0.66	-1.93	-0.04	0.22
G04	120	-0.23	-0.66	0.01	0.07	-0.52	-1.53	0.01	0.17
G05	160	-0.22	-0.66	0.01	0.07	-0.51	-1.52	0.02	0.16
G06	200	-0.22	-0.65	0.01	0.07	-0.52	-1.49	0.01	0.17
G07	240	-0.23	-0.76	0.02	0.08	-0.54	-1.76	0.05	0.18
G08	280	-0.32	-0.99	-0.02	0.11	-0.75	-2.29	-0.04	0.25
G09	320	-0.21	-0.73	0.19	0.09	-0.48	-1.68	0.43	0.20
H01	0	-0.25	-0.78	-0.01	0.08	-0.58	-1.80	-0.03	0.18
H02	60	-0.27	-0.86	-0.02	0.09	-0.62	-1.99	-0.04	0.20
H03	120	-0.23	-0.72	0.00	0.07	-0.53	-1.66	-0.01	0.17
H04	180	-0.23	-0.66	0.00	0.07	-0.52	-1.53	0.01	0.17
H05	240	-0.24	-0.77	0.00	0.08	-0.56	-1.78	0.00	0.18
H06	300	-0.28	-0.91	-0.01	0.10	-0.65	-2.11	-0.02	0.22

LIST OF REFERENCES

- ACI 318.99. 1999. Building code requirements for reinforced concrete. American Concrete Institute. Farmington Hills, MI.
- Adrezin, R., P. Bar-Avi and H. Benoraya. 1996. Dynamic response of compliant offshore structures-review. *Journal of Aerospace Engineering*. 9 (4): 114-131.
- Aldrich, R.A. and G.S. Weaving. 1979. Structural response of an inflated roof greenhouse. *Transactions of ASAE* 22(1). 1390-1397.
- Aldrich, R.A. and D.A. Wells. 1979. Estimating wind loads on glasshouses. *Transactions of ASAE* 22(1). 1122-1128.
- Almroth, B.O. 1962. Buckling of a cylindrical shell subjected to non-uniform external pressure. *Journal of Applied Mechanics, Transactions of ASME*. 29 (4): 675-682.
- Ambrose, J and D. Vergun. 1994. Simplified Building Design for Wind and Earthquake Forces. Third Edition, John Wiley & Sons, Inc., New York, N.Y.
- Andrade, L.J., C. Calil, and C.F. Carril. 2001. The structural behavior of cylindrical silos under wind loading-state of the art. *AAWE Americas Conference on Wind Engineering – 2001*. Clemson, S.C.
- ANSI. 1982. American national standard minimum design loads for buildings and other structures. ANSI A58.1-82, American National Standards Institute, New York, N.Y.
- ASAE. 1980. *Agricultural Engineering Yearbook*. ASAE, St. Joseph, Michigan.
- ASAE Standards. 1998. EP 288.5 DEC92. Agricultural building snow and wind loads. ASAE Standards, St. Joseph, Michigan.
- ASCE. 1961. Wind forces on structures. *Transactions of ASCE*. 126 (2): 1124-1198.
- ASCE. 1987. Wind tunnel model studies of buildings and structures. *Manuals and Reports on Engineering Practice*. No. 67. American Society of Civil Engineers. New York, N.Y.

- ASCE. 1987b. Wind Loading and Wind-induced Structural Response. A state-of-the-art prepared by committee on wind effects of the committee on dynamic effects of the structural division of the American Society of Civil Engineers. New York, N.Y.
- ASCE. 1988. ASCE Task Committee on Drift Control of Steel Building Structures of the Committee on Design of Steel Building Structures. Wind drift design of steel-framed buildings: State-of-the-art report. *Journal of Structural Engineering*. 114 (9): 2085-2108.
- ASCE 7-88. 1988. Minimum design loads for buildings and other structures. American Society of Civil Engineers, New York, N.Y.
- ASCE. 1996. Aerospace Division Task Committee on Wind Tunnel Studies of Buildings and Structures. Wind tunnel studies of buildings and structures. *Journal of Aerospace Engineering*. 9 (1): 19-36.
- ASCE/ANSI 7-95. 1996. Minimum design loads for buildings and other structures. American Society of Civil Engineers, New York, N.Y.
- ASCE 7-98. 2000. Minimum design loads for buildings and other structures. American Society of Civil Engineers, New York, N.Y.
- Balendra, T., G.K. Nathan and K.H. Kang. 1989. Deterministic model for wind-induced oscillations of buildings. *Journal of Engineering Mechanics*. 115 (1): 179-199.
- Billington, D.P. 1982. Thin Shell Concrete Structures. Second Edition, McGraw-Hill, New York, N. Y.
- Bishop, R.E.D. and A.Y. Hassan. 1964. The lift and drag forces on a circular cylinder oscillating in a flowing fluid. *Proceedings of the Royal Society of London*, London, England, A 227.
- Blackler, M.J. and P. Ansourian. 1983. Buckling of stiffened cylindrical bins under wind loading. *Proceedings of the International Conference on Bulk Materials, Storage, Handling and Transportation*. Newcastle, Australia. 317-339.
- BOCA National Building Code. 1984, 1987, 1993. Building Officials and Code Administrators International Inc. Country Club Hills, IL.
- Boggs, D.W. and J.A. Peterka. 1989. Aerodynamic model tests of tall buildings. *Journal of Engineering Mechanics*. 115 (3): 618-635.
- Bose, P.R. and T.K. Datta. 1994. Lateral-torsional motion of tall buildings to along-wind forces. *Computers & Structures*. 53 (4): 897-905.
- Binder, R.C. 1973. *Fluid Mechanics*. Fifth Edition. Prentice Hall, Inc., Englewood Cliffs, N.J.

- Briassoulis, D. 1985. Analysis of the behavior of steel silos under wind loading. Ph.D. Dissertation (unpublished), University of Illinois at Urbana-Champaign. Urbana, IL.
- Briassoulis, D. and D.A. Pecknold. 1986a. Anchorage requirements for wind-loaded empty silos. *Journal of the Structural Division, ASCE*. 112 (2): 308-325.
- Briassoulis, D. and D.A. Pecknold. 1986b. Behavior of empty steel grain silos under wind loading: Part 1: the stiffened cylindrical shell. *International Journal of Engineering Structures*. 8(4): 260-275.
- Briassoulis, D. and D.A. Pecknold. 1988. Behavior of empty steel grain silos under wind loading: Part 2: the stiffened conical roof shell. *International Journal of Engineering Structures*. 10: 57-64.
- British Standard Code. 1972. Code of practice, CP3, code of basic data for the design of buildings, chap V., loading, wind loads. British Standard Institution, London, England.
- Cermak, J.E., 1977. Wind tunnel testing of structures, *Journal of the Engineering Mechanics Division, ASCE*. 103(EM6): 1124-1140.
- Chan, C. 1998. Optimal stiffness design to limit static and dynamic wind responses of tall steel buildings. *Engineering Journal*. 3 (3): 94-105.
- Chandrashekhara, K. 1989. Analysis of long cantilever cylindrical shell subjected to wind loading. *Journal of Engineering Mechanics*. 115 (9): 2101-2105.
- Changery, M. 1979. Data collection and storage by the national climatic center. *Proceedings, Workshop on Wind Climate, Asheville, N.C.* 1: 99-106.
- Chen, Y. and G. Ahmadi. 1992. Wind effects on base-isolated structures. *Journal of Engineering Mechanics*. 118 (8): 1708-1727.
- Chen, J. 1994. Analysis of engineering structures response to random wind excitation. *Computers & Structures*. 51 (6): 687-693.
- Chiu, G.L.F. and D.C. Perry. 1997. Low-rise building wind load provisions-where are we and where do we need to go? *Engineering Journal*, fourth quarter, pp.135-150.
- Cook, N.J. 1993. Wind Engineering. 1st IAWQ European and African Regional Conference, Redwood Books, Trowbridge, Great Britain.
- Corotis, R.B. and V.A. Jaria. 1979. Stochastic nature of building live loads. *Journal of the Structural Division, ASCE*. 493-510.

- Davenport, A.G., 1960: Wind Loads on Structures, Technical Paper No. 88, Division of Building Research, National Research Council of Canada, Ottawa, Canada.
- Davenport, A.G., 1961. The application of statistical concepts to the wind loading of structures. Proceedings, Institution of Civil Engineers, Vol. 19, Paper 6480.
- Davenport, A.G. and N. Isyumov. 1968. The application of the boundary layer wind tunnel to the prediction of wind loading. Proceedings of the International Research Seminar on Wind Effects on Buildings and Structures. Ottawa. University of Toronto Press. Toronto, Canada.
- Davenport, A.G. and D. Surry. 1974. The pressures on low-rise buildings in turbulent wind. Canadian Structural Engineering Conference. Toronto, Canada.
- Davenport, A.G., D. Surry, and T. Stathopoulos. 1977. Wind loads on low rise buildings: Final report of phases I and II – parts 1 and 2. The University of Western Ontario, BLWT Report, SS8-1977, Second edition. Toronto, Canada.
- Davenport, A.G., D. Surry, and T. Stathopoulos. 1978. Wind loads on low rise buildings: Final report of phase III – part 1. The University of Western Ontario, BLWT Report, SS4-1978, Second edition. Toronto, Canada.
- Davenport, A.G., D. Surry, and T. Stathopoulos. 1984. External pressures on low buildings-the code and beyond. Fourth Canadian Workshop on Wind Engineering, pp. 11-19. Toronto, Canada.
- Devlin, P.A. 1997. Wind endurance. Civil Engineering. 67 (Dec.): 60-62.
- DIN. 1985. Thin-walled cylindrical steel tower silos (Dünwandige rundsilos aus stahl). DIN 18914. Deutsche Normen, Berlin, Germany.
- DIN. 1987. Lastannahmen für bauten--lasten in silozellen. DIN 1055, Teil 6. Deutsche Normen, Berlin.
- Dyrbye, C. and S.O. Hansen. 1996. Wind Loads on Structures. John Wiley & Sons Inc., New York, N. Y.
- Ellingwood, B. 1983. Statistical tests of environmental load data. Journal of Structural Engineering. 110 (6): 1400-1404.
- Ellingwood, B. and A. Tallin. 1984. Serviceability limit states: induced vibrations. Journal of Structural Engineering. 110 (10): 2424-2437.
- European Prestandard, 1995. ENV 1991-4, Eurocode1: Basis of design and actions on structures-Part4: Actions in silos and tanks. European Committee for Standardization (CEN), Brussels.

- Florida Building Code. 2000. Florida Building Commission. Tallahassee, FL.
- Fur, L., H.T.Y. Yang, and S. Ankireddi. 1996. Vibration control of tall buildings under seismic and wind loads. *Journal of Structural Engineering*. 122 (8): 948-957.
- Gaylord, E.H. and C.N. Gaylord. 1984. Design of Steel Bins for Storage of Bulk Solids. Prentice Hall, Englewood Cliffs, New Jersey.
- Gopacacharyulu, S. and D.J. Johns. 1979. Cantilever cylindrical shells under assumed wind pressures. *Journal of Structural Division, ASCE*. Paper 10085. ASCE, Reston, VA.
- Gorenc, B.E., T.J. Hogan, and J.M. Rotter. 1986. Guidelines for the assessment of loads on bulk solids containers. National Committee on Structural Engineering, The Institution of Engineers, Australia.
- Gould, P.L. and S.H. Abu-Sitta. 1980. Dynamic Response of Structures to Wind and Earthquake Loading. John Wiley & Sons, New York, N.Y.
- Greiner, R. 1998. Cylindrical shells: wind loading. In: Silos, Fundamentals of Theory, Behavior and Design. Edited by C.J. Brown and J. Nielson. E&FN Spon. London. pp 378-399.
- Griffis, L.G. 1993. Serviceability limit states under wind load. *Engineering Journal*, First Quarter, (1): 1-16.
- Grossman, R.B. 1993. Wind loads on conical roofs. Paper No. 93-4005. ASAE, St. Joseph, MI.
- Gurley, K. and A. Kareem. 1997. Analysis, interpretation, modeling and simulation of unsteady wind and pressure data. *Journal of Wind Engineering and Industrial Aerodynamics*, 69-71: 657-669.
- Gurley, K., M. Tognarelli, and A. Kareem. 1997. Analysis and simulation tools for wind engineering. *Probabilistic Engineering Mechanics*. 12 (1): 9-31.
- Hands, K.N. and B.L. Clarkson, 1968: Response of Tall Structures to Atmospheric Turbulence, Proceedings, Wind Effects on Buildings and Structures, Loughborough University of Technology, England, Vol. 1, Paper 14.
- Harmon, J.D., G.F. Grandle, and C.L. Barth. 1992. Effects of hurricane Hugo on agricultural Structures. *Transactions of ASAE*. 8(1): 93-96.
- Hartlen, R.T. and I.G. Currie. 1970. Lift-oscillator model of vortex-induced vibration. *Journal of Engineering Mechanics Division, ASCE*. (5): 577-591.

- Holroyd, R.J. 1983. On the behavior of open-topped oil storage tanks in high winds. Part I. Aerodynamic aspects. *Journal of Wind Engineering and Industrial Aerodynamics*. (12): 329-352.
- Holroyd, R.J. 1985a. On the behavior of open-topped oil storage tanks in high winds. Part II. Structural aspects. *Journal of Wind Engineering and Industrial Aerodynamics*. (18): 55-73.
- Holroyd, R.J. 1985b. On the behavior of open-topped oil storage tanks in high winds. Part III. A structural dynamic instability mechanism. *Journal of Wind Engineering and Industrial Aerodynamics*. (21): 339-341.
- Hoxey, R.P. 1984. Design wind loads for closed farm buildings. *Journal of Agricultural Engineering Research*. 29: 305-311.
- Hoxey, R.P. and G.M. Richardson. 1984. Measurements of wind loads on full-scale film plastic clad greenhouses. *Journal of Wind Engineering and Industrial Aerodynamics*. 16: 57-83.
- Iannuzzi, A. and P. Spinelli. 1987. Artificial wind generation and structural response. *Journal of Structural Engineering*. 113 (12): 2382-2398.
- IBC. 2000. International Building Code. BOCA International, Inc. Country Club Hills, IL.
- Islam, M.S., B. Ellingwood, and R.B. Corotis. 1990. Transfer function modeling of dynamic wind loads on buildings. *Journal of Engineering Mechanics*. 116 (7): 1473-1488.
- Jensen, M. and N. Franck. 1965. *Model-Scale Tests in Turbulent Wind*. Danish Technical Press.
- Jerath, S. and A.P. Boreisi. 1979. Stress analysis of bins by shell bending theory. *Journal of the Structural Division, ASCE*. 105 (ST6): 1069-1082.
- Jerath, S. and H. Sadid. 1985. Buckling of orthotropic cylinders due to wind load. *Journal of Engineering Mechanics*. 111 (5): 610-622.
- Jesien, W., T. Stathopoulos, and H.K. Ha. 1993. Dynamic along-wind response of buildings: comparative study. *Journal of Structural Engineering*. 119 (5): 1498-1515.
- Kareem, A. 1985a. Wind induced response analysis of tension leg platforms. *Journal of Structural Engineering*. 111 (1): 37-55.
- Kareem, A. 1985b. Lateral-torsional motion of tall buildings to wind loads. *Journal of Structural Engineering*. 111 (11): 2479-2496.

- Kareem, A., M. Tognarelli, and K. Gurley. 1998. Modeling and analysis of quadratic term in the wind effects on structures. *Journal of Wind Engineering and Industrial Aerodynamics*. 74-76: 1101-1110.
- Kebeli, H.V. and R.A. Bucklin. 1999. Structural failure modes of grain bins. Paper No. 994141. ASAE, St. Joseph, MI.
- Kebeli, H.V., R.A. Bucklin, K. Gurley, and T. Reinhold. 2001a. Wind pressure coefficients of conical roofs on grain bins. AAWE Americas Conference on Wind Engineering – 2001. Clemson, S.C.
- Kebeli, H.V., R.A. Bucklin, and K. Gurley. 2001b. Wind tunnel tests to establish pressure coefficients for grain bins. Paper No. 01-4017. ASAE, St. Joseph, MI.
- Krauthammer, T., P.A. Rowekamp, and R.T. Leon. 1987. Experimental assessment of wind-induced vibrations. *Journal of Engineering Mechanics*. 113 (9): 1387-1403.
- Kundurpi, P.S., G. Samaredan, and D. Johns. 1975. Stability of cantilever shells under wind loading. *Journal of Engineering Mechanics Division, ASCE*. 101(EM5): 517-530.
- Kurth, F. 1985. Design of the external steel framework of Eurosilos to resist wind loading. *Bulk Solids & Handling*. 5(2): 417-423.
- Levitan, M.L. and K.C. Mehta. 1991a. Texas Tech field experiments for wind loads part I: Building and pressure measuring system. *Proceedings of the Eight International Conference on Wind Engineering*, London, Ontario, Canada.
- Levitan, M.L. and K.C. Mehta. 1991b. Texas Tech field experiments for wind loads part II: Meteorological instrumentation and terrain parameters. *Proceedings of the Eight International Conference on Wind Engineering*, London, Ontario, Canada.
- Lew, M. and G.C. Hart. 1979. Microzonation in wind engineering. *Journal of the Structural Division, ASCE*. (1): 975-989.
- Liu, H. 1991. Wind Engineering: A Handbook for Structural Engineers. Prentice Hall, Englewood Cliffs, N.J.
- Macdonald, A.J. 1975. Wind Loading on Buildings. Applied Science Publishers, London, UK.
- Macdonald, P.A., J.D. Holmes, and K.C.S. Kwok. 1988. Wind loads on circular storage bins, silos and tanks. I. Point pressure measurements on isolated structures. *Journal of Wind Engineering and Industrial Aerodynamics*. 31: 165-188.

- Macdonald, P.A., J.D. Holmes, and K.C.S. Kwok. 1990a. Wind loads on circular storage bins, silos and tanks. II. Effects of grouping. *Journal of Wind Engineering and Industrial Aerodynamics*. 34: 77-95.
- Macdonald, P.A., J.D. Holmes, and K.C.S. Kwok. 1990b. Wind loads on circular storage bins, silos and tanks. III. Fluctuating and peak pressure distributions. *Journal of Wind Engineering and Industrial Aerodynamics*. 34: 319-337.
- Maher, F.J. 1966. Wind loads on dome-cylinder and dome-cone shapes. *Journal of Structural Division, ASCE*. 92(ST5): 79-85.
- Mahoney, G.W.A., R. Gaddis, A.F. Butchbaker, and S. Moustafa. 1978. Storage pattern effects on wind force reaction on roofs of open buildings. *Transactions of ASAE*. 172-145.
- Mahoney, G.W.A. 1984. Wind forces on flat roofs, stack pattern effect. ASAE paper No. 84-4006. ASAE, St. Joseph, MI.
- Mahoney, G.W.A. and J.I. Fryrear. 1985. Lee wall vent openings in open front shelters, effects on wind pressures. *Transactions of ASAE*. 538-541.
- Marshall, R.D. 1973. Aerodynamics of structures and wind tunnel modeling-development of improved design criteria to better resist the effects of extreme winds for low-rise buildings in developing countries. Center of Building Technology, National Bureau of standards, Washington, DC.
- Marshall, R.D., T.A. Reinhold, and H.W. Tielman. 1976. Wind pressures on single-family dwellings. ASCE-EMD Specialty Conference, Dynamic Response of Structures. University of California, Los Angeles, CA.
- Marshall, R.D. 1977. The measurement of wind loads on a full-scale mobile home. Center of Building Technology, National Bureau of standards, Washington, DC.
- Marzouk, O.A., and G. Abdel-Sayed. 1973. Linear theory of orthotropic cylindrical shells. *Journal of the Structural Division, ASCE*. 99 (ST11): 2287-2306.
- Math Works Inc. 2001. Math Lab Release 12. Math Works Inc., USA.
- Mcfadden, V.J., D.S. Bundy, and A.D. Lukens. 1991. Evaluation of the loading of a post-frame structure. *Transactions of ASAE*. 34(4): 1860-1865.
- Mehta, K.C. 1984. Wind-induced damage: Observations and their implications for design practice. *Engineering Structures*. 6 (4): 242-247.
- Mehta, K.C. and R.D. Marshall. 1997. Guide to the use of the wind load provisions of ASCE 7-95. ASCE Press. American society of Civil Engineers, Reston, VA.

- Michot, B.J. 1999. Full-scale wind pressure measurement utilizing unobtrusive absolute pressure transducer technology. Unpublished Master Thesis. Civil Engineering Department, Clemson University, Clemson, SC.
- Microsoft Corporation. 2001. Microsoft Office Suite- Excel 2000. Microsoft Co., Richmond, WA.
- Monroe, J.S. 1996. Wind tunnel modeling of low rise structures in a validated open country simulation. Master's thesis. Civil Engineering Department, Clemson University, Clemson, SC.
- Moriarty, W.W. 1985. On the directional uncertainty of strong wind gusts. *Journal of Wind Engineering and Industrial Aerodynamics*. 21: 155-166.
- Motorola. 2000. MPX2010 10kPa On-Chip Temperature Compensated and Calibrated Silicon Pressure Sensors. Motorola Sensor Service Data. Motorola Inc., USA.
- National Instruments. 2000. Lab VIEW 5.0. National Instruments Co., Austin, TX.
- National Instruments. 2001. Data Acquisition Designer Manual 2001. National Instruments Co., Austin, TX.
- Nelson, J.K. and T.A. Reinhold. 1999. Tower Version 1.9. Software for use with the Clemson University mobile wind measurement tower. Clemson University, Clemson, SC.
- Niemann, H.J. 1980. Wind effects on cooling tower shells. *Journal of the Structural Division, ASCE*. 106 (ST3): 643-661.
- Noakowski, P. and K.H. Gerstle. 1990. Tower structures subjected to temperature and wind. *ACI Structural Journal*. 87 (4): 479-487.
- NRCC. 1990a: National Building Code of Canada, 1985, Associate Committee on the National Building Code, National Research Council of Canada, NRCC No. 23174, Ottawa, Canada.
- NRCC. 1990b: The Supplement to the National Building Code of Canada, 1985, Associate Committee on the National Building Code, National Research Council of Canada, NRCC No. 23178, Ottawa, Canada.
- Pecknold, D.A. 1989. Load transfer mechanisms in wind-loaded cylinders. *Journal of Engineering Mechanics*. 115 (11): 2353-2367.
- Peterka, J.A. and J.E Cermak. 1975. Adverse Wind Loading Induced by Adjacent Buildings, ASCE Meeting Preprint No. 2456, ASCE, New York, NY.

- Porterfield, M.L., and J.P. Jones. Full-scale measurements on a low-rise structure in Southern Shores, North Carolina: Structure and instrumentation systems. The Eight U.S. National Conference on Wind Engineering, The John Hopkins University, Baltimore, M.D.
- Prabhu, K.S., S. Gopalacharyulu, and D.J. Johns. 1975. Cantilever cylindrical shells subjected to wind loading. *Journal of Applied Mechanics*. American Society of Mechanical Engineers. 41(1): 233-234.
- Purdy, D.M., F.J. Meher, and D. Frederick. 1967. Model studies of wind loads on flat-top cylinders. *Journal of the Structural Division, ASCE*. 93(ST2): 379-395.
- Rao, P.S. and K. Ramanjaneyulu. 1993. Stability of cooling tower shell with modified wind pressure coefficients. *Journal of Engineering Mechanics*. 119(11): 2207-2225.
- Reed, D.A. 1987. Use of field parameters in wind engineering design. *Journal of Structural Engineering*. 113 (7): 1570-1585.
- Reinhold, T.A., Ed., 1983. *Wind Tunnel Modeling for Civil Engineering Applications*, Proceedings, International Workshop (April 1982, Gaithersburg, MD), Cambridge University Press, New York, NY.
- Richardson, G. M. 1993. Full-scale wind load measurements on a single-span film plastic-clad livestock building. *Journal of Agricultural Engineering Research*. 55: 251-264.
- Robertson, A.P. and P. Moran. 1984. Wind loads on a dutch barn. *Journal of Agricultural Engineering Research*. 29: 207-213.
- Robertson, A.P., R.P. Hoxey, and P. Moran. 1985. A full-scale study of wind loads on agricultural ridged canopy roof structures and proposals for design. *Journal of Wind Engineering and Industrial Aerodynamics*. 21: 167-205.
- Rouse, H., 1938. Fluid Mechanics for Hydraulic Engineers. McGraw-Hill, New York, NY.
- Sabransky, I.J. and W.H. Melbourne. 1987. Design pressure distribution on circular silos with conical roofs. *Journal of Wind Engineering and Industrial Aerodynamics*. 26: 66-84.
- Sachs, P. 1977. Wind Forces in Engineering. 2. Edition, Pergamon Press. Elsevier Science Publishing Co. New York, N.Y.
- Samali, B., J.N. Yang, and C.T. Yeh. 1985. Control of lateral-torsional motion of wind-excited buildings. *Journal of Engineering Mechanics*. ASCE. 111(6): 777-796.

- Shiau, L. and T.Y. Yang. 1987. Two-cylinder model for wind vortex-induced vibration. *Journal of Engineering Mechanics*. 113 (5): 780-789.
- Shiau, L. 1989. Wind-induced vibration of two flexible cylindrical structures. *Journal of Engineering Mechanics*. 115 (9): 2089-2098.
- Simiu, E., S.D. Leigh, and W.A. Nolan. 1985. Environmental load direction and reliability bounds. *Journal of Structural Engineering*. 112 (5): 1199-2229.
- Simiu, E. and Scanlan, R.H., 1986. Wind Effects on Structures. 2nd Edition, John Wiley and Sons, New York, NY.
- Simiu, E. and R.H. Scanlan. 1996. Wind Effects on Structures: Fundamentals and Applications to Design. John Wiley & Sons Inc., New York, N. Y.
- Singer, J., M. Baruch, and O. Harari. 1966. Inversion of the eccentricity effect in stiffened cylindrical shells buckling under external pressure. *Journal of Mechanical Engineering Science*. 8(4): 363-373.
- Skop, R.A. and O.M. Griffin. 1975. On a theory for the vortex-excited oscillations of flexible cylindrical structures. *Journal of Sound Vibrations*. 41(3): 263-274.
- Smart, H.R., L.K. Stevens, and P.N. Joubert. 1967. Dynamic structural response to natural wind. *Proc. Wind Effects on Buildings and Structures*, University of Toronto Press. 1: 595-630.
- Solari, G. 1985. Mathematical model to predict 3-d wind loading on buildings. *Journal of Engineering Mechanics*. 111 (2): 254-276.
- Solari, G. 1988. Equivalent wind spectrum technique: theory and applications. *Journal of Structural Engineering*. 114 (6): 1303-1323.
- Solari, G. 1989. Wind response spectrum. *Journal of Engineering Mechanics*. 115 (9): 2057-2073.
- Sollenberger, N.J., and R.H. Scanlan. 1974. Pressure differences across the shell of a hyperbolic natural-draft cooling tower. *Proceedings of the Second USA-Japan Research Seminar On Wind Effects on Structures*. University of Tokyo Press, Tokyo, Japan.
- Sollenberger, N.J., R.H. Scanlan, and D. P. Billington. 1980. Wind loading and response of cooling towers. *Journal of the Structural Division, ASCE*. 106 (ST3): 601-621.
- SPSS Inc. 2001. Sigma Plot 2001 for Windows version 7. Math Works Inc., USA.
- Srinivasan, C.N. and C.R. Arvind. 1993. Wind loads on buildings with sawtooth roofs. *Journal of Structural Engineering*. 119 (3): 994-996.

- Standard Building Code. 1997. Southern Building Congress International Inc. Birmingham, Alabama.
- Standards Australia. 1996. Loads on bulk solid containers. AS 3774-1996. Standards Australia, Homebush, NSW, Australia.
- Stathopoulos, T. 1984. Adverse wind loads on low buildings due to buffering. *Journal of Structural Engineering*, ASCE. 111(1): 2374-2392.
- Stathopoulos, T. and R. Kozutsky. 1985. Wind-induced internal pressures in buildings. *Journal of Structural Engineering*, ASCE. 112(9): 2012-2026.
- Stathopoulos, T. and H.D. Luchian. 1989. Transient wind-induced internal pressures. *Journal of Engineering Mechanics*, ASCE. 115(7): 1501-1514.
- Stathopoulos, T. and P. Saathoff. 1994. Codification of wind-pressure coefficients for multispan gable roofs. *Journal of Structural Engineering*. Vol. 120, No. 8, pp. 2495-2519. ASCE.
- Tallin, A. and B. Ellingwood. 1984. Serviceability limit states: Wind induced vibrations. *Journal of Structural Engineering*. 110 (10): 2424-2437.
- Tallin, A. and B. Ellingwood. 1985. Wind induced lateral-torsional motion of buildings. *Journal of Structural Engineering*. 111 (10): 2197-2213.
- Tielman, H.W., D. Surry, and K.C. Mehta. 1993. Full/model scale comparisons of surface pressures on the Texas Tech experimental building. Seventh U. S. National Wind Engineering Conference, Los Angeles, CA.
- Torkamani, M.A.M. and E. Promono. 1985. Dynamic response of tall building to wind excitation. *Journal of Structural Engineering*. 111 (4): 805-825.
- Uniform Building Code, 1982, 1991, and 2000. International Conference of Building Officials, Whittier, CA.
- Uematsu, Y. and K. Uchiyama. 1985. Deflection and buckling behavior of thin, circular cylindrical shells under wind loads. *Journal of Wind Engineering and Industrial Aerodynamics*. (18): 245-261.
- U.S. National Weather Service. 2001. Weather conditions in Gainesville Regional Airport, Gainesville, FL. Online. <http://weather.noaa.gov/weather/current/KGNV.html>
- Vellozzi, J.W. and E. Cohen. 1968. Gust response factors. *Journal of the Structural Division*, ASCE. 94(ST6): 1295-1313.

- Vickery, P.J. 1984. Wind loads on the Aylesbury experiment house: A comparison between full scale and two different scale models. Master of Science Thesis, University of Western Ontario, Canada.
- Wang, Y., and D.P. Billington. 1974. Buckling of cylindrical shells by wind pressure. *Journal of the Engineering Mechanics Division, ASCE*, Vol. 100, No. EM5, pp. 1005-1021.
- Wen, Y. 1983. Wind direction and structural reliability: II. *Journal of Structural Engineering*. 110 (6): 1253-1264.
- Wickstrom, L.L. 1980. Loads applied to grain bin roofs. ASAE Paper No. 80-4505. American Society of Agricultural Engineers, St Joseph, Michigan.
- Zdravkovich, M.M. 1985. Flow induced oscillations of two interfering circular cylinders. *Journal of Sound Vibrations*. 101(4): 511-521.

BIOGRAPHICAL SKETCH

H. Volkan Kebeli was born on July 6, 1971, in Karabük, Türkiye. He graduated from Ankara-Atatürk Anatolia High School in 1989 and enrolled in the Agricultural Structures and Irrigation Department at the Faculty of Agriculture at Ankara University and graduated with the second highest GPA in 1994.

He started his M.Sc. studies in agricultural engineering in 1994 and worked in the Agricultural Structures and Irrigation Department at the Faculty of Agriculture at Ankara University, for one year as a research and teaching assistant. In 1995, he succeeded in a competitive and nationwide exam offered by the Turkish government to pursue both M.Sc. and Ph.D. degrees in agricultural engineering in the U.S.A.

Volkan came to the U.S.A. in February 1996 and studied English in the Academic English Program at the University of Texas at Austin. Since May of 1996, he has worked with Dr. Ray A. Bucklin to pursue his Master's and Ph.D. degrees. He received his Master of Engineering degree in May 1998. Volkan expects to receive his doctor of philosophy degree in agricultural and biological engineering with a minor degree in structural engineering in May 2002, and plans to start working at Sukup Manufacturing Company as structural engineer after his graduation. He is currently a member of the Florida Gamma Beta Chapter of Alpha Epsilon, American Society of Agricultural Engineering (ASAE), American Society of Civil Engineering (ASCE), The Society of

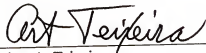
Turkish Agricultural Engineers, University of Florida Alumni Association, and Ankara University Alumni Association.

I certify that I have read this study and that in my opinion it conforms to acceptable standards of scholarly presentation and is fully adequate, in scope and quality, as a dissertation for the degree of Doctor of Philosophy.



Ray A. Bucklin, Chairman
Professor of Agricultural and Biological
Engineering

I certify that I have read this study and that in my opinion it conforms to acceptable standards of scholarly presentation and is fully adequate, in scope and quality, as a dissertation for the degree of Doctor of Philosophy.



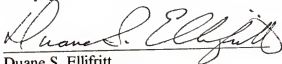
Arthur A. Teixeira
Professor of Agricultural and Biological
Engineering

I certify that I have read this study and that in my opinion it conforms to acceptable standards of scholarly presentation and is fully adequate, in scope and quality, as a dissertation for the degree of Doctor of Philosophy.




Michael T. Talbot
Associate Professor of Agricultural and
Biological Engineering

I certify that I have read this study and that in my opinion it conforms to acceptable standards of scholarly presentation and is fully adequate, in scope and quality, as a dissertation for the degree of Doctor of Philosophy.



Duane S. Ellifritt
Professor of Civil and Coastal Engineering


I certify that I have read this study and that in my opinion it conforms to acceptable standards of scholarly presentation and is fully adequate, in scope and quality, as a dissertation for the degree of Doctor of Philosophy.



Kurtis R. Gurley
Assistant Professor of Civil and Coastal
Engineering

This dissertation was submitted to the Graduate Faculty of the College of Engineering and to the Graduate School and was accepted as partial fulfillment of the requirements for the degree of Doctor of Philosophy.

August 2002



Pramod P. Khargonekar
Dean, College of Engineering

Winfred M. Phillips
Dean, Graduate School